# Power Spectra of a Three-Phase Inverter with Random Pulse Width Modulation Modes

by



Samuel Kwok

B.Eng.,University of Victoria , Canada, 1991

A Thesis Submitted in Partial Fulfillment of the
Requirements for the Degree of

MASTER OF APPLIED SCIENCE

in the Department of Electrical and Computer Engineering

We accept this thesis as conforming
to the required standard

[redacted]

Dr. R. L. Kirlin, Supervisor, Dept. of Elect. & Comp. Eng.

[redacted]

Dr. J. M. S. Kim, Departmental Member, Dept. of Elect. & Comp. Eng.

[redacted]

Dr. Z. Dong, Outside Member, Dept. of Mech. Eng.

[redacted]

Dr. C. J. Konzelman, External Examiner , Dept. of Mech. Eng.

Supervisor: Dr. R. L. Kirlin.

# Abstract

Power inverters convert DC voltage to single- or multi-phase AC voltage. For three-phase inversion, the voltage control is realized by means of Pulse-Width Modulation (PWM) of the switching variables a, b, and c which represent the control signals for individual phases of the inverter. In this thesis, analysis of the harmonic power spectra of the three-phase, voltage-controlled inverter with randomized lead-lag modes of operation will be presented. In these modes, the pulses of switching variables are either leading- or lagging-edge modulated. The randomized PWM technique provides non-repetitive switching patterns which result in spreading of distinct harmonic power over a wider frequency range. Experimental confirmation of the derived closed-form equations of both continuous and discrete spectra is provided. Further, a brief outline of the future work, which is to find the optimal switching pattern (i.e. probability density function) based on certain optimization criteria, is also presented.

Examiners:

Dr. R. L. Kirlin, Supervisor, Dept. of Elect. & Comp. Eng.

Dr. J. M. S. Kim, Departmental Member, Dept. of Elect. & Comp. Eng.

Dr. Z. Dong, Outside Member, Dept. of Mech. Eng.

Dr. C. J. Konzelman, External Examiner , Dept. of Mech. Eng.

# Contents

# List of Figures

# Acknowledgements

I would like to thank my supervisor, Dr. R. Lynn Kirlin for giving me the opportunity to participate in this research. His patient guidance and Research Assistantship support are greatly appreciated. I would like to thank Dr. J.M.S. Kim for his helpful comments on power electronic concepts. I would also like to thank Dr. A. M. Trzynadlowski, University of Nevada, and Dr. S. Legowski, University of Wyoming, for their helpful comments and experimental results on the random pulse-width modulation.

I also wish to thank several fellow graduate students for their help on preparing this manuscript. In particular, Pavan Kumar's discussion on power electronic concepts and Alex Andekian's help on using LaTeX are appreciated. I would also like to thank the ECE department secretary, Maureen Denning, for typing part of the formulas of Chapter 4 of this thesis. Finally, I wish to thank Dr. W.S. Lu for his helpful discussions and encouragement during my time as a graduate student at UVic.

**To my Parents.**

# Chapter 1

# Introduction

## 1.1 Background

Pulse-Width Modulation (PWM) techniques are used in inverter circuits such as the one shown in figure 1.1 to allow control of the fundamental output voltage and to reduce the magnitude of the harmonic voltage. When the inverter load is an AC motor, the lower order harmonics cause undesirable effects on the load such as heating, pulsating torque and cogging. As a result, the efficiency of the motor is less than that of a motor driven by a pure sinusoidal voltage. Ideally, the best PWM technique is the one that eliminates the highest number of low-order harmonics of the inverter output voltage while maintaining a high fundamental output voltage. For a given maximum inverter switching frequency, the problem is to choose a PWM control technique which will maximize the fundamental voltage amplitude and mimimize the harmonic power losses within the motor.

Since the publication of the classical papers [10, 11], a number of PWM schemes

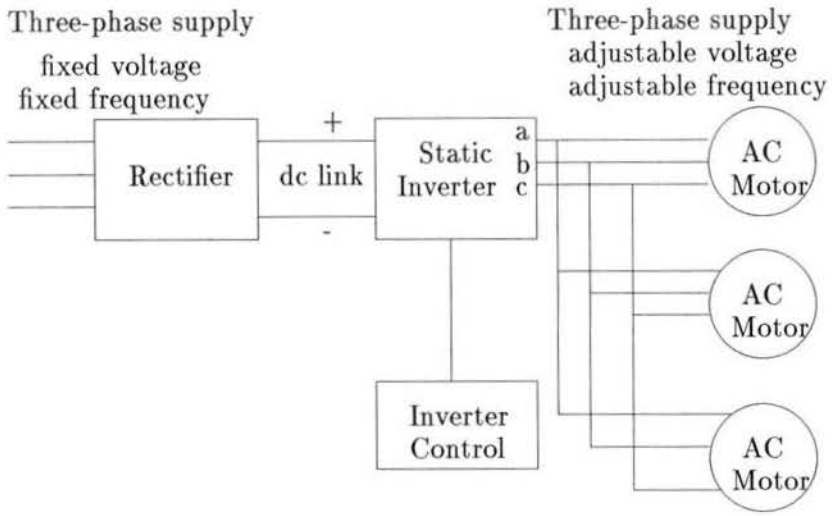


Figure 1.1: Block diagram of PWM inverter for a multimotor AC drive.

have been proposed for the control of inverters or converters. We only discuss the more important aspects that can later be used for comparison with the random PWM strategy discussed in Chapter 3.

The sinusoidal PWM (SPWM) is the most common method in industrial applications. This method has been reviewed extensively in the literature [24, 25, 26, 28]. The idea is simple. A sinusoidal reference wave with the desired fundamental frequency of the inverter output is compared with a triangular carrier wave using a comparator. From Fourier analysis, the resulting pulse-waveform is shown to contain the fundamental and a number of unwanted harmonic content. This modulation is called sinusoidal PWM because the pulse width of the output waveform is a sinusoidal function of its angular position in the cycle. The implementation of this method is usually done in analog components. However, the circuitry needed to achieve precise generation of a variable-frequency three-phase sinusoidal modulat-

ing wave is generally costly. For high-precision control, this method is not reliable due to phase and frequency drift problems associated with the analog components.

The improved method, called programmed PWM, provides the minimization of the undesirable harmonic content (in particular, low-order harmonics) in the inverter output spectra. Programmed PWM is an optimal scheme which takes certain optimization criteria into account. This may include : selective harmonic elimination [10, 11, 12], optimization of efficiency [13, 14], optimal drive dynamics (i.e. minimization of torque pulsations and position ripples) [15], and electromagnetic interference (EMI) minimization [19]. Thus, the calculated waveforms represent the optimum solution for the given objective function under certain constraints.

Programmed PWM offers the following distinct advantages in comparison to the SPWM method :

1. Elimination of low-order harmonics minimizes torque pulsations and increases motor efficiency.

2. Reduction in the size of the input filter is achieved due to the high quality of output voltage and current.

The control systems for SPWM and programmed PWM are normally implemented using dedicated analog and digital hardware. However, microprocessor-based implementation is receiving wide attention. A detailed comparative study of the various microprocessor-based methods of generating PWM control is presented in [18]. The main features which are advantageous for the control tasks are summarized as follows :

1. For complex drive-control systems, the simplification of hardware saves control electronics cost and improves system reliability.

2. Digital control inherently provides noise immunity, which is particularly important because of large switching transients in the converters.

3. The software control algorithm can easily be altered or improved in the future without change of hardware.

4. Powerful diagnostic functions can be incorporated in software.

Natural sampling (or sinusoidal PWM) is essentially an analog technique, and this form of digital implementation is not very effective. In a microprocessor-controlled PWM inverter, it is difficult to calculate the pulse widths of the naturally sampled waveform in real time. In other words, the on-line computation of instants of intersection of the triangular carrier and sinusoidal reference waveform is not possible as there is no closed-form solution yielding these instants. It is possible to simulate the process of natural sampling in software, but, again, this is not an effective technique [17]. The uniform sampled PWM inverter control was first proposed in 1975 [17]. It is recognized to have certain advantages over the sinusoidal PWM (or natural sampling PWM) when implemented using microprocessor-based techniques.

The optimum PWM waveforms based on programmed PWM can not be generated with analog control circuitry, and the switching angles can not be computed in real time. The usual technique adopted involves storing the pre-computed switching information for a number of different fundamental voltage levels as a look-up table in memory and accessing this information by hardwired digital logic or by a microprocessor. The memory requirement is related to the number of discrete levels of inverter output voltage and the look-up table format.

The difficulties encountered in the programmed PWM method are:

1. The amount of memory required grows with the resolution and accuracy of the output waveform.

2. In most cases only the local minimum can be obtained after considerable amount of computational effort (e.g. in the selective harmonic elimination technique); hence, the switching waveform computed is not truly optimal.

## 1.2 Purpose and Contributions

The PWM schemes that we have mentioned so far are referred to as deterministic, since the waveforms generated are fixed and repeated periodically. The adverse effect of the repeated switching pattern is the generation of a periodic ripple current, which in turn results in fluctuating output torque from the AC motor driven by the inverter. As a result, the motor could have high noise level, poor vibration characteristics and low efficiency.

As an alternative to the existing deterministic PWM methods for voltage-controlled power inverters, a novel and high-performance PWM technique, called Random PWM (RPWM), was initially introduced in [1]. RPWM is based on randomization of the switching pattern.

The concept of randomized switching, which has a very rich mathematical foundation based on probability theory and harmonic analysis, has long been studied extensively in the area of signal processing and communications [29, 30]. It is not until recently that the concept of randomization was found useful in applications to power converters. This application is based on the observation that the operation of an AC motor is not sensitive to a small variation in the inverter output voltage

or current. Thus, a randomization factor with certain statistical properties can be introduced to the PWM technique. The result of this is that the power spectrum of the inverter output can be altered in a controlled manner such that the proper operation of the AC motor is not affected significantly.

The RPWM strategy possesses several distinct advantages over the deterministic PWM technique [6].

1. Varying switching patterns result in the spreading of the inverter output power spectra. This provides better noise and vibration characteristics of a drive system supplied from the inverter.

2. High-quality output current at low switching frequency can be obtained.

3. Simplicity of the hardware implementation can be achieved by using an integrated microcontroller system.

Since the publication of the initial paper [1], the RPWM strategy has received wide spread attention from researchers and has been employed successfully in numerous applications [1, 2, 5, 6, 8], where the focus is mainly on the implementation issues. However, the analytical content of the existing RPWM literature is very limited. The authors of [20] have provided the initial efforts to generalize the spectral analysis of randomly modulated converters. In this thesis, we provide analytical expressions to theoretically confirm the inverter harmonic power spectra obtained from the experimental results of A.M. Trzynadlowski and S. Legowski [2, 3, 6].

## 1.3 Outline of Thesis

In Chapter 2, the operating principle of the voltage-fed three-phase power inverter based on the deterministic PWM is reviewed. In Chapter 3, we present the circuit description of the RPWM technique, and introduce three kinds of inverter control functions for explaining the principle of the RPWM. We also discuss the randomized pulse position (RPP) technique. In Chapter 4 we analyze the RPPM technique with the so-called lead-lag and uniform PWM modes. We also give closed-form expressions that describe the output spectra (both discrete and continuous) of the power inverter. MATLAB plots are provided to verify the experimental results based on [2, 3, 6]. We also outline the optimization procedures for spectral design as future work. In Chapter 5 we conclude with a brief summary of the results and suggestions for future work.

# Chapter 2

# Power Inverter Fundamentals

## 2.1 Introduction

Switching techniques can be used for the conversion of DC power to AC power. If switches $S1$ and $S2$ in the single-phase inverter circuit shown in figure 2.1 are alternately opened and closed in antiphase, then a square-wave alternating voltage is developed across the load with a frequency determined by the switching rate. Obviously, the DC supply will be short circuited when both switches are turned on simultaneously. It is also uneconomical to employ mechanical switches in these circuits, because semiconductor switches have turn-on and turn-off times of the order of microseconds, or less, permitting high-frequency operations and giving very fast transient response. Fast switching speeds are important in DC to AC applications for high quality of output current.

The importance of the described technique is that the fundamental output voltage can be varied and low-order harmonic content can be eliminated by switching in a specific manner. Thus, voltage control can be achieved while operating with a constant supply voltage. This general method of voltage control is termed Pulse-

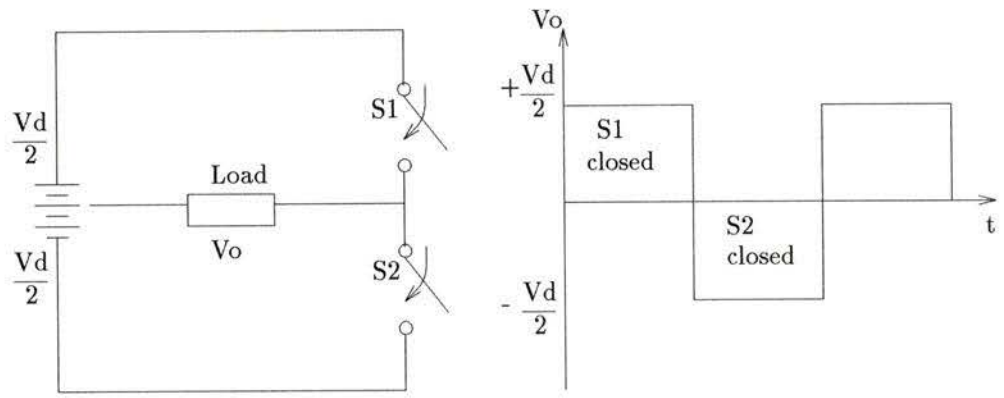


Figure 2.1: Single phase inverter circuit.

Width Modulation (PWM). In the following sections, the basic operating principles of the deterministic PWM inverter are reviewed. This serves as a background for its more advanced non-deterministic counterpart, known as Random Pulse-Width Modulation (RPWM). The detailed treatment of the deterministic PWM methods can be found in most standard power electronic texts [24, 25, 26, 27].

## 2.2 Three-Phase Voltage Source Inverter

The power circuit of a three-phase voltage-fed inverter is shown in figure 2.2. The inverter circuit consists of six self-commutated semiconductor switches $S_1$ to $S_6$ with the antiparalled fast recovery diodes $D_1$ to $D_6$. When the inverter feeds an inductive load such as an AC motor (with lagging power factor) , these diodes (also called free-wheeling diodes) are necessary to allow load current to circulate during the off-period of the transistors. It can be shown that triplen harmonics are absent from both the line-to-line and line-to-neutral voltage waveforms [24, 25, 27].

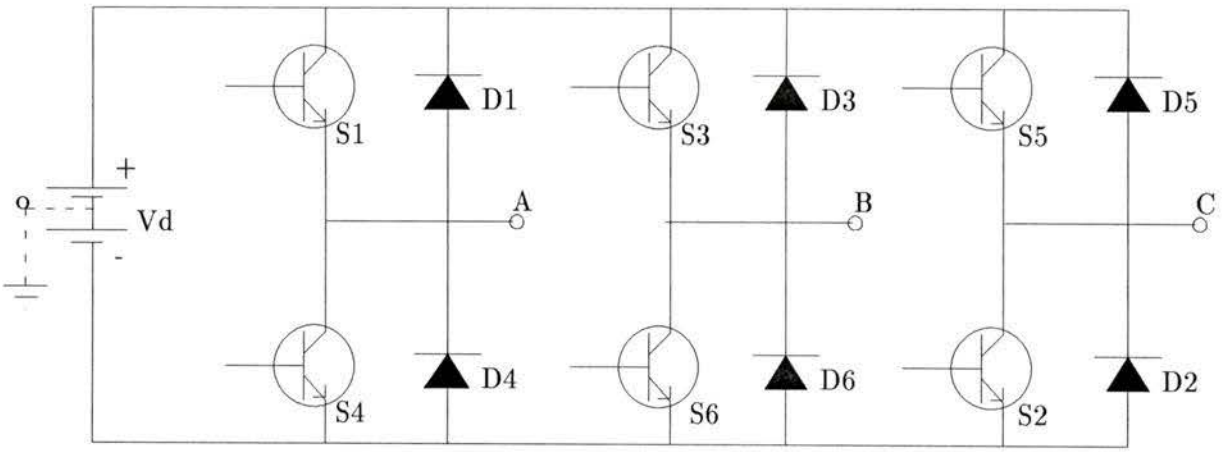


Figure 2.2: Three phase voltage source inverter.

## 2.3 Review of PWM Techniques

### 2.3.1 PWM with Natural Sampling

This section describes the most common and simplest control method, PWM with natural sampling (or sinusoidal PWM). The principle of PWM with natural sampling is shown in figure 2.3.

Three-phase reference voltages (or modulating functions) $V_a$, $V_b$ and $V_c$ of a variable amplitude $A$ are compared with a common triangular carrier $V_T$ of fixed amplitude $A_m$ using three separate comparators (see figure 2.3(a)). The outputs of comparators $a$, $b$, and $c$ form the control signals for the three legs of the inverter formed by switch pairs $(S_1, S_4)$, $(S_3, S_6)$, and $(S_5, S_2)$ respectively (see figure 2.2 and 2.3). Figure 2.3(b) shows the operation of the pair $(S_1, S_4)$ which controls the voltage of the motor phase $A$ with respect to the imaginary middle point of the

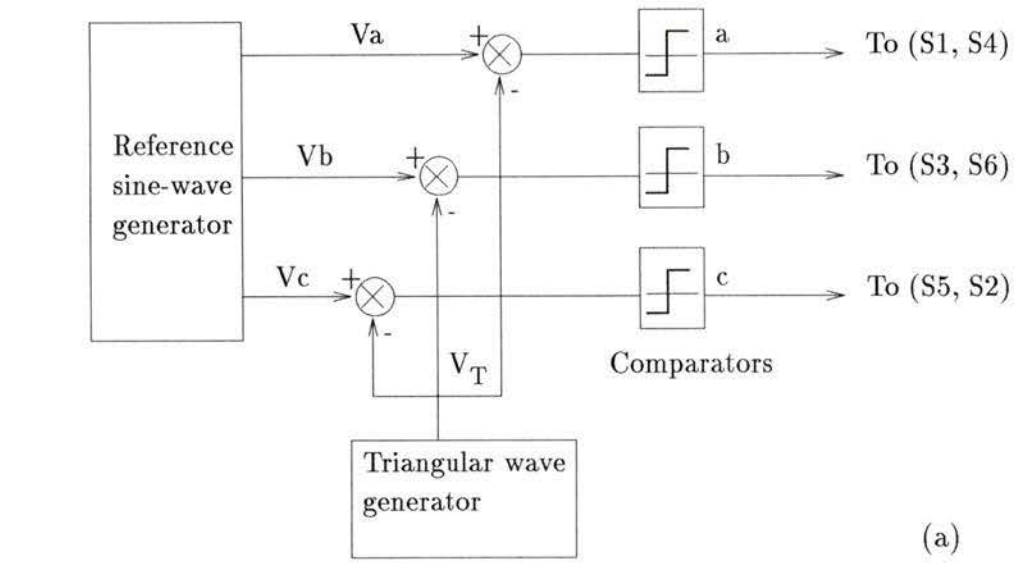


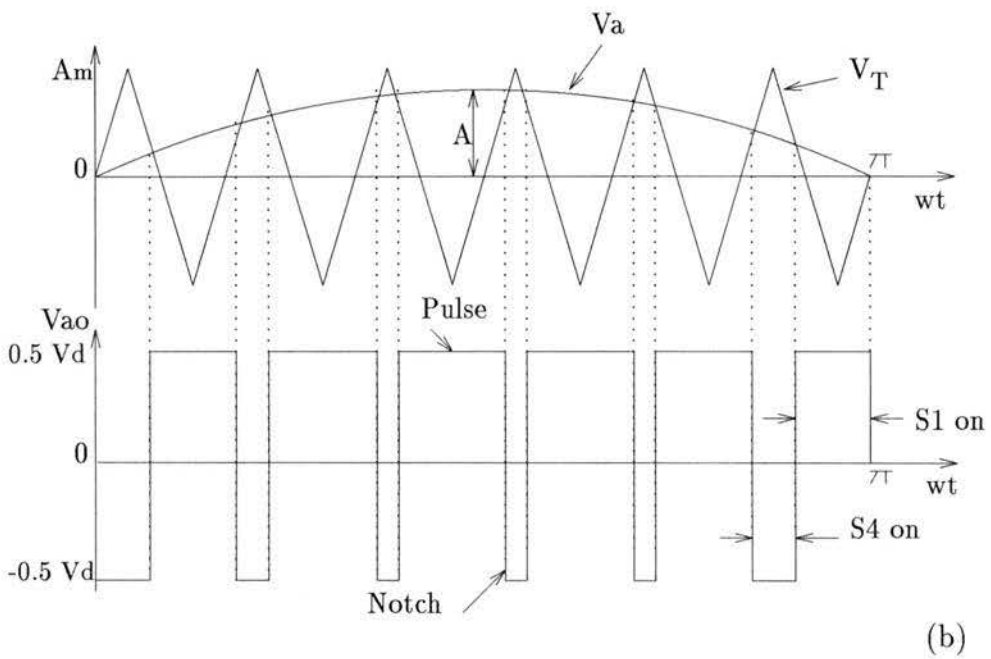


Figure 2.3: Principle of sinusoidal pulse-width modulation.

DC source. The positive half-cycle of the phase $A$ reference voltage $V_a$ and the carrier wave $V_T$ are drawn on the common time axis. The switches turn on and off according to the following rule:

$$S_1 = ON \quad and \; S_4 = OFF \quad if \; V_a > V_T \tag{2.1}$$
$$S_1 = OFF \; and \; S_4 = ON \quad if \; V_T > V_a$$

The resultant waveform of $V_{ao}$ is shown in the figure. Similar operations apply to switch pairs $(S_3, S_6)$ and $(S_5, S_2)$. The line-to-line voltage $V_{ab}$ is obtained by subtracting $V_{bo}$ from $V_{ao}$. The line-to-line voltages for $V_{bc}$ and $V_{ca}$ are obtained similarly. Figure 2.4 shows the line-to-line voltage $V_{ab}$ obtained from the individual phase voltage $V_{ao}$ and $V_{bo}$.

The frequency of the fundamental component of the motor terminal voltage is the same as that of the reference sinusoidal voltages. Hence, the frequency of the motor voltage can be changed by changing the frequency of the reference sinusoidal voltages. The modulation index, $m$ , is defined as the ratio of the reference wave amplitude $A$ to the triangular carrier wave amplitude $A_m$. The waveform $V_{ao}$ shown in figure 2.3(b) indicates that the value of $m$ determines the notch width in the modulated phase voltage waveform and therefore controls the fundamental output voltage of the inverter. Normally, the triangular carrier amplitude is fixed, and the reference wave amplitude controls the modulation index, $m$, and the output voltage. When $m$ is zero, the phase voltage of figure 2.3(b) is a symmetric unmodulated square wave. For small values of $m$, the line voltage pulses are very narrow but, as $m$ increases, the pulse width increases proportionately, thereby increasing the volt-seconds area per half-cycle and thus the fundamental voltage amplitude. Thus,

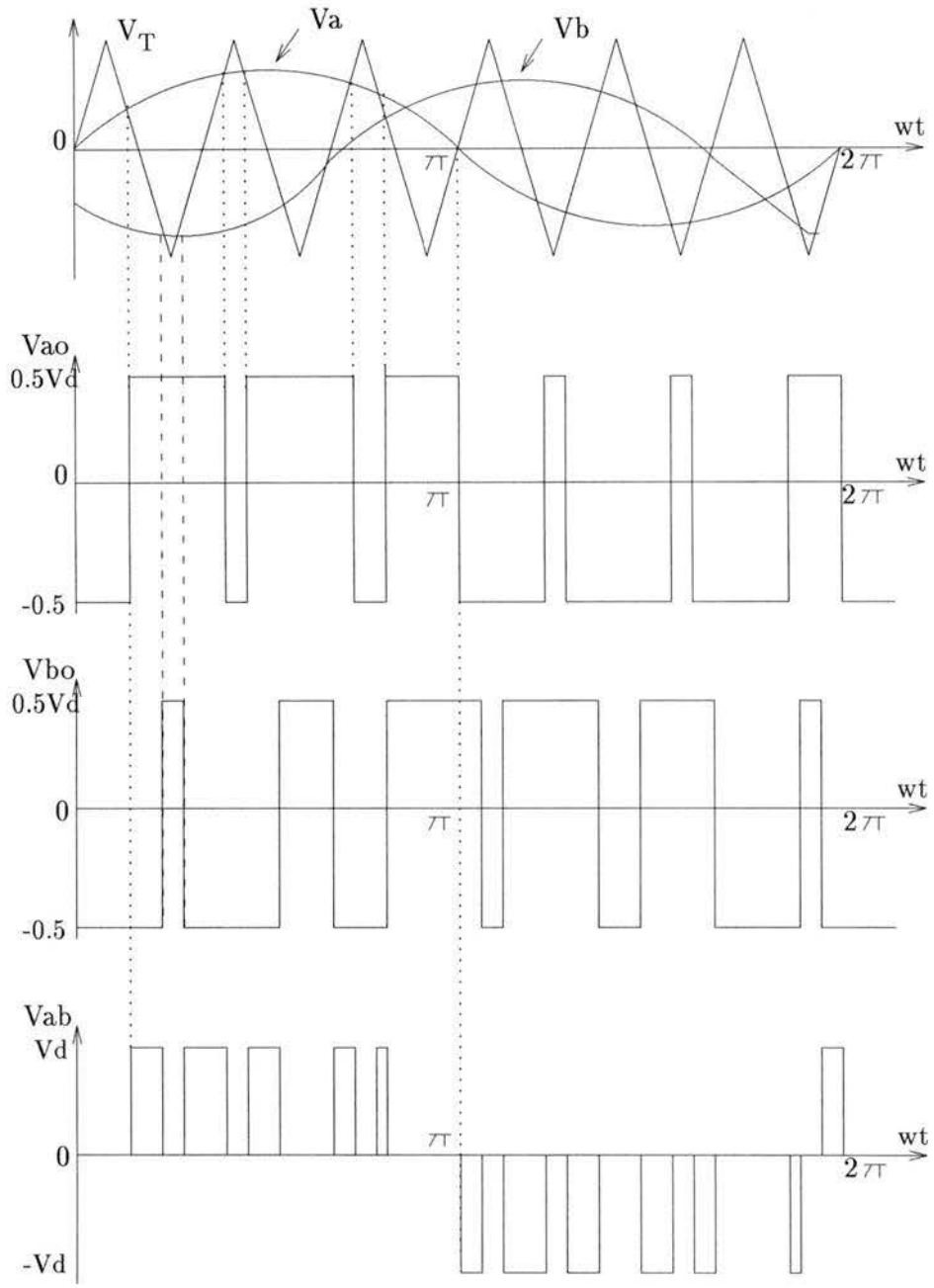


Figure 2.4: Sinusoidal PWM (line and phase voltage relation).

the fundamental voltage increases linearly with $m$ until $m = 1$ (that is, when the amplitude of the reference wave becomes equal to that of the carrier wave). As $m$ increases above unity, the number of pulses in $V_{ao}$ becomes less and the modulation ceases to be sinusoidal PWM. This condition is termed over-modulation. Some of the intersections between the modulating and carrier waves are lost. As a result, pulses are dropped in the output phase voltage waveform. For large values of $m$, the only intersections are those at the zero crossings of the sine wave. The phase voltage waveform becomes an unmodulated square wave. Because of over-modulation, the sinusoidal modulation strategy is lost and the low-order harmonics reappear in the output voltage waveform, causing a considerable increase in machine losses.

### 2.3.2 Harmonic Analysis

Fourier analysis shows that the output waveform from PWM with natural sampling contains carrier frequency-related harmonics with modulating frequency-related sidebands in the form of $f_{side} = Mf_c \pm Nf_r$, where $f_c$ is the carrier frequency, $f_r$ the modulating (or reference) frequency, $M$ and $N$ are integers, and $M + N$ is an odd integer. The occurance of sidebands is analogous to the sidebands introduced in the modulation techniques used in communications theory.

For even values of $M$, there is an odd sideband spectrum because the harmonics are nonexistent when $M$ and $N$ are both even. Thus, for $M = 2$, there are harmonics of order $2f_c \pm f_r$, $2f_c \pm 3f_r$, $2f_c \pm 5f_r$, ... in the phase voltage waveform, but harmonic amplitude diminishes rapidly with increasing values of $M$ and $N$. It is also found that odd values of $M$ gives an even sideband spectrum, because $M+N$ must be odd. Thus, for $M = 1$, there are harmonics of order $f_c \pm 2f_r$, $f_c \pm 4f_r$, $f_c \pm 6f_r$, ...

and so on. When the carrier frequency ratio, $p = \frac{f_c}{f_r}$ is large, the frequencies of major harmonics are large compared to the fundamental. The nominal leakage inductance of the machine is able to filter out the harmonics and the current approaches an ideal sinusoidal waveform. Furthermore, in a three-phase system, the carrier ratio $p$ is selected to be a multiple of three to give a balanced three-phase output. The phase voltage waveform has a particularly large harmonic at the carrier frequency. Since $p$ is a multiple of three, this carrier harmonic is a triplen harmonic and does not appear across the three-phase system [24].

### 2.3.3 PWM with Uniform Sampling

In PWM with natural sampling, the triangular carrier is compared directly with the modulating wave (reference voltage) to determine the switching instants. The second method, called uniform sampling, is based on the sample-and-hold principle, wherein the sampling frequency is equal to the carrier frequency (see figure 2.5). The figure shows the generation of the phase $A$ voltage $V_{ao}$. The reference wave $V_a$ is sampled by a sample-and-hold circuit at a regular interval $T_c$, the period of the common triangular carrier. This results in the modulating waveform $V_R$ shown in figure 2.5.

The waveform $V_R$ is compared with the triangular carrier (figure 2.5 (b)). The inverter switch $S_1$ is turned on when $V_R > V_T$ and $S_4$ is turned on when $V_R < V_T$. This results in the modulated waveform $V_{ao}$ shown in figure 2.5 (c). The fundamental component of $V_{ao}$ is also shown. It has the same frequency as that of the reference wave $V_a$ and its amplitude is proportional to the amplitude of the reference wave.

As a result, the frequency and magnitude of the motor voltage can be controlled

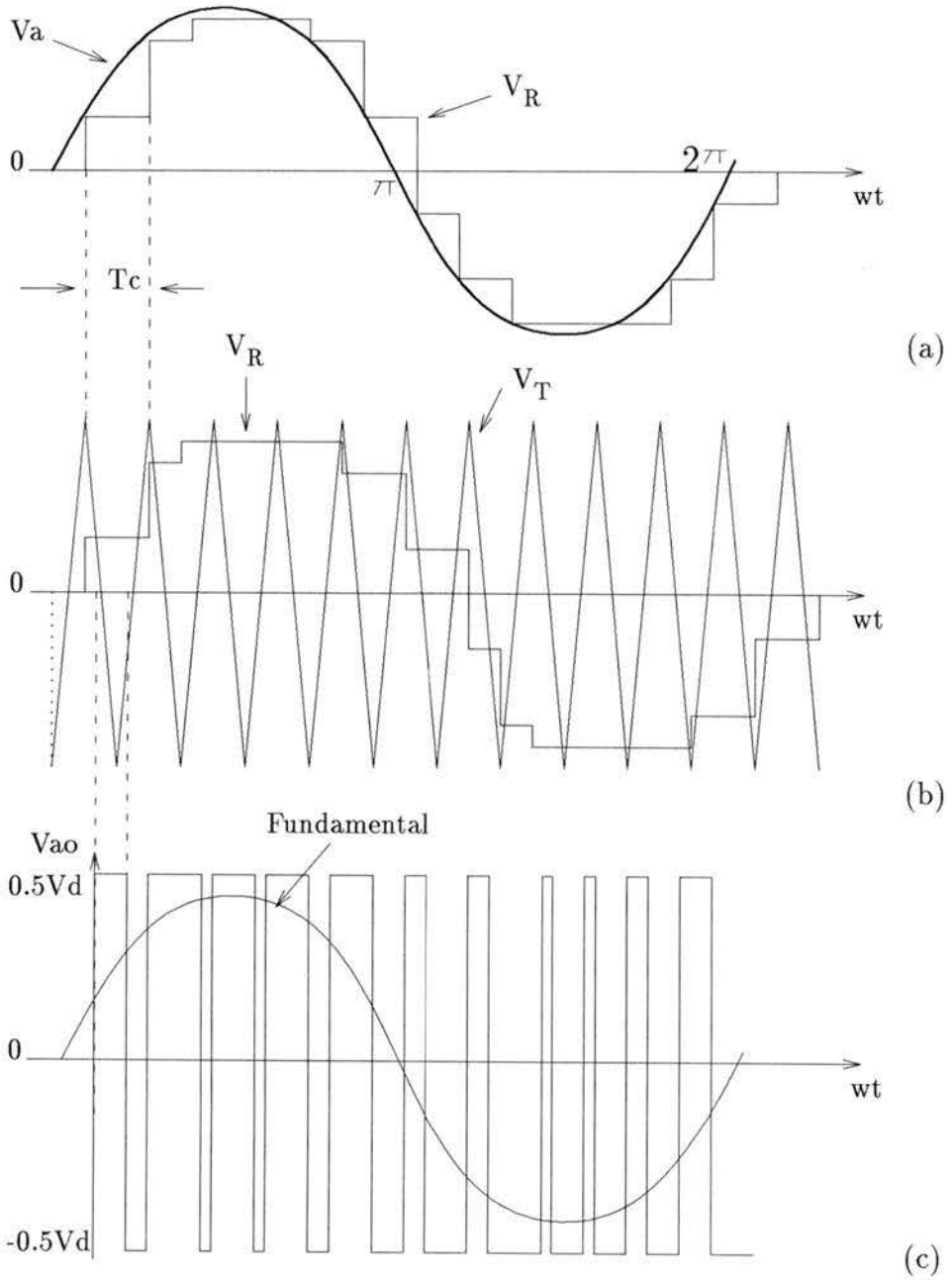


Figure 2.5: Pulse width modulation with uniform sampling.

by controlling the reference wave.

### 2.3.4 Harmonic Elimination

In controlling the fundamental output voltage of the inverter for AC motor control, the PWM strategy introduces additional harmonic components which are detrimental to motor performance and efficiency. The proposed methods from [10, 11] allow the specific low-order harmonics to be eliminated and they can be effectively implemented with microprocessor-based control techniques.

In these methods, the undesirable harmonics can be eliminated and the fundamental voltage component can be controlled. The waveform shown in figure 2.6 can be represented by the general Fourier series:

$$f(\omega t) = \sum_{k=1}^{\infty} [a_k \sin(k\omega t) + b_k \cos(k\omega t)] \tag{2.2}$$

where

$$a_k = \frac{1}{\pi} \int_0^{2\pi} f(\omega t) \sin(k\omega t) d(\omega t) \tag{2.3}$$

$$b_k = \frac{1}{\pi} \int_0^{2\pi} f(\omega t) \cos(k\omega t) d(\omega t) \tag{2.4}$$

Fourier analysis shows that the amplitudes of the harmonic voltages may be expressed in terms of the switching (or commutation) angles $\alpha_1, \alpha_2, \ldots, \alpha_n$. It can be shown that if $M$ is the number of harmonics to be eliminated, then $n$ is chosen to satisfy $M = n - 1$. The magnitude of the fundamental as well as the magnitude of the harmonics can be controlled [10, 11]. In general, the more switching angle $\alpha_i$ are used, the better the solutions to the specific optimization problems can be obtained.

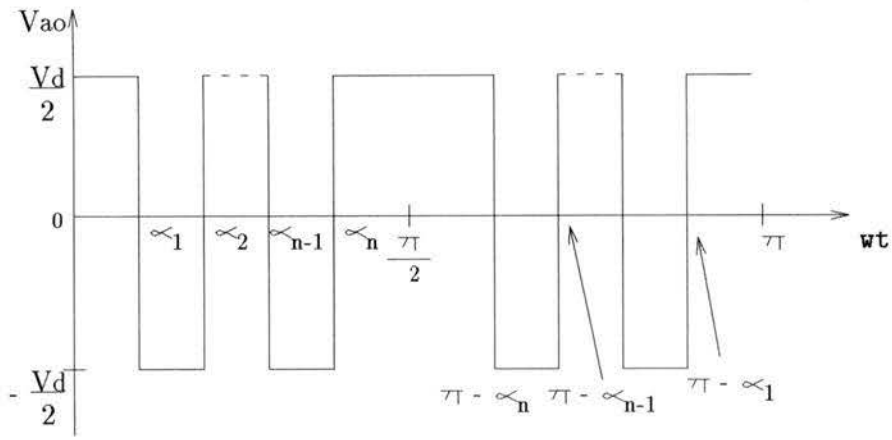


Figure 2.6: Selective harmonic elimination.

From the above Fourier series expressions, we can see that only odd harmonics may exist when quarter-wave symmetry of the waveform is assumed. For the $k^{th}$ harmonic, we have

$$b_k = 0 \tag{2.5}$$

and

$$\begin{aligned} a_k &= \frac{4}{\pi}\int_0^{\pi/2} V_{ao}\sin(k\omega t)d(\omega t) \\ &= \frac{2V_d}{k\pi}[1+2(-\cos(k\alpha_1)+\cos(k\alpha_2)- \ \ldots+\cos(k\alpha_n))] \\ &= \frac{2V_d}{k\pi}[1+2\sum_{p=1}^{n}(-1)^p\cos(k\alpha_p)] \end{aligned} \tag{2.6}$$

Furthermore, the meaningful and realizable solutions are subject to the constraint condition

$$0 < \alpha_1 < \alpha_2 \ldots < \alpha_n < \pi/2 \tag{2.7}$$

A total of $n$ simultaneous equations are needed to solve for the values of unknowns $\alpha_1, \alpha_2, \ldots, \alpha_n$. These equations are obtained by assigning the required value to the fundamental and zero values to the $(n-1)$ harmonics to be eliminated. In a symmetrical three-phase system, the triplen harmonics are automatically suppressed in the load voltage waveform, and there are no even harmonics when the phase voltage has the symmetry property as shown in figure 2.6. Consequently, the four lowest order harmonics of significance are the $5^{th}$, $7^{th}$, $11^{th}$, and $13^{th}$, and these can cause torque pulsations and speed fluctuations in AC motor drives at low rotational speeds. Elimination of these four harmonics produces a waveform in which there is no harmonic of order lower than the $17^{th}$. Control of the fundamental voltage and the suppression of four harmonics requires 5 switchings per phase per quarter cycle, or 22 switchings per cycle, including the switchings at 0 and 180 degrees.

The procedures just described is explained by the following example. Since the number of harmonics to be eliminated is four (i.e. M = 4), hence, $n = 5$. From equation (2.6), we have

$$a_1 = \frac{2V_d}{\pi} \cdot [1 + 2 \cdot (-\cos\alpha_1 + \cos\alpha_2 - \cos\alpha_3 + \cos\alpha_4 - \cos\alpha_5)] \quad (2.8)$$

$$a_5 = \frac{2V_d}{5\pi} \cdot [1 + 2 \cdot (-\cos 5\alpha_1 + \cos 5\alpha_2 - \cos 5\alpha_3 + \cos 5\alpha_4 - \cos 5\alpha_5)] = 0 \quad (2.9)$$

$$a_7 = \frac{2V_d}{7\pi} \cdot [1 + 2 \cdot (-\cos 7\alpha_1 + \cos 7\alpha_2 - \cos 7\alpha_3 + \cos 7\alpha_4 - \cos 7\alpha_5)] = 0 \quad (2.10)$$

$$a_{11} = \frac{2V_d}{11\pi} \cdot [1 + 2 \cdot (-\cos 11\alpha_1 + \cos 11\alpha_2 - \cos 11\alpha_3 + \cos 11\alpha_4 - \cos 11\alpha_5)] = 0 \quad (2.11)$$

$$a_{13} = \frac{2V_d}{13\pi} \cdot [1 + 2 \cdot (-\cos 13\alpha_1 + \cos 13\alpha_2 - \cos 13\alpha_3 + \cos 13\alpha_4 - \cos 13\alpha_5)] = 0 \quad (2.12)$$

The nonlinear algebraic equations (2.8) through (2.12) can be solved numerically for a specificed value of the fundamental amplitude $a_1$ and subjected to the constraints of equation 2.7. By solving these equations for different fundamental amplitudes, the variations of $\alpha_1, \alpha_2, \ldots, \alpha_5$ with the fundamental can be obtained. A look-up table of these angles can then be generated for a microprocessor-based implementation. The numerical method used to solve the set of non-linear equations is presented in [10, 11].

It has been assumed that eliminating low-order harmonics completely would automatically lead to optimal motor behaviour. However, it is worth mentioning that the elimination of low-order harmonics is obtained at the expense of an increase in the next significant low-order and high-order harmonics. Therefore, in order to achieve optimal motor behaviour, it is important to consider not only the low-order harmonic elimination, but also for the minimization of the overall harmonic losses for the specific application at hand.

## 2.4 Summary

Inverters provide three-phase AC voltages from a fixed DC voltage. For adjusting the fundamental output voltage, pulse-width modulation (PWM) method is used. In case of the sinusoidal PWM, the fundamental voltage increases linearly with modulation index $m$, which is defined as ratio of the reference wave amplitude to

the triangular carrier wave amplitude.

Two types of PWM methods are described, namely PWM with natural sampling and PWM with uniform sampling. The latter is suitable for microprocessor implementation.

Fourier analysis shows that the PWM output waveform contains carrier frequency-related harmonics with modulating frequency related sidebands. Due to waveform symmetries, only odd-order harmonics may exist. All triplen harmonics are also absent due to the cancellation effect in three-phase systems.

The Selective Harmonic Elimination (SHE) technique is one of the many optimization method available for inverter applications. The general solution for the SHE method leads to a set of nonlinear equations that can be solved numerically using the optimization procedures presented in [10, 11].

# Chapter 3

# Random Pulse Width Modulation Technique

## 3.1 Introduction

In this Chapter we describe the operating principle and hardware implementation of the Random Pulse Width Modulation (RPWM) strategy. In Section 3.2 we describe the prototype of a so called "hypersonic" three-phase medium power, voltage controlled inverter [3]. In Section 3.3 we describe the inverter control functions. They are the parameters used in describing the operation of the RPWM technique. In Section 3.4 we present the operating principles of the RPWM technique. The control of the hypersonic inverter is realized by mean of the RPWM technique. This novel method was initially introduced in [1]. The Random Pulse Position Modulation (RPPM), based on RPWM principle, is described in Section 3.5. The practical implementation of the RPPM strategy is described in [6] under the name of Grey-Noise PWM (GNPWM). In this implementation, the position of the pulse is assumed to have randomized position, which is either leading or lagging in its switching interval. The pulse width in each switching interval is determined by the

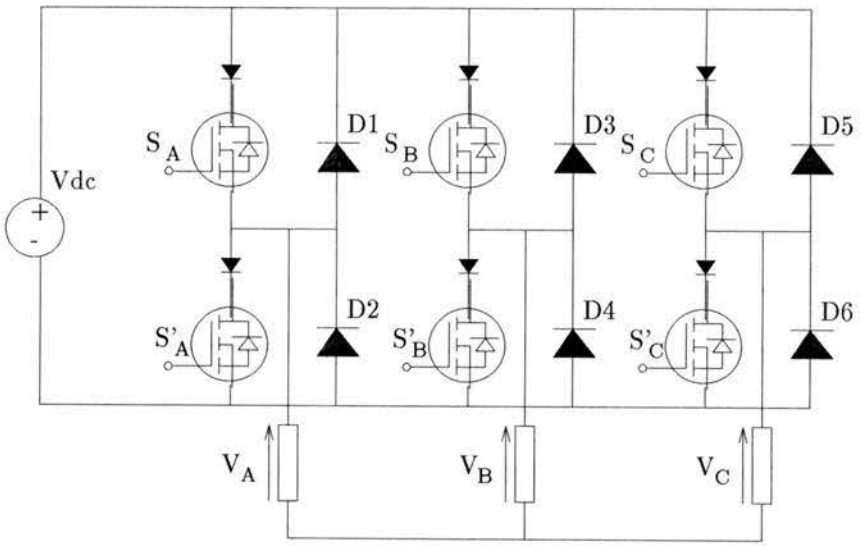


Figure 3.1: Power circuit of the inverter [1].

value of the switching variable. In Section 3.6 we point out the distinct advantages of the RPWM technique over the conventional PWM method. Finally, this Chapter is concluded with a brief summary.

## 3.2 Circuit Description

We have shown a general PWM circuit configuration in figure 1.1, Chapter 2, where the conventional PWM technique is reviewed. The circuit for the Random Pulse-Width Modulation (RPWM) technique is similar; it consists of three parts : the power circuit, the drivers, and the microprocessor-based controller of the inverter. The circuit described in this Chapter is capable of operating within 62.5 - 125 kHz average switching frequency range and has power rating of 25 kVA, 230V. This device

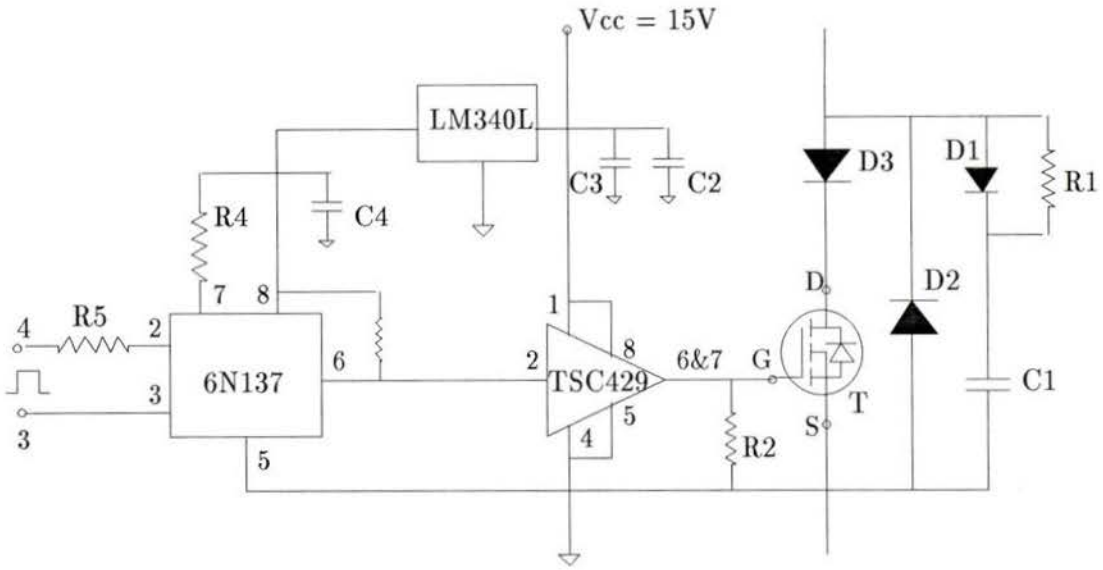


Figure 3.2: Driver for a single switch of the inverter.

is built based upon the APT5025BN 500V, 25A power MOSFETs from Advanced Power Technology. It has turn-on and turn-off delay times not exceeding 20 nsec and 70 nsec respectively [3].

Power circuit of the three-phase inverter is shown in figure 3.1. It consists of six power MOSFETs $S_A$ to $S'_C$ with the anti-parallel fast-recovery feedback diodes, $D_1$ to $D_6$. Their roles are to allow reverse current flow during reactive power flow and regeneration, and also to clamp the load voltage to the input level. The additional series connecting blocking diodes are used to block the flyback path through the slow-recovery internal diode of the MOSFET [3].

A high-speed CMOS power MOSFET driver TSC429, developed by the Teledyne Semiconductor [9], is used to drive a single switch of the inverter (see figure 3.2). Floating 15V supply is used for the driver, and through an LM340L

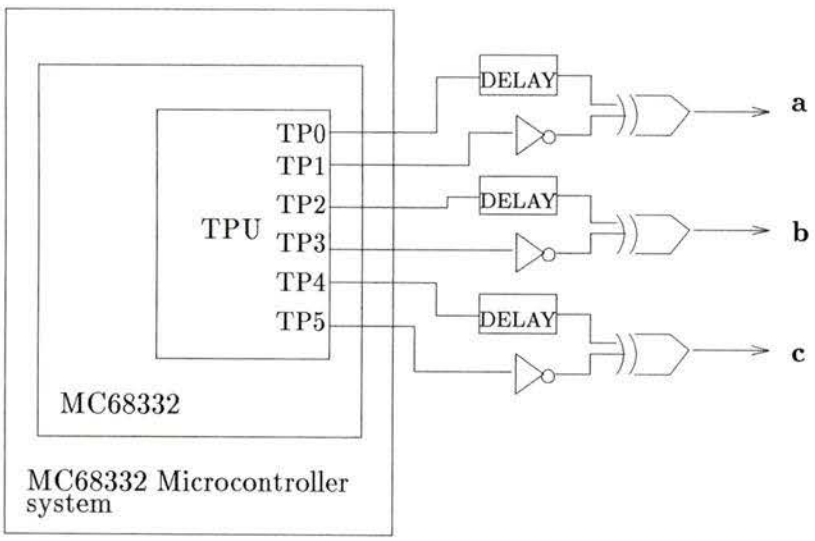


Figure 3.3: Block diagram of MC68332 microcontroller system interface.

voltage regulator for the optocoupler (6N137), which acts as an interface between the microprocessor-based control system of the inverter and driver. Fast-recovery rectifiers D2 and D3 act as the flyback and blocking diodes, respectively.

Diode D1, resistor R1 and capacitor C1 shown in figure 3.2 constitute a snubber circuit, which protects the device from supply- and load- side voltage transients, and reduces the device's switching loss [25].

A simple logic network of a controller based on the MC68332 integrated microcontroller system by Motorola is shown in figure 3.3. It constitutes the interface between the system and the drivers of the power switches of the inverter. The MC68332 has a high-performance timer processor unit (TPU), which allows single-chip implementation of the RPWM strategy described in the following sections. The function of the TPU is to locate precisely the required switching instants [6].

## 3.3 Inverter Control Functions

Three kinds of inverter control functions are described in this section. They are essential for the understanding of the RPWM operating principle.

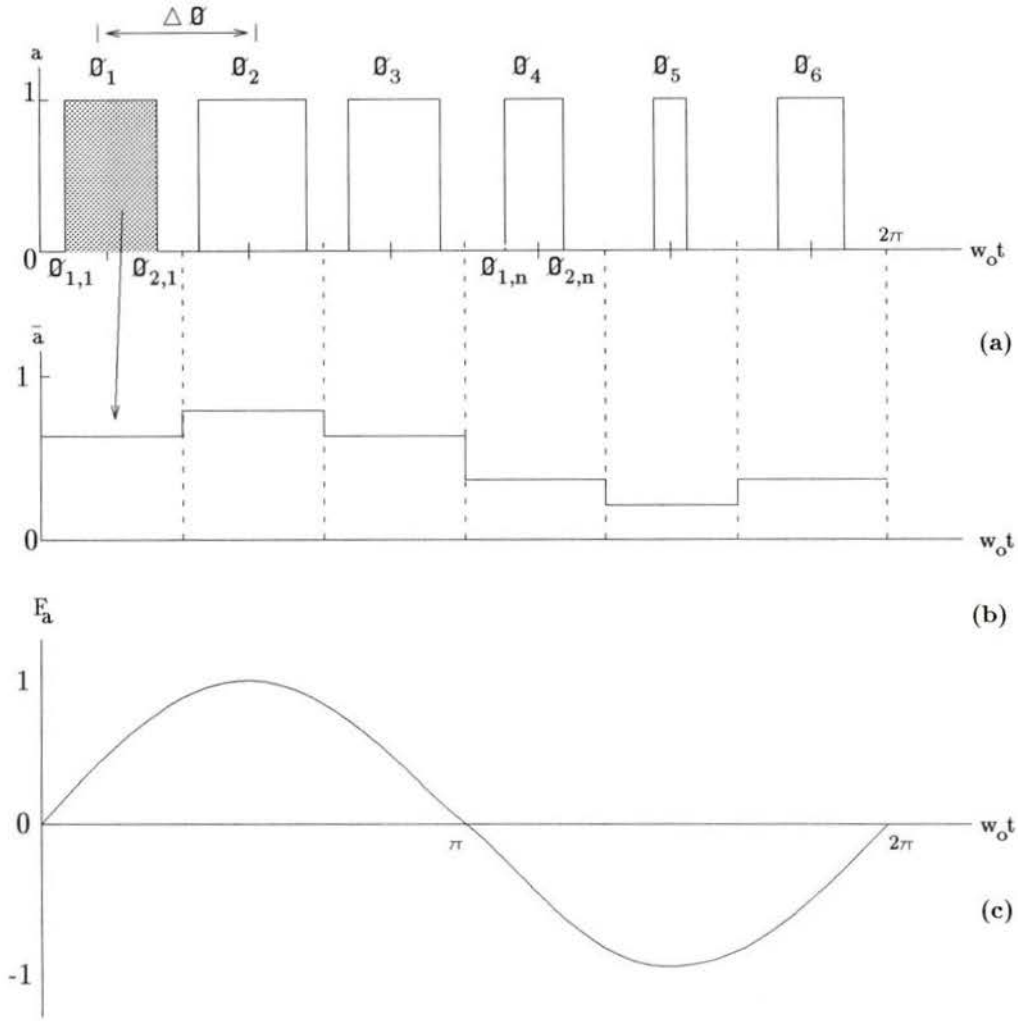


Figure 3.4: Illustration of the inverter control functions.

### 3.3.1 Switching Functions

A switching function is a binary function assigned to each phase of the power circuit of the inverter. For phase $A$ of the inverter, a binary switching function $a(\omega_o t)$, where $\omega_o$ denotes the output radian frequency of the inverter, is defined as follows:

$$a(\omega_o t) = \begin{cases} 0 & \text{if } S_A \text{ is 'OFF' and } S'_A \text{ is 'ON'} \\ 1 & \text{if } S_A \text{ is 'ON' and } S'_A \text{ is 'OFF'} \end{cases}$$

A switching function of the inverter is shown in figure 3.4(a). The actual output line-to-line voltage of the inverter equals

$$V_{XY} = V_{dc}(x - y). \tag{3.1}$$

where $X, Y$ and $x, y$ denote any two phases and the corresponding switching variables respectively. $V_{dc}$ is the DC supply voltage of the inverter.

### 3.3.2 Average Switching Functions

Let the output frequency period (or $2\pi$ radians period) be divided into $N$ equal modulation intervals $\Delta\phi$. A discrete average switching function $\bar{a}(\phi_n)$ is defined as the average value of the switching function $a(\omega_o t)$ within the n-th modulation interval, centered about the angle $\phi_n = 2\pi(n-1/2)/N,\ n = 1, 2, \ldots, N$. As shown in figure 3.4(a), $\phi_{1,n}$ and $\phi_{2,n}$ stand for the switch-on and switch-off angles, respectively. The discrete average switching function $\bar{a}(\phi_n)$ can be defined as

$$\bar{a}(\phi_n) = \frac{\phi_{2,n} - \phi_{1,n}}{\Delta\phi}, \quad n = 1, 2, \ldots, N. \tag{3.2}$$

The fundamental of the output line-to-line or line-to-neutral voltage of the inverter form the balanced three-phase sets if the following condition is satisfied :

$$\bar{a}(\omega_o t) = \bar{b}(\omega_o t + 2\pi/3) = \bar{c}(\omega_o t + 4\pi/3) \tag{3.3}$$

Elimination of low-order harmonics can be achieved by increasing the number of modulation intervals N. The selection of $N$ depends on the balance between the inverter switching loss, which increases with increasing $N$, and machine harmonic loss, which decreases with increasing $N$. Therefore, higher values of $N$ can be used when high speed switching devices are being employed.

### 3.3.3 Modulating Functions

Let $F_A(\omega_o t)$ be a periodic function having the period equal to that of the desired output voltage of the inverter, and the magnitude not greater than unity. It was shown in [4] that if

$$\bar{a}(\omega_o t) = [1 + mF_A(\phi_n)]/2 \tag{3.4}$$

where $m$ is a magnitude control ratio (modulation index), adjustable within the range 0 to 1, then the *rms* value of the fundamental output line-to-line voltage of the inverter equals $\sqrt{6}mF_1V_{DC}/4$, where $F_1$ is the fundamental of the modulating function and $V_{DC}$ is the DC supply voltage of the inverter. From equation 3.4, the average switching function is adjustable within the range 0 and 1. Figure 3.4(c) gives an example of a sinusoidal modulating function, $F_A(\omega_o t)$ =sin($\omega_o t$). In order to produce a balanced three-phase output of the inverter, the switching pattern generated must satisfy the conditions (3.3) and (3.4). Notice that the pulse width in figure 3.4(a) is a sinusoidal function of its angular position in cycle (figure 3.4(c)).

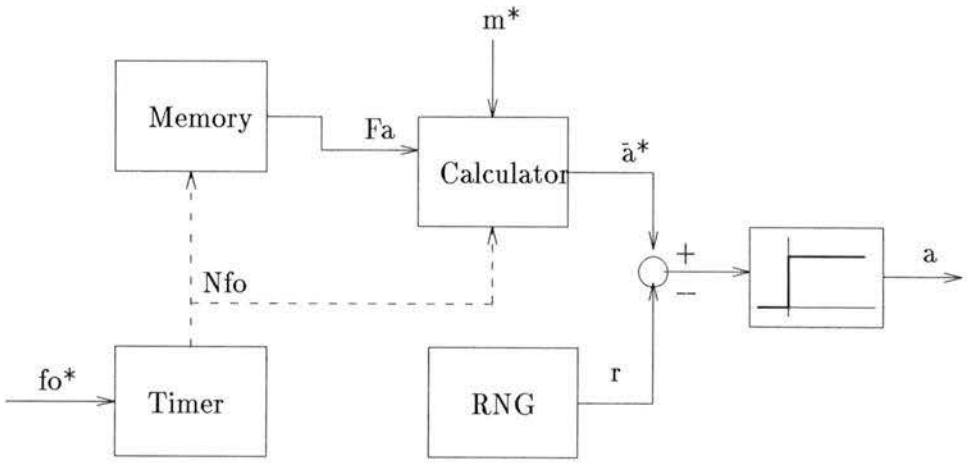


Figure 3.5: Random generation of an inverter switching function using RPWM.

## 3.4 Principle of RPWM

The principle of Random Pulse Width Modulation (RPWM) is described by the block diagram shown in figure 3.5 for phase A of the inverter. This block diagram represents the inverter control block (microprocessor-based controller) shown earlier in figure 1.1.

The desired output frequency $f_o^*$ of the inverter is applied to a timer from a microprocessor-based control system. This generates the timing signal $Nf_o$ for both the memory unit and the calculator, resulting in $N$ switching intervals per cycle of the output frequency. Consecutive values of the modulation function $F_A$, which is being stored in discrete form in memory, are released. Consequently, the reference duty ratio $\bar{a}^*$ corresponding to the desired magnitude control ratio (modulation index) $m^*$ can be computed in the calculator using the formula :

$$\bar{a}^* = [1 + m^* \, F_A]/2 \tag{3.5}$$

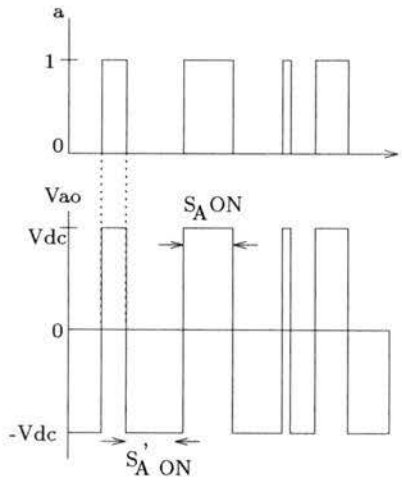


Figure 3.6: Switching function and its corresponding phase voltage waveform.

The reference duty ratio $\bar{a}^*$ is then compared with a signal $r$ generated by a random number generator (RNG). The random numbers $r$ take on values between 0 and 1 with a uniform probability distribution having unity area. The comparator generates the switching signal according to the following rule :

$$a = \begin{cases} 0 & \text{if } r > \bar{a}^* \\ 1 & \text{if } r \leq \bar{a}^* \end{cases}$$

At $a = 1$, the switch $S_A$ (common-anode) in branch A of the power circuit of the inverter (figure 3.1) is turned on and the switch $S'_A$ (common-cathode) is turned off. At $a = 0$, the reverse combination of states of the switch is realized. An example switching function and its corresponding phase voltage waveform $V_{ao}$ is shown in figure 3.6.

Because of the uniform probability density of the random variable $r$, the probability of the random number generated being less than the desired average reference

value $\bar{a}^*$, is just $\bar{a}^*$ (see figure 3.7). Hence, the average value of the switching function $a$, denoted as $\bar{a}$ (as shown in the shaded area in figure 3.8), within a given switching interval approaches the desired value $\bar{a}^*$. The higher the number of random number generated (*i.e.* $f_r >> Nf_o$) within a single modulation interval, the closer $\bar{a}$ and $\bar{a}^*$ become. For instance, if $\bar{a}^* = 0.7$, then 70% of the random numbers generated over the switching period are below $\bar{a}^*$ and 30% are above. In other words the power switches are turned on for 70% of the time during a given switching period and 30% of the time they are turned off. An illustration of the operation of a random pulse-width modulator is shown in figure 3.8.

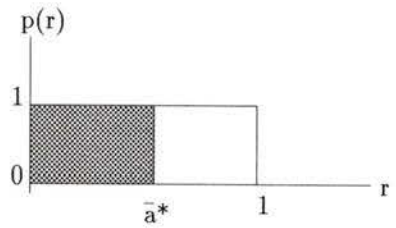


Figure 3.7: Uniform probability density function between 0 and 1.

### 3.4.1 Tracking of the Modulating Function

Another property of the RPWM technique is related to the modulation index $m^*$. In essense, the modulation index $m^*$ has the ability to track the outline of the modulating function.

We first use $m^* = 0$ as an example to illustrate the above concept (see figure 3.9(a)). From the equation $\bar{a}^* = [1 + m^* F_A]/2$, we have $\bar{a}^* = 0.5$, which is a constant in the figure, and the probability of the random number being greater and

less than 0.5 is equal. This probability value is just $\bar{a}^* = 0.5$. This means that the switching function $a$ at the output of the RPWM modulator will have, on average, an equal number of 1's and 0's as its value. In the actual voltage waveform, this results in the zero average value of the output voltage per given switching period. In other words this corresponds to no modulation and the fundamental of this output voltage is zero.

We now increase the modulation index to $m^* = 0.7$. Hence, we have $\bar{a}^* = [1 + 0.7\ F]/2$ as shown in figure 3.9(b). As stated earlier, it is necessary that the modulating function has values $|F(\omega_o t)| \leq 1$ for $\bar{a}^*$ to have values between 0 and 1. The curve $\bar{a}^*$ shown in the figure clearly outlines the shape of a sinusoidal modulating function. The figure also shows that there are more random numbers falling below than above the $\bar{a}^*$ curve. As a result, the switching function $a$ at the output of the RPWM modulator will have more 1's than 0's resulting in more pulses occuring over the switching period as compared to the case for $m^* = 0$. In the actual voltage waveform, this results in an increase of volt-seconds area per given switching period; hence, the fundamental voltage amplitude also increases proportionally. Consequently, as the modulation index $m^*$ increases from 0 to 1, the number of random numbers falling below the average switching function $\bar{a}^*$ also increases. This corresponds to an increase of the fundamental voltage amplitude.

The tracking of the modulating function using $m^*$ becomes inaccurate when the value of $m^*$ is close to zero. At low values of $m^*$, the desired switching variable $\bar{a}^*$ over the whole period appears almost as a flat line. In order to track the outline of the modulating function, extremely high switching frequencies are required (i.e. a great number of random number are required to be generated within each switching interval). In the extreme case, when $m^* = 0$, and $\bar{a}^* = 0.5$, this corresponds to no

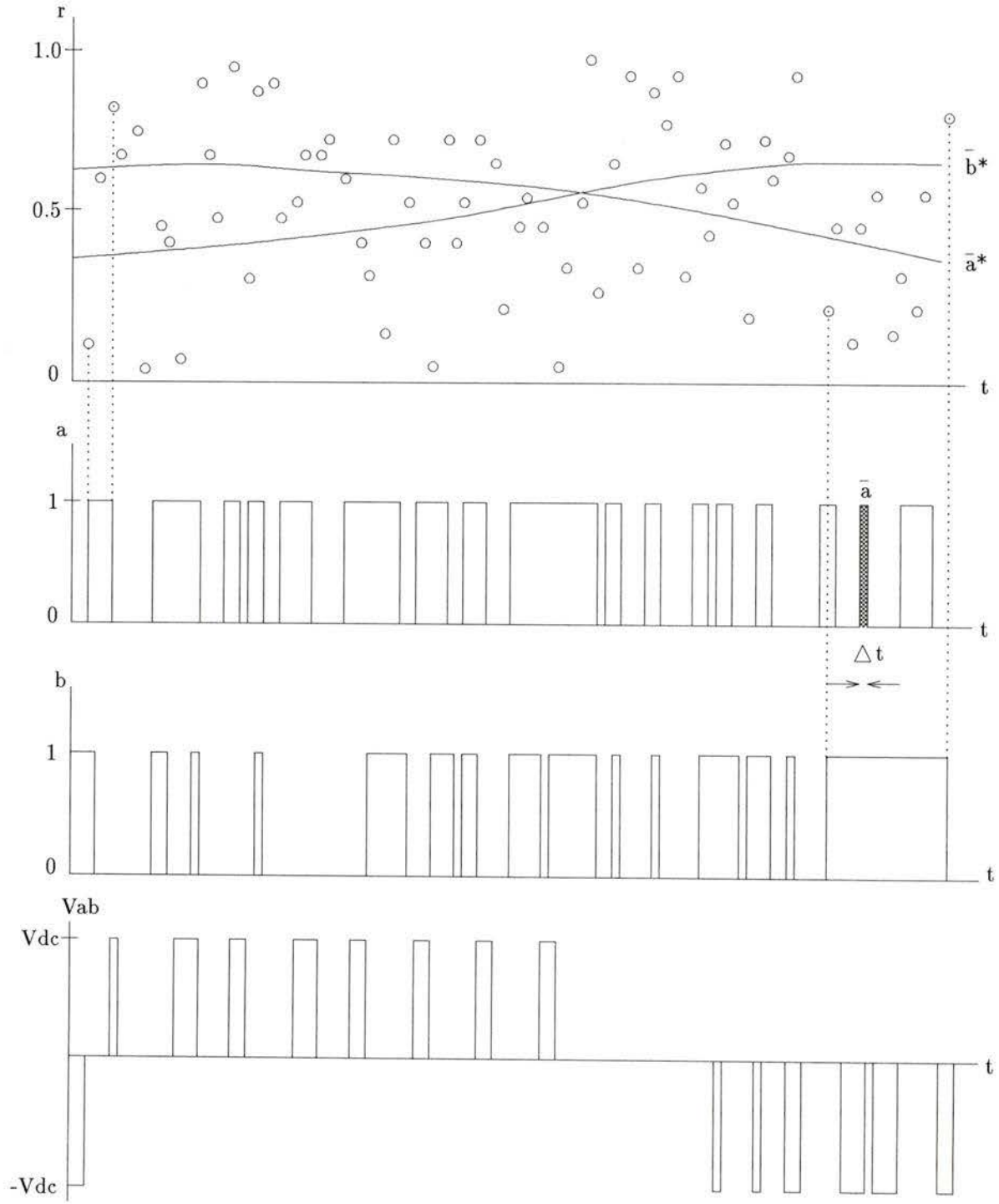


Figure 3.8: Operation of a random pulse-width modulator.

modulation and $\bar{a}^*$ becomes a horizontal line as discussed above. This is the major drawback of this randomized technique. In order to become effective, the value of the modulation index $m^*$ is usually chosen to be close to unity.

## 3.5 Randomized Pulse Position PWM Strategy

### 3.5.1 Introduction

In the RPWM technique discussed so far, the switching pattern (or pulse) occurred at the center within each modulation interval and the pulse width is determined by the product of the required duty ratio and duration of the modulation interval.

The implementation of the random pulse position (RPP) strategy is described in [6] under the name of Grey-Noise PWM (GNPWM). The term "grey noise" is used for this technique is because the resulting higher order harmonics are distributed thinly, but not perfectly uniformly (i.e. white noise), over a wider frequency range. In this strategy, the cycle of the output frequency $f$ of the inverter is divided into $N$ equal switching intervals of width $\Delta t$. As illustrated in figure 3.10, pulses of the switching variables $a$, $b$, and $c$ are either starting at the beginning of the switching interval, which we called lead-mode (trailing-edge modulated) or starting at the end of the interval, which we called lag-mode (leading-edge modulated). The modulation modes are selected at random prior to each switching interval. The pulse width within each interval is determined by the duty ratio of the switching variable.

It is important to mention that the randomization modes are fixed for all three phases. However, the duty ratios of the switching variables $b$ and $c$ are phase shifted by $-120^o$ and $-240^o$, respectively. Corresponding averaged duty ratios $\bar{a}$, $\bar{b}$, and

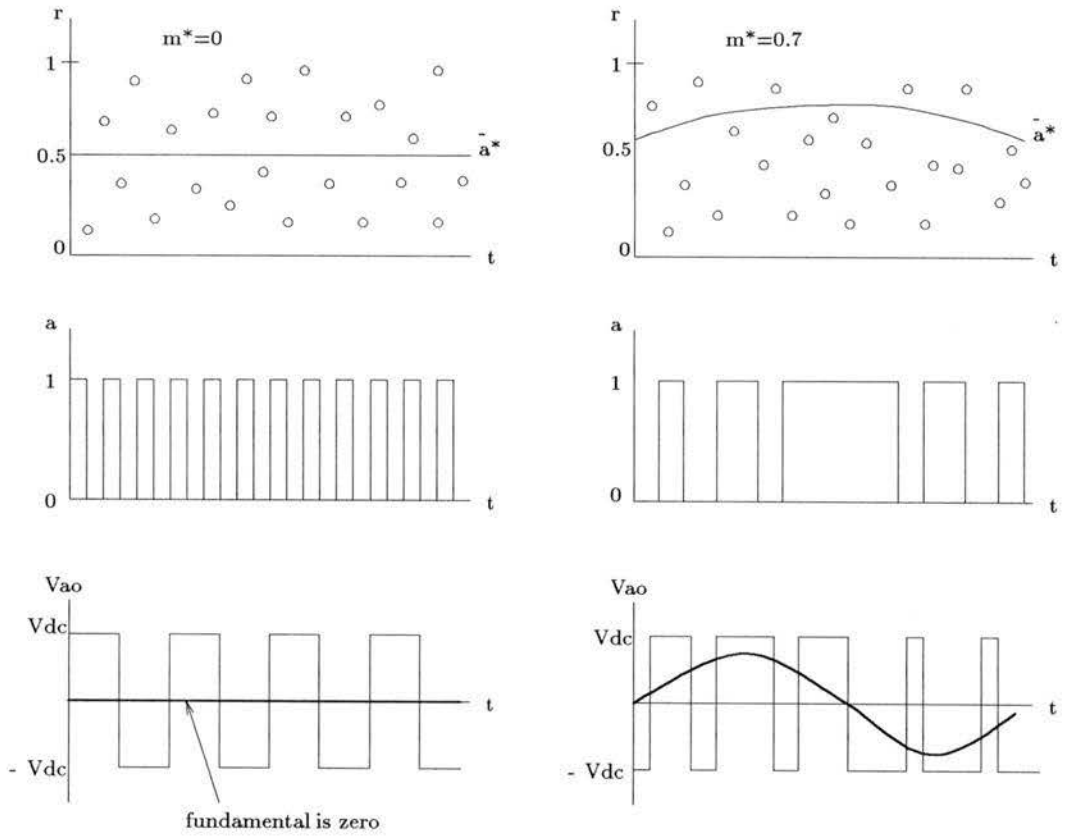


(a) (b)

Figure 3.9: Tracking of the modulation function.

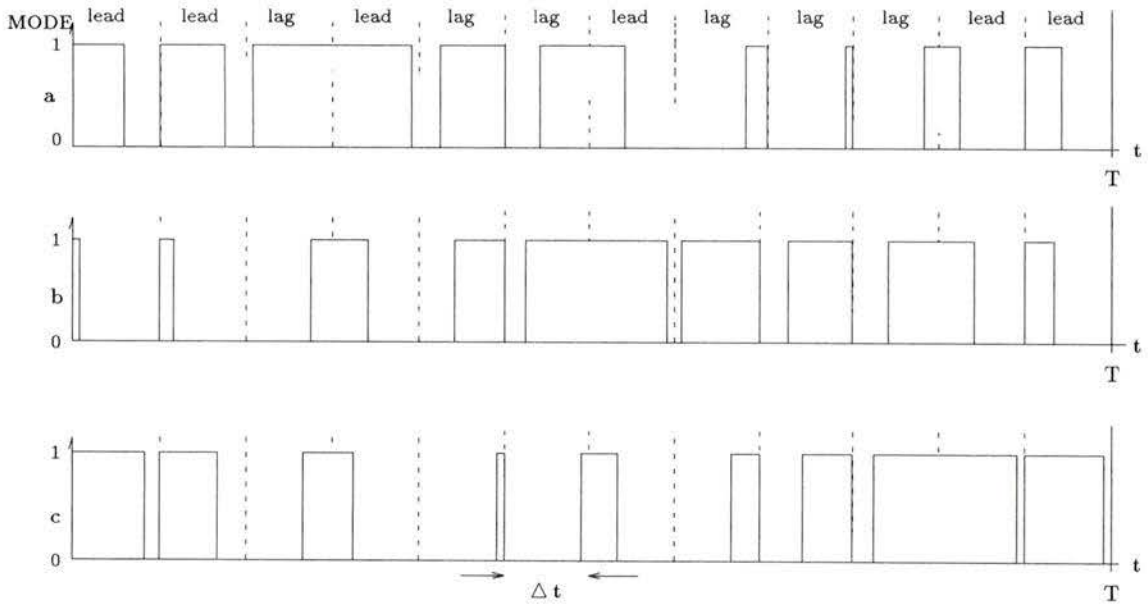


Figure 3.10: Lead-lag mode randomization of switching variables.

$\bar{c}$ are shown in figure 3.11 (also see Fig. 4.1 for pule width determined by the average switching variable). When such duty ratios are realized, the fundamental line-to-line output voltage of the inverter will be proportional to the fundamental of the function $a(\omega_o t)$. In fact there are two possible versions (symmetrical and asymetrical modulation, (3.4) is the former) of the $\bar{a}$ and $F$ relation (see Section 4.2.3 for details).

### 3.5.2 Principle of GNPWM

Let the variable $r$ be defined as the pulse position within each modulation interval. The ON-OFF switching pattern (lead-mode) corresponds to $r = 1$, while $r = 0$ corresponds to the OFF-ON sequence (lag-mode). If the values of $r$ for consecutive

modulation intervals are generated by a single-bit random generator with uniform probability density, switching patterns for individual cycles of the output frequency will be different. Hence, harmonic spectra of the output voltage vary from cycle to cycle. In fact, there are a total of $2^N$ different switching patterns per cycle of the output frequency. In addition, the single-bit random generator to enforce the mode randomization is readily available (e.g. National Semiconductor's MM5437 chip).

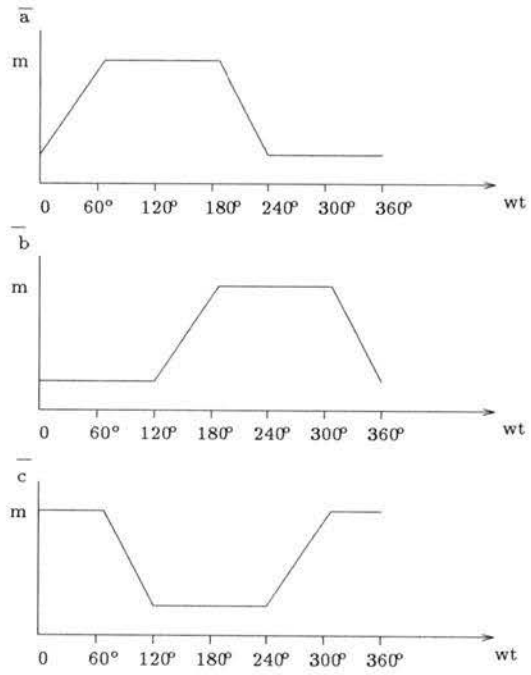


Figure 3.11: Averaged duty ratios of the switching variables.

Figure 3.12 shows the block diagram illustrating the principle of GNPWM. This block is similar to the one shown for the RPWM in figure 3.5. The only difference is that the threshold device is replaced by the pulse-positioning device, which will position the pulses of switching variable $a$ at either leading-edge or lagging-edge within each modulation interval. The random numbers $r$ generated from the RNG

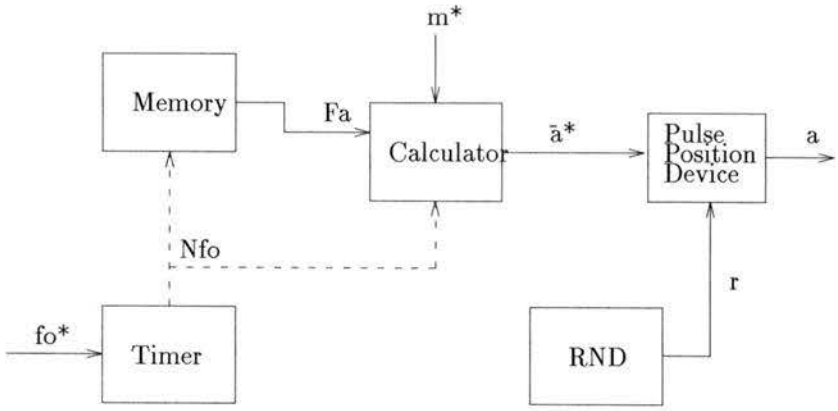


Figure 3.12: Random generation of an inverter switching function using GNPWM.

take on only two discrete values, which can either be 0 for leading-edge modulated or 1 for lagging-edge modulated.

GNPWM results in less switching in comparison to the RPWM strategy. This is illustrated in figure 3.13 showing variables $a$ and $r$ in the RPWM and the GNPWM operating modes. We can see from the figure that the latter technique results in a lower number of switchings than the former one.

There are six switchings for the RPWM (see figure 3.13(a)) and only four switching for the GNPWM (see figure 3.13(b)). In the extreme case, when $r$ follows the $1-0-1-0-1$ ... pattern, the GNPWM technique gives $f_s = 0.5Nf$, where $f$ and $f_s$ are the fundamental and output switching frequency, respectively. The average number of switchings within a single cycle of the output frequency is 25% lower than the RPWM. Therefore, the average switching frequency equals $f_{sw,ave} = 0.75Nf$. For example, at $N = 48$ and $f = 60Hz$, the average switching frequency is 2.16 KHz which is a fully acceptable value even for low-power switches.

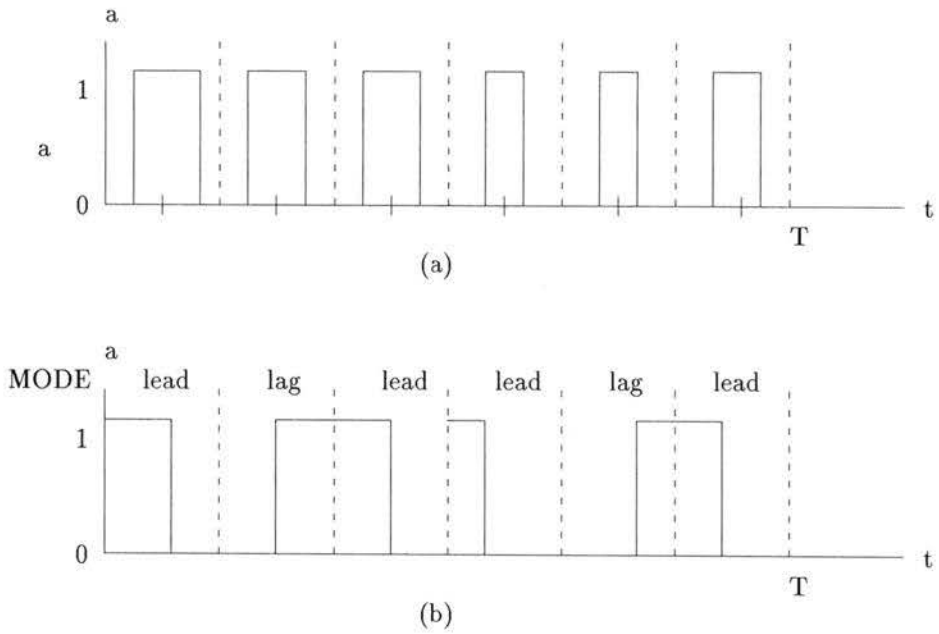


Figure 3.13: Distribution of the switching variable pulses in RPWM and GNPWM.

## 3.6 Deterministic versus Random PWM

The main advantage of the RPWM technique provides a non-periodic switching pattern which results in the spreading of distinct harmonic power over a wider frequency range. In constrast, a deterministic repeated switching pattern is characterized by distinct clusters of pronounced higher harmonics. Spectra posessing distinct power concentration at particular frequencies will create undesirable effects on certain systems having frequency-dependent sensitivity to these harmonics. The typical adverse effects are : annoying tonal noise, resonant vibrations, and electromagnetic interference (EMI). These effects are less pronounced in the case of the randomly varying frequency spectrum produced by RPWM. For instances, the tonal noise appears as a soothing hissing sound. Also, the resonant frequency of the me-

chanical portion of the affected system is unlikely to be excited by the spectrum produced from the RPWM. This prominant feature of RPWM has been confirmed in numerous publications [1, 2, 3, 5, 6, 8].

RPWM has other advantage. It can be implemented in a relatively simple microprocessor system to produce extremely high operation frequency for the control of the inverter. The method also provides real-time control of the inverter, since the modulation index $m$ can be changed in real-time to allow the control of the inverter operation. In contrast, with the deterministic PWM method, the optimal switching patterns for different modulation index have to be pre-computed and stored as a look-up table in memory. Hence, this does not allow real-time control of the inverter [4, 6]. As shown in Chapter 2, using the harmonic elimination technique, the optimal switching patterns or angles are pre-computed off-line by solving a set of nonlinear equations numerically. Improved method based on approximate computations have yielded promising results. However, the proposed solution does not produce a truly optimal switching pattern [21].

## 3.7 Summary

The prototype circuit of the hypersonic three-phase voltage controlled inverter, based on medium power MOSFETs, is described. Three kinds of inverter control functions, namely, the switching function, the average switching function and the moduation function, are described. In order to produce a balanced three-phase output, the conditons stated in (3.3) and (3.4) must be satisfied.

The control of the hypersonic inverter is performed by means of the RPWM strategy. The block diagram illustrating the random generation of the inverter

switching function is given. The tracking ability of the modulation index to the modulating function is also described. When low values of the modulation index are used, higher switching frequencies are required to produce an acceptable resolution at the output.

Another form of RPWM strategy known as random pulse-position modulation (RPPM), or Grey-Noise PWM in the literature, is presented. In this implementation, only two randomization modes are possible. The switching pattern can either occur at the beginning (lead-mode) or at the end (lag-mode) of the switching interval. The lead-lag modes provide fewer switchings as compared to the RPWM technique. This implies less switching loss in the system being fed by the inverter.

In contrast to the deterministic PWM, the switching patterns resulting from the RPWM are different from cycle to cycle. Since the various switching patterns generate different harmonic profiles, the power spectra tend to spread over a wider frequency range. As a result, the adverse effects associated with the deterministic PWM method are greatly alleviated. For instance, the tonal noise appears as a "static" sound, and the resonant vibrations are unlikely to be excited in the absence of a prolonged exposure to periodic harmonic torques and forces generated from the conventional PWM.

# Chapter 4

# Spectral Analysis of Random Pulse-Width Modulation

## 4.1 Introduction

In this chapter we present a detailed analysis of the RPWM strategy described in the previous chapter. In section 4.2 the time domain and frequency domain characterization of the RPPM signal are presented. Three modulating functions (sinusoidal, trapezoidal, and harmonic) and two different types of randomization modes (lead-lag and uniform) are described. The analysis for a single switching variable is presented in section 4.3. The results verify that the higher the number of switching intervals used, the smaller the low-order harmonics are. In section 4.4 we present the multiphase spectral analysis of the inverter output. The resulting spectra can be expressed in terms of the probability density function of the randomization modes. In section 4.5 the analytical formulas for line-to-line voltage are plotted for the two modulating functions (sinusoidal and trapezoidal) with two different randomization modes, and these are compared with the scope traces from the actual microprocessor implementation of the scheme.

## 4.2 Characterization of the RPPM Signal

### 4.2.1 Time Domain Description of RPPM

In the PWM schemes for voltage-controlled inverters, the period $T$ of output frequency $f$ is divided into $N$ equal modulation intervals of width $\triangle$. Each interval $\triangle$ contains a unit-height pulse of width $\bar{a}(n)\triangle$. The duty ratio $\bar{a}(n)$ of variable $a$ in the $n$-th interval equals

$$\bar{a}(n) = [1 + mF(\alpha_n)]/2 \tag{4.1}$$

where $M$ is the modulation index, $F$ is an arbitrarily chosen modulating function of half-wave symmetry and unity amplitude, and $\alpha_n$ is the central angle of the $n$-th modulation interval. The modulating function $F(\alpha_n)$ is introduced to modulate $\bar{a}$ in such a way that a strong sinusoidal component is present in the inverter output voltage. If $F(\alpha_n)$ is assumed to be a periodic function with peaks at $+1$ and $-1$, the relation between $F(\alpha_n)$ and $\bar{a}$ is linear. The change in $F(\alpha_n)$ from $-1$ to $+1$ results in the change in $\bar{a}$ from 0 to 1. Figure 4.1 shows the pulses with the duty ratio of a trapezoidal modulating function. Analogous equations express duty ratios $b$ and $c$, with the angle $\alpha_n$ replaced with $\alpha_n - 120°$ and $\alpha_n - 240°$, respectively.

Considering the phase A switching variable $a$, the operation of an RPPM (or GNPWM) inverter can be described by means of a Bernoulli random variable $\theta_n$, where $\theta_n = -1$ indicates a pulse at the beginning of the $n$th interval (lead mode) and $\theta_n = 1$ indicates a pulse at the end of the $n$th interval (lag mode). The density of $\theta_n$ in the Bernoulli randomization is

$$p(\theta_n) = \frac{1}{2}[\delta(\theta_n - 1) + \delta(\theta_n + 1)] \tag{4.2}$$

Since $\bar{a}(n)$ is known and periodic with period $T = N\triangle$, a period of this random

pulse train can be written as:

$$v_a(t) = \sum_{n=0}^{N-1} \Omega \left( \frac{t - \left( n\triangle + \theta_n \left( \frac{1-\bar{a}(n)}{2} \right) \triangle \right)}{\bar{a}(n)\triangle} \right) \tag{4.3}$$

where $\Omega(t/\alpha) = u(t + \alpha/2) - u(t - \alpha/2)$, $\theta_n$ is a Bernoulli random variable giving the position of the $n$th pulse, and $0 \leq \bar{a}(n) \leq 1$ is the relative width of the $n$th pulse with respect to $\triangle$. A more general formulation replaces the position value $\theta_n \frac{(1 - \bar{a}(n))}{2} \triangle$ with $g(\theta_n)$.

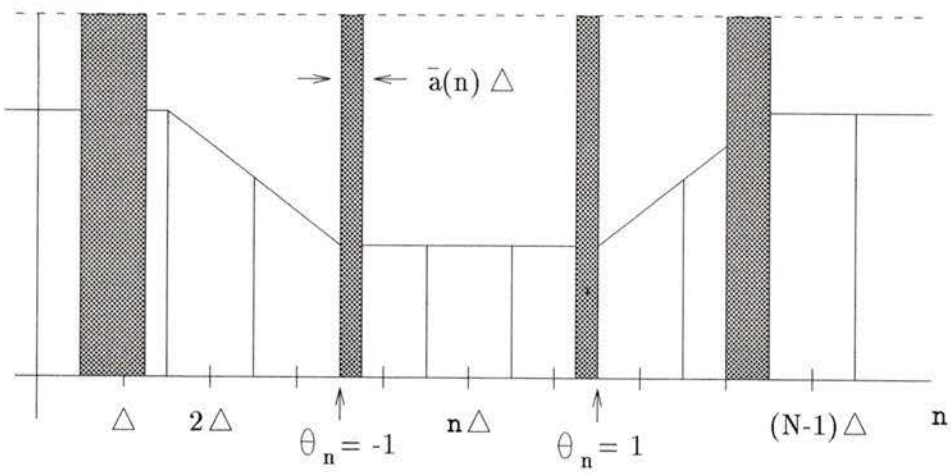


Figure 4.1: PWM with $\bar{a}$(n), randomized position in each delta-interval.

### 4.2.2 Frequency Domain Description of RPPM

For such a cyclic random waveform, a power spectral density has been found [28, pg. 52]. It has a continuous part (power per Hz) and a discrete part with finite power (infinite density) at harmonics of the fundamental $1/(N\triangle)$ Hz.

The spectrum is

$$\begin{aligned} S_x(f) &= \frac{1}{T}E\{|V_a|^2\} - \frac{1}{T}|E\{V_a\}|^2 \quad \text{(continuous spectral density)} \\ &+ \frac{1}{T^2}\sum_{n=-\infty}^{\infty} |E\{V_a\}|^2 \delta\left(f - \frac{n}{T}\right) \text{(harmonic power spectrum)} \end{aligned} \tag{4.4}$$

where $V_a = V_a(f)$ is the Fourier transform of $v_a(t)$ in (4.3) .

The delta functions in the discrete part of the spectrum represent power concentrated at integer multiples of $1/T$. The amount of power at these frequencies depends on the squared magnitude of the Fourier transform of the waveform, $v_a(t)$. If the mean value $E\{V_a\}$ of the waveform is zero, there will be no discrete spectrum even though the waveform is periodic. However, the output spectrum of the inverter we consider always gives discrete components, since the modulation index is always greater than zero. As far as the modulation is concerned, the discrete components other than the fundamental represent wasted power. The relative magnitude of the harmonics (discrete components) can be controlled by modifying the modulating function $F$, and/or the density of the random phase variable $\theta_n$.

### 4.2.3 Average Switching and Modulating Functions

The three most commonly employed modulating functions are considered in our analysis. They are the sinusoidal, trapezoidal, and harmonic modulating functions as shown in figure 4.3. The relative merits of these modulating functions can be found in [3, 4, 5].

There are two possible versions of the $\bar{a}$ versus $F$ relation :

$$\bar{a}(n) = [1 + mF(\alpha_n)]/2 \tag{4.5}$$

$$\bar{a}(n) = m[1 + F(\alpha_n)]/2 \tag{4.6}$$

Both (4.5) and (4.6) result in the same modulation of the inverter voltage, since the d.c. term, 1/2 in (4.5) and $m/2$ in (4.6) does not affect the output voltage. The relations between the instantaneous values of output voltages of an inverter and the switching singals $a$, $b$, and $c$ are:

Line-to-Neutral voltages:

$$\begin{aligned} V_a &= V_{dc}(2a - b - c)/3 \\ V_b &= V_{dc}(2b - c - a)/3 \\ V_c &= V_{dc}(2c - a - b)/3 \end{aligned} \tag{4.7}$$

Line-to-Line voltages:

$$\begin{aligned} V_{ab} &= V_a - V_b = V_{dc}(a - b) \\ V_{bc} &= V_b - V_c = V_{dc}(b - c) \\ V_{ca} &= V_c - V_a = V_{dc}(c - a) \end{aligned} \tag{4.8}$$

Since $\bar{b}$ and $\bar{c}$ are phase shifted by 120° and 240° with respect to $\bar{a}$, the d.c. component in all three switching variables is the same and it becomes zero in the above two set of equations (4.7) and (4.8).

The two modulations do not produce identical performance of the inverter. Symmetrical modulation tends to result in a slightly lower harmonic distortion of the inverter output current, particularly at low values of the modulation index, than the asymmetrical modulation. On the other hand, assuming availability of the sequential values $F(\alpha_n)$ of the modulating functions stored in a look-up table of the microprocessor based modulator, the symmetrical modulation requires three mul-

tiplications and three additions to be performed for each switching interval. The asymmetrical modulation involves only three multiplication, since the individual values of the whole $[1 + F(\alpha_n - \ldots)]/2$ term can be stored and retrieved from the look-up table [7].

The sinusoidal modulation is considered classic and obsolete, due to poor utilization of the supply voltage. In an ideal (lossless) inverter, sinusoidal modulation yields a peak value of the fundamental output line-to-neutral voltage equal to $M/2$ of the DC supply voltage $V_{dc}$. Hence, assuming the DC voltage is obtained from a six-pulse rectifier, the maximum a.c./a.c. conversion ratio if the rectifier-inverter cascade equals $0.827M$, can be obtained as follows (also see figure 4.2).

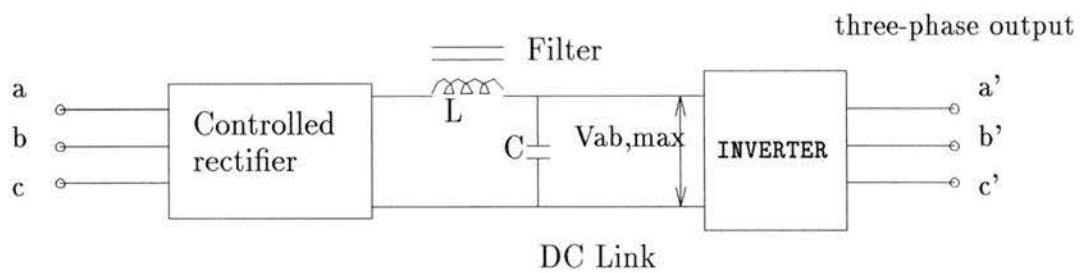


Figure 4.2: Voltage control in six-step inverter drive.

The input line-to-line voltage between phase A and B is given by

$$\begin{aligned} V_{ab} &= V_p \sin \omega t \\ &= \sqrt{2} V_{rms} \sin \omega t \end{aligned} \tag{4.9}$$

where $V_{rms}$ and $V_p$ are the $rms$ and peak voltage, respectively.

$$\therefore V_{aN} = \frac{|V_{ab}|}{\sqrt{3}} = \frac{\sqrt{2} V_{rms}}{\sqrt{3}} \tag{4.10}$$

where $V_{aN}$ is the line-to-neutral voltage. The maximum DC link voltage $V_{ab,max}$ as shown in the figure is

$$V_{ab,max} = \frac{3\sqrt{2}V_{rms}}{\pi} \tag{4.11}$$

With $V_{ab,max}$ as the input voltage for the second stage, the peak value of the inverter fundamental output line-to-neutral voltage equals $M/2$ of the supply voltage. Therefore,

$$\begin{aligned} V_{aN'} &= \left(\frac{M}{2}\right) V_{ab,max} \\ &= \left(\frac{M}{2}\right)\left(\frac{3\sqrt{2}V_{rms}}{\pi}\right) \end{aligned} \tag{4.12}$$

For maximum a.c./a.c. conversion, we have $\frac{V_{aN'}}{V_{aN}} = \frac{V_{bN'}}{V_{bN}} = \frac{V_{cN'}}{V_{cN}}$. For phase A only, using (4.10) and (4.12), we have $\frac{V_{aN'}}{V_{aN}} = \frac{3\sqrt{3}}{2\pi} = 0.827M$. This ratio can be increased by 15.5% by employing the so-called harmonic modulating function [22]. The equation of this function is given by

$$F(\alpha_n) = 2[\sin(\alpha_n) + \sin(3\alpha_n)/6]/\sqrt{3}. \tag{4.13}$$

The harmonic modulating function results in a peak line-to-neutral fundamental voltage of $\frac{MV_{dc}}{\sqrt{3}}$ and a maximum a.c./a.c. voltage conversion ratio of 0.955. Further increase of this voltage by another 5% is possible when trapezoidal modulation is used. In this case, the voltage in question equals $\frac{6MV_{dc}}{\pi^2}$. The maximum a.c./a.c. voltage conversion ratio reaches the theoretical (for pulse-width modulated inverters) limit of 1.005 [23].

### 4.2.4 Probability Density Functions

In addition to the Bernoulli density described in the previous sections, we also consider the PWM pulses modulated in position by the uniform probability density.

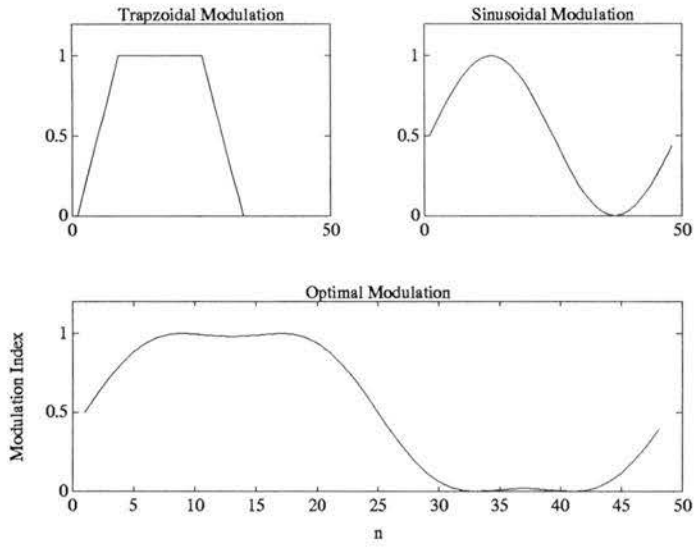


Figure 4.3: Trapezoidal (Top Left), Sinusoidal (Top Right) and Harmonic (Bottom) Modulating Functions (N=48).

In this case the time position of pulses is assumed to be uniformly distributed over the modulation interval $\triangle$. In contrast the time position of pulses in the Bernoulli density is assumed to be either at the beginning (lead-mode) or at the end (lag-mode) of the modulation interval as described before.

The mathematical expressions describing the two density functions are the following. For the Bernoulli density as shown before,

$$p(\theta_n) = \frac{1}{2}[\delta(\theta_n - 1) + \delta(\theta_n + 1)]$$

where $\theta_n$ is a random variable for the position of the pulse within each modulation interval. Note that the probability of occurance of the pulse position is weighted equally with a probability of 1/2 (see figure 4.4).

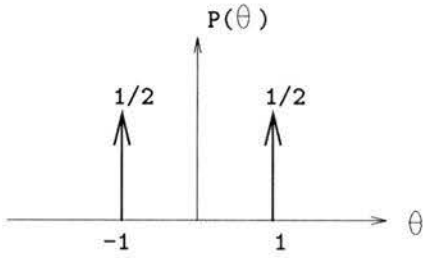


Figure 4.4: Probability density function of Bernoulli trail.

For the uniform density, we have

$$p(\theta) = \begin{cases} \frac{1}{b-a} & \text{for a} \leq \theta \leq \text{b} \\ 0 & \text{otherwise} \end{cases}$$

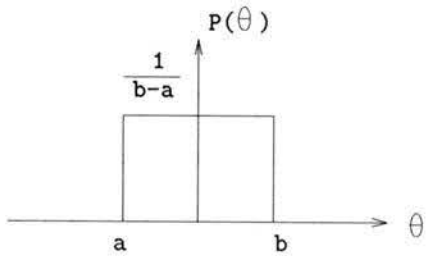


Figure 4.5: Probability density function of uniform distribution.

The shape of the uniform distribution is very simple as shown in figure 4.5. The random variable $\theta$ may take on any value in the interval between $a$ and $b$ with equal probability of being chosen (i.e. the pulse will center at any location in this interval).

It is well known that Fourier series can be used to decompose a periodic signal into an infinite sum of sinusoidal components. The Fourier transform performs

a similar role in the analysis of non-periodic signals. Basically, from the signal processing point of view, the primary motivation of using Fourier analysis is to obtain the frequency spectrum of the signal. In effect, it is often more revealing to view the signal in the frequency domain than in the time domain. It will be shown later in this chapter that the derived spectral formulas are expressed in terms of the Fourier transform of the probability density function.

In our inverter spectral analysis we merely use the Fourier transform as a mathematical tool. Since we have assumed that the probability density functions are even, their Fourier transforms are real.

We can write the Fourier transform of the probability density functions as shown in the following. But first we have to define the Fourier transform pair.

$$\Psi(f) = \int_{-\infty}^{\infty} p(\theta) e^{-j2\pi f\theta} d\theta \tag{4.14}$$

$$p(\theta) = \int_{-\infty}^{\infty} \Psi(f) e^{j2\pi f\theta} df \tag{4.15}$$

where $\Psi(f)$ is the Fourier transform of $p(\theta)$. In general, $\Psi(f)$ is a complex function.

For the Bernoulli density we have

$$\begin{aligned} \Psi(f) &= \int_{-\infty}^{\infty} \frac{1}{2}[\delta(\theta+1) + \delta(\theta-1)] e^{-j2\pi f\theta} d\theta \\ &= \cos(2\pi f) \end{aligned} \tag{4.16}$$

Similarly, for the uniform density,

$$\begin{aligned} \Psi(f) &= \int_{a}^{b} \frac{1}{b-a} e^{-j2\pi f\theta} d\theta \\ &= \frac{\sin(\pi f)}{\pi f} \end{aligned} \tag{4.17}$$

where $b = 1/2$ and $a = -1/2$ are used in order to satisfy the condition of $\int_{-\infty}^{\infty} p(\theta) d\theta = 1$.

## 4.3 Analysis for a Single Switching Variable

### 4.3.1 Preliminary Analysis

We now proceed to find $V_a$, $E\{V_a\}$ and $E\{|V_a|^2\}$ and subsequently consider the resulting $S_x(f)$.

The Fourier transform of $v_a(t)$, defined in (4.3), over $N\triangle$ seconds is

$$\begin{aligned} V_a(f,\ \underline{\theta}) &= \sum_{n=0}^{N-1} \frac{\sin(\pi f \bar{a}(n)\triangle)}{\pi f} e^{-j2\pi f\left[n\triangle+\left(\triangle\frac{1-\bar{a}(n)}{2}\right)\theta_n\right]}, \\ \underline{\theta} &= (\theta_1,\ \theta_2,\ \ldots,\ \theta_N)' \end{aligned} \tag{4.18}$$

where we have used the time scaling and shifting properties of Fourier transform. Since $\theta_n$ is independent from interval to interval, the joint density of $\{\theta_0,\ \theta_1,\ \cdots,\ \theta_{N-1}\}$ is

$$p(\theta_0,\ \theta_1,\ \cdots,\ \theta_{N-1}) = \prod_{n=0}^{N-1} p(\theta_n) = p(\underline{\theta})$$

Thus the expected $V_a(f)$ is

$$\begin{aligned} E\{V_a\} &= \int\int\cdots\int p(\underline{\theta}) V_a(f,\ \underline{\theta}) d\underline{\theta} \\ &= \sum_{n=0}^{N-1} \frac{e^{-j2\pi f n\triangle}}{\pi f} \sin(\pi f \bar{a}(n)\triangle)\cos(\pi f\triangle(1-\bar{a}(n))) \end{aligned} \tag{4.19}$$

Since $\sin\alpha\cos\beta = \frac{1}{2}[\sin(\alpha+\beta)+\sin(\alpha-\beta)]$ and $\sum_{n=0}^{N-1} a^n = \frac{1-a^N}{1-a}$

$$\begin{aligned} E\{V_a\} &= \sum_{n=0}^{N-1} \frac{e^{-j2\pi f n\triangle}}{2\pi f}[\sin(\pi f\triangle)+\sin(\pi f\triangle(2\bar{a}(n)-1))] \\ &= \frac{\sin(\pi f\triangle)}{2\pi f}\,\frac{1-e^{-j2\pi f N\triangle}}{1-e^{-j2\pi f\triangle}} \\ &\qquad + \sum_{n=0}^{N-1} \frac{e^{-j2\pi f n\triangle}}{2\pi f} \sin\left(2\pi f\triangle\left(\bar{a}(n)-\frac{1}{2}\right)\right) \end{aligned} \tag{4.20}$$

In (4.20) we let $z = e^{-j2\pi f'}$, $\alpha_n = 2\pi\left(\bar{a}(n) - \frac{1}{2}\right)$, $f' = f\triangle$, then write

$$\bar{\alpha}_{f'} = \begin{bmatrix} \sin f'\alpha_0 \\ \sin f'\alpha_1 \\ \vdots \\ \sin f'\alpha_{N-1} \end{bmatrix}, \bar{z}_{f'} = \begin{bmatrix} z^0 \\ z^1 \\ \vdots \\ z^{N-1} \end{bmatrix},$$

to give

$$E\{V_a\} = \frac{\sin \pi f\triangle}{2\pi f} \frac{1 - e^{-j2\pi fN\triangle}}{1 - e^{-j2\pi f\triangle}} + \frac{\bar{\alpha}_{f'}^T \bar{z}_{f'}}{2\pi f} \tag{4.21}$$

$$|E\{V_a\}|^2 = \left(\frac{\sin \pi f\triangle}{2\pi f}\right)^2 \left|\frac{1 - e^{-j2\pi fN\triangle}}{1 - e^{-j2\pi f\triangle}}\right|^2 + 2\frac{\sin(\pi f\triangle)}{(2\pi f)^2} \text{ Re } \left(\frac{1 - e^{-j2\pi fN\triangle}}{1 - e^{-j2\pi f\triangle}} (\bar{\alpha}_{f'}^T \bar{z}_{f'})^*\right) + \frac{1}{(2\pi f)^2} |\bar{\alpha}_{f'}^T \bar{z}_{f'}|^2 \tag{4.22}$$

where we have used $|a + b|^2 = |a|^2 + |b|^2 + 2\cdot\text{Re}(ab^*)$ and $(\cdot)^*$ denotes complex conjugation.

In order to find $E\{|V_a|^2\}$, we have to know

$$\begin{aligned} \int\int\cdots\int V_a(\underline{\theta}) V_a(\underline{\theta})^* p(\underline{\theta}) d\underline{\theta} &= \int\int\cdots\int V_a(\underline{\theta}) V_a(\underline{\theta})^* p(\theta_0) p(\theta_1) \cdots p(\theta_i) \cdots p(\theta_k) \\ &\qquad \cdots p(\theta_{N-1}) d\theta_0 d\theta_1 \cdots d\theta_i \cdots d\theta_k \cdots d\theta_{N-1} \\ &= \int\int V_a(\theta_i, \theta_k) V_a(\theta_i, \theta_k)^* p(\theta_i) p(\theta_k) d\theta_i d\theta_k \end{aligned} \tag{4.23}$$

where $\int p(\theta_n) d\theta_n = 1$ for $n \neq i, k$.

Also,

$$p(\theta_i)p(\theta_k) = \frac{1}{4}[\delta(\theta_i + 1)\delta(\theta_k + 1) + \delta(\theta_i + 1)\delta(\theta_k - 1) + \delta(\theta_i - 1)\delta(\theta_k + 1) + \delta(\theta_i - 1)\delta(\theta_k - 1)] \qquad for \ \ i \neq k$$

$$p(\theta_i)p(\theta_k) = \frac{1}{2}[\delta(\theta_i+1)+\delta(\theta_i-1)] \qquad for \quad i=k$$

Substituting (4.18) into (4.23) and using the above expressions, we have

$$\begin{aligned}
E\{|V_a|^2\} &= \int\int\cdots\int p(\underline{\theta})V_a(f,\ \underline{\theta})(V_a(f,\ \underline{\theta}))^* d\underline{\theta} \\
&= \frac{1}{4}\int\int \sum_{i,\ k=0,\ i\neq k}^{N-1} \frac{\sin(\pi f\bar{a}(i)\triangle)}{\pi f}\ \frac{\sin(\pi f\bar{a}(k)\triangle)}{\pi f} e^{-j2\pi f\triangle(i-k)} \\
&\qquad \cdot e^{-j2\pi f\left[\left(\triangle\frac{1-\bar{a}(i)}{2}\right)\theta_i-\left(\triangle\frac{1-\bar{a}(k)}{2}\right)\theta_k\right]}[\delta(\theta_i+1)\delta(\theta_k+1)+ \\
&\qquad \delta(\theta_i+1)\delta(\theta_k-1)+\delta(\theta_i-1)\delta(\theta_k+1)+\delta(\theta_i-1)\delta(\theta_k-1)]d\theta_i d\theta_k \\
&\quad +\frac{1}{2}\int\sum_{i=0}^{N-1}\left(\frac{\sin(\pi f\bar{a}(i)\triangle)}{\pi f}\right)^2[\delta(\theta_i+1)+\delta(\theta_i-1)]d\theta_i
\end{aligned} \tag{4.24}$$

The double summation term is for the summation index $i \neq k$ and the single summation term is for $i = k$.

Since $E\{|X|^2\} = |E\{X\}|^2 - (diag.terms)_{|E\{X\}|^2} + (diag.terms)_{E\{|X|^2\}}$,

$$\begin{aligned}
E\{|V_a|^2\} &= |E\{V_a\}|^2 - \sum_{i=0}^{N-1}\left(\frac{\sin(\pi f\bar{a}(i)\triangle)}{\pi f}\right)^2 \\
&\qquad -\frac{1}{4}\sum_{i=0}^{N-1}\left(\frac{\sin(\pi f\bar{a}(i)\triangle)}{\pi f}\right)^2 e^{-j2\pi f\left[\triangle\left(\frac{1-\bar{a}(i)}{2}\right)\right]\times 2} \\
&\qquad -\frac{1}{4}\sum_{i=0}^{N-1}\left(\frac{\sin(\pi f\bar{a}(i)\triangle)}{\pi f}\right)^2 e^{j2\pi f\left[\triangle\left(\frac{1-\bar{a}(i)}{2}\right)\right]\times 2} \\
&\qquad +\frac{1}{2}\sum_{i=0}^{N-1}\left(\frac{\sin(\pi f\bar{a}(i)\triangle)}{\pi f}\right)^2 \\
&= |E\{V_a\}|^2 + \frac{1}{2}\sum_{i=0}^{N-1}\left(\frac{\sin(\pi f\bar{a}(i)\triangle)}{\pi f}\right)^2 \\
&\qquad -\frac{1}{2}\sum_{i=0}^{N-1}\left(\frac{\sin(\pi f\bar{a}(i)\triangle)}{\pi f}\right)^2 \cos[2\pi f\triangle(1-\bar{a}(i))]
\end{aligned} \tag{4.25}$$

Subtracting $|E\{V_a\}|^2$ from both sides of (4.25),

$$
\begin{aligned}
E\{|V_a|^2\} - |E\{V_a\}|^2 &= \frac{1}{2}\sum_{i=0}^{N-1}\left(\frac{\sin(\pi f\bar{a}(i)\triangle)}{\pi f}\right)^2 [1-\cos(2\pi f\triangle(1-\bar{a}(i))] \\
&= \frac{1}{2}\sum_{i=0}^{N-1}\left(\frac{\sin(\pi f\bar{a}(i)\triangle)}{\pi f}\right)^2 2\sin^2[\pi f\triangle(1-\bar{a}(i))] \\
&= \sum_{i=0}^{N-1}\frac{[\cos(2\pi f\triangle(\bar{a}(i)-0.5)) - \cos\pi f\triangle]^2}{(2\pi f)^2} \\
&= \frac{1}{(2\pi f)^2}\left\{\frac{1}{2}\sum_{i=0}^{N-1}(1+\cos(4\pi f\triangle(\bar{a}(i)-0.5))) \right. \\
&\qquad \left. +N\cos^2(\pi f\triangle) - 2\cos(\pi f\triangle)\sum_{i=0}^{N-1}\cos(2\pi f\triangle(\bar{a}(i)-0.5))\right\} \\
&= \frac{\frac{N}{2}+N\cos^2(\pi f\triangle)}{(2\pi f)^2} + \frac{1}{(2\pi f)^2}\sum_{i=0}^{N-1}\frac{1}{2}\cos(4\pi f\triangle(\bar{a}(i)-0.5)) \\
&\qquad -\frac{\cos(\pi f\triangle)}{(2\pi f)^2}\sum_{i=0}^{N-1}2\cos(2\pi f\triangle\ (\bar{a}(i)-0.5)) \qquad (4.26)
\end{aligned}
$$

We have now found the expressions for $V_a$, $E\{V_a\}$ and $E\{|V_a|^2\}$.

### 4.3.2 Evaluation of the Spectral Density

From (4.4) we have

$$
\begin{aligned}
S_x(f) &= \frac{1}{T}E\{|V_a|^2\} - \frac{1}{T}|E\{V_a\}|^2 \text{ (continuous spectrum)} \\
&\qquad +\frac{1}{T^2}\sum_{n=-\infty}^{+\infty}|E\{V_a\}|^2\delta(f-\frac{n}{T}) \text{ (discrete spectrum)} \qquad (4.27) \\
&= S_c(f) + S_d(f). \qquad (4.28)
\end{aligned}
$$

where $S_c(f)$ is the continuous part and $S_d(f)$ the discrete. First we consider the discrete spectral coefficients, i.e. $\frac{1}{T^2}|E\{V_a\}|^2$ at $f = k/T$. From (4.22) we have

$$
|E\{V_a\}|_k^2 = \frac{1}{(2\pi f)^2}|\bar{\alpha}_{f'}^T\bar{z}_{f'}|^2_{f=k/T} \qquad (4.29)
$$

where (with $f' = f\triangle$ and $T = N\triangle$, so that $f' = (k/T)(T/N) = k/N$ in $\bar{\alpha}_{f'}$ and $\bar{z}_{f'}$)

$$\bar{\alpha}_k = \begin{bmatrix} \sin(\alpha_0 k/N) \\ \sin(\alpha_1 k/N) \\ \vdots \\ \sin(\alpha_N k/N) \end{bmatrix}, \bar{z}_k = \begin{bmatrix} 1 \\ z^1 \\ \vdots \\ z^{N-1} \end{bmatrix}_{z=e^{-j2\pi k/N}} . \tag{4.30}$$

Therefore the discrete spectrum $S_d(f)$ is

$$S_d(f) = \frac{1}{T^2} \sum_{k=-\infty}^{+\infty} |E\{V_a\}|^2 \delta\left(f - \frac{k}{T}\right)$$

and the $k$th harmonic power is

$$P_k = \frac{2}{(2\pi k)^2} |\bar{\alpha}_k^T \bar{z}_k|^2 = \frac{1}{2(\pi k)^2} \left| \sum_{n=0}^{N-1} \sin\left(2\pi \frac{k}{N}\left(\bar{a}(n) - \frac{1}{2}\right)\right) e^{-j2\pi \frac{kn}{N}} \right|^2 \tag{4.31}$$

Similarly the continuous spectrum $S_c(f)$ is

$$\begin{aligned} S_c(f) &= \frac{1}{T}[E\{|V_a|^2\} - |E\{V_a\}|^2] \\ &= \frac{N(1 + 2\cos^2(\pi f\triangle))}{8(\pi f)^2 T} + \frac{1}{8(\pi f)^2 T} \sum_{i=0}^{N-1} \cos(4\pi f\triangle(\bar{a}(i) - 0.5)) \\ &\quad - \frac{\cos(\pi f\triangle)}{2(\pi f)^2 T} \sum_{i=0}^{N-1} \cos(2\pi f\triangle(\bar{a}(i) - 0.5)) \end{aligned} \tag{4.32}$$

We have now obtained both the discrete spectrum (4.31) and the continuous spectrum (4.32) for a single phase output of an inverter. The spectral formulas are programmed using MATLAB (see m-file discrete.m and continuous.m in Appendix). The plots for both the discrete and continuous spectrum with three different switching interval values ($N_1 = 48$, $N_2 = 120$, and $N_3 = 480$) are shown in figures 4.6, 4.7, and 4.8, respectively. The fundamental frequencies for all plots are set to be unity. Trapezoidal modulation is used for all three cases.

From the figures we see that as the number of the switching intervals N increases, the next significant low-order harmonics move higher up in the discrete spectrum (i.e. less harmonic distortion). As a result the current waveform generated from the inverter with $N = 480$ will be closer to an ideal sinusoidal waveform than the one generated with $N = 48$ or $N = 120$.

These results are in agreement with the observation made in the previous chapter (the section on average switching function). It was mentioned that the machine harmonic loss will decrease with increasing N. This is exactly what we have obtained from the plots of the discrete spectral formula.

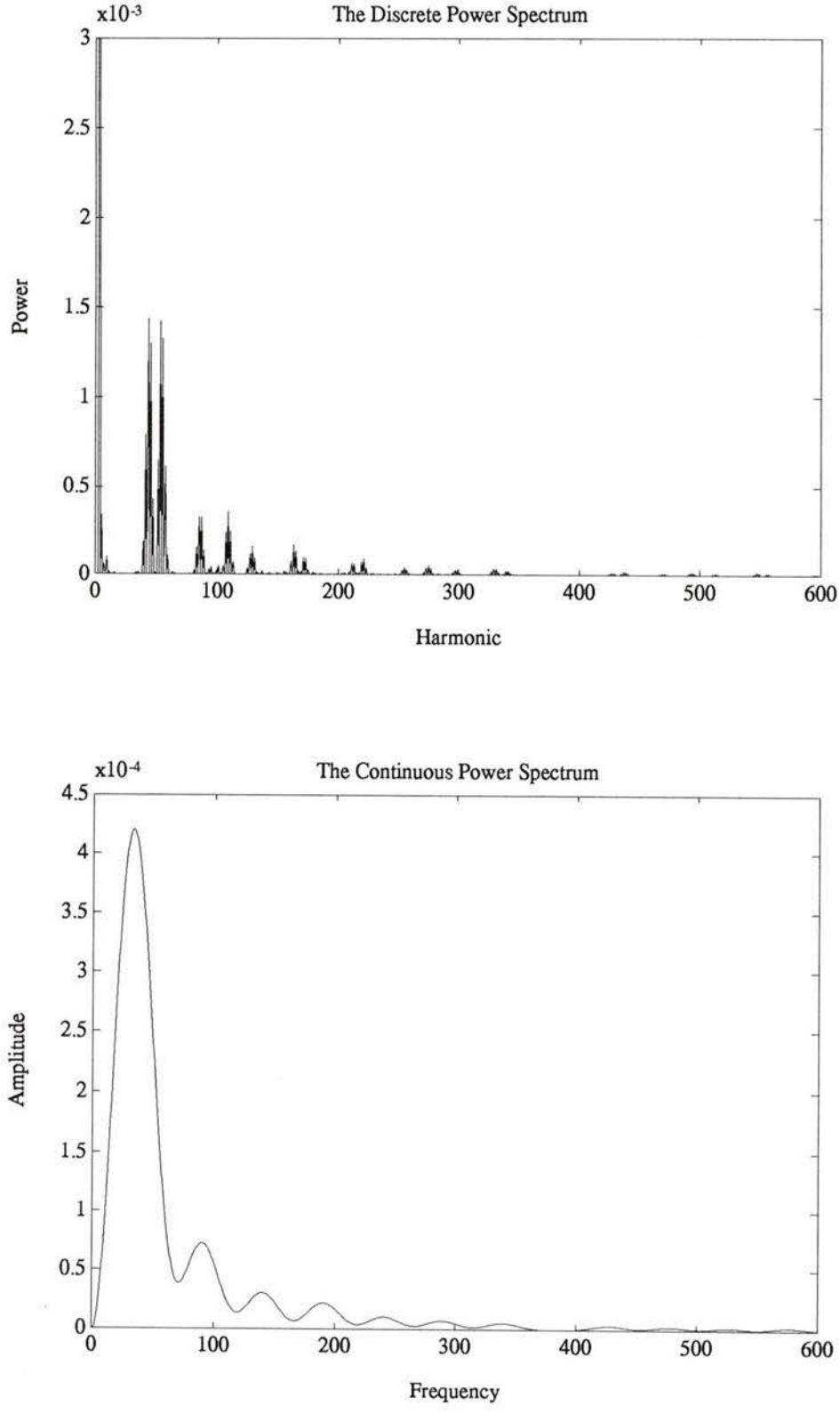


Figure 4.6: Discrete (Top) and Continuous (Bottom) Spectrum with Trapezoidal Modulation (N=48).

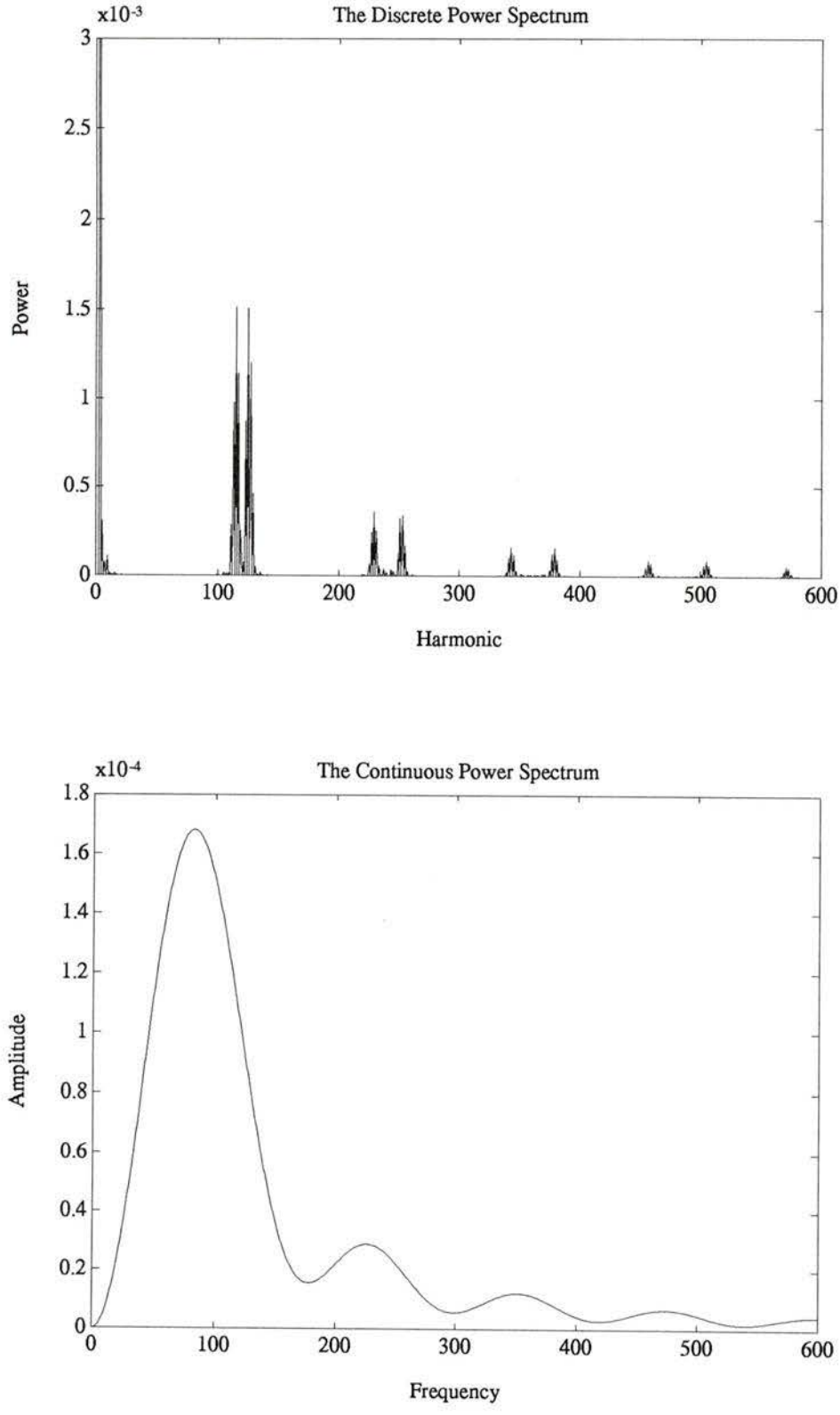


Figure 4.7: Discrete (Top) and Continuous (Bottom) Spectrum with Trapezoidal Modulation (N=120).

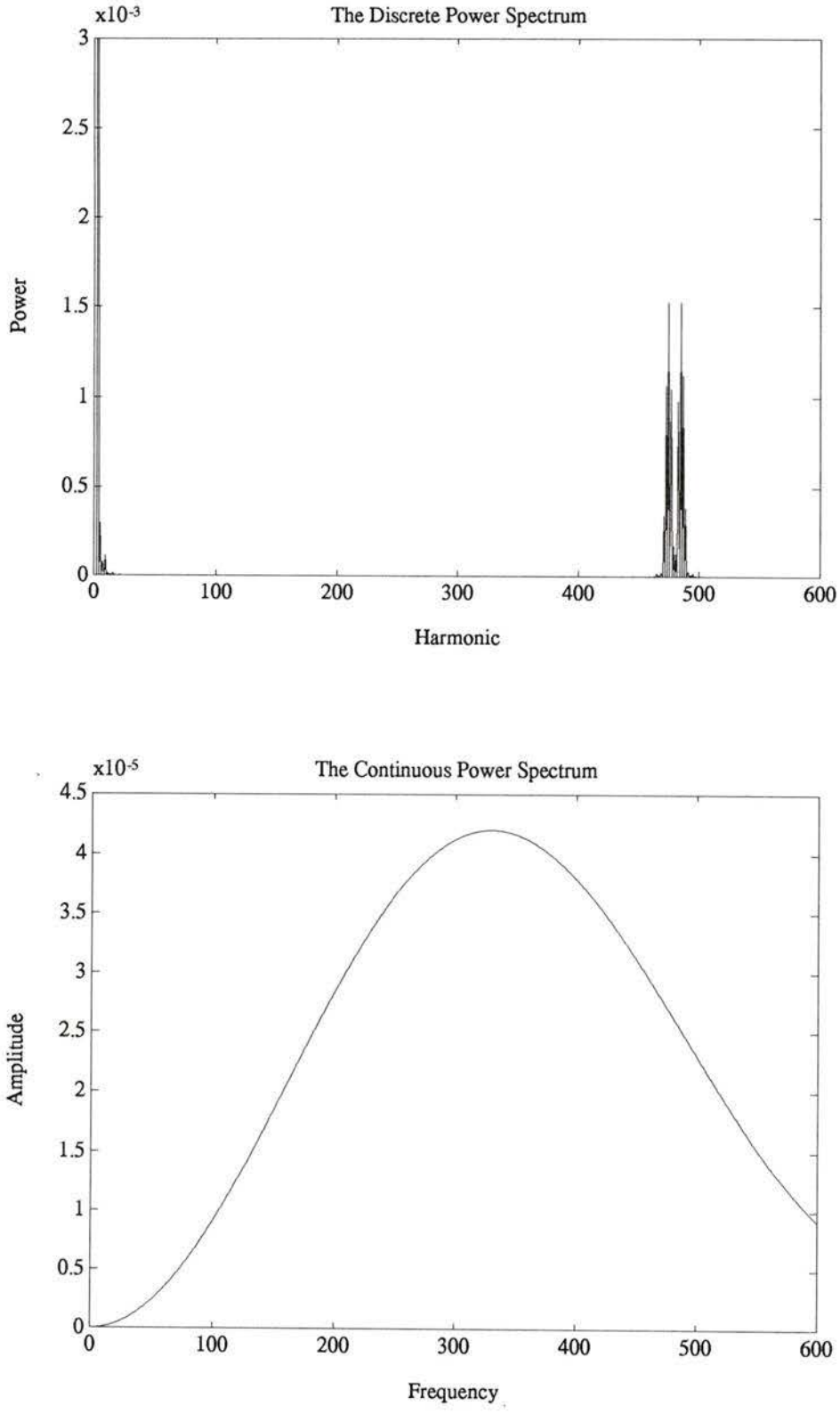


Figure 4.8: Discrete (Top) and Continuous (Bottom) Spectrum with Trapezoidal Modulation (N=480).

## 4.4 Multiphase Spectra

Electric power systems are three-phase systems in that power is generated by three-phase generators (e.g. inverters) and transmitted to the three-phase load. In the following sections we present a detailed analysis of the line-to-line and line-to-neutral of the inverter output harmonic power spectra.

### 4.4.1 Line-to-Line Harmonic Power Spectra

An example line-to-line inverter output voltage between phase A and phase B is shown in figure 3.8. We can write the expression for this waveform as

$$v_{ab}(t) = v_a(t,\ \bar{a}(n),\ \theta^a) - v_b(t,\ \bar{a}(n),\ \theta^a) \tag{4.33}$$

where $\theta^a$ denotes the Bernoulli sequence for phase $a$, $\theta^b$ for phase $b$, and $\theta^c$ for phase $c$; $\theta^a_n$ denotes the $n$th value in $\theta^a$.

Thus

$$v_a = v_a(t,\ \bar{a}(n),\ \theta^a) = \sum_{n=0}^{N-1} \Omega\left(\frac{t - (n\triangle + \theta^a_n(\frac{1-\bar{a}(n)}{2})\triangle)}{\bar{a}(n)\triangle}\right) \tag{4.34}$$

and

$$v_b = v_a(t,\ \bar{a}(n - N/3),\ \theta^a) = \sum_{n=0}^{N-1} \Omega\left(\frac{t - (n\triangle + \theta^a_n(\frac{1-\bar{a}(n-N/3)}{2})\triangle)}{\bar{a}(n - N/3)\triangle}\right) \tag{4.35}$$

The width modulation on $v_b(t)$ is $T/3$ lagging that on $v_a(t)$, but the position-dithering sequence is identical and time-coincident on all three phases (see figure 3.10). Therefore, we have $v_b = v_a(t,\ \bar{a}(n - N/3),\ \theta^a)$ in (4.35).

Letting $k = n - N/3$ in (4.35) gives

$$v_b(t,\ \bar{a}(k),\ \theta^a) = \sum_{k=0}^{N-1} \Omega\left(\frac{t - \left((k + N/3)\triangle + \theta^a_{k+N/3}(\frac{1-\bar{a}(k)}{2})\triangle\right)}{\bar{a}(k)\triangle}\right) \tag{4.36}$$

where the summation limits on $k$ are the same as on $n$ due to the periodicity of $\bar{a}(n)$, $v_a(t)$ and $v_b(t)$.

Noting $\theta^a_{k+N/3}$ is independent of $\theta^a_n$ unless $k = n - N/3$, thus we may let $\theta^b_k = \theta^a_{k+N/3}$ and write

$$v_b(t,\ \bar{a}(k),\ \theta^b) = v_a(t - T/3,\ \bar{a}(k),\ \theta^b) \tag{4.37}$$

Notice that the position-dithering sequence (or the randomization mode) is not shifted, but the width modulation (or the duty ratio) is phase shifted by $T/3$ or $-120°$.

The Fourier transform of $v_a(t) = v_a(t,\ \bar{a}(n),\ \theta^a)$ is

$$V_a(f) = \sum_{n=0}^{N-1} X(f,\ n) e^{-j2\pi f(\frac{1-\bar{a}(n)}{2})\triangle\theta^a_n} \tag{4.38}$$

where

$$X(f,\ n) = \frac{\sin(\pi f \bar{a}(n)\triangle)}{\pi f} e^{-j2\pi f n\triangle}. \tag{4.39}$$

Similarly,

$$V_b(f) = \sum_{n=0}^{N-1} X(f,\ n) e^{-j2\pi fT/3} e^{-j2\pi f(\frac{1-\bar{a}(n)}{2})\triangle\theta^b_n}, \tag{4.40}$$

Therefore, the Fourier transform of the line-to-line voltage is given by

$$V_{ab}(f) = \sum_{n=0}^{N-1} X(f,\ n) e^{-j2\pi f\left(\frac{1-\bar{a}(n)}{2}\right)\triangle\theta^a_n} - e^{-j2\pi fT/3} \sum_{n=0}^{N-1} X(f,\ n) e^{-j2\pi f\left(\frac{1-\bar{a}(n)}{2}\right)\triangle\theta^b_n} \tag{4.41}$$

where we have used the linearity property of the Fourier transform.

Taking the expectation of $V_{ab}(f)$ over the $2N$ joint variables in $\theta^a$ and $\theta^b$ gives

$$\begin{aligned} E\{V_{ab}(f)\} &= \sum_{n=0}^{N-1} X(f,\ n) \Psi\left(f\frac{1-\bar{a}(n)}{2}\triangle\right)(1 - e^{-j2\pi fT/3}) \\ &= E\{V_a(f,\ \bar{a}(n),\ \theta^a\}(1 - e^{-j2\pi fT/3}) \end{aligned} \tag{4.42}$$

and

$$|E\{V_{ab}(f)\}|^2 = 2(1 - \cos(2\pi fT/3))|E\{V_a(f)\}|^2 \tag{4.43}$$

where $\Psi(f) = \int_{-\infty}^{\infty} p(\theta) e^{-j2\pi f\theta} d\theta$ is the Fourier transform of the probability density function $p(\theta)$ and $E\{V_a(f)\} = \sum_{n=0}^{N-1} X(f,\ n)\Psi\left(f\frac{1-\bar{a}(n)}{2}\triangle\right)$.

Note for the Bernoulli randomization mode we have $p(\theta) = \frac{1}{2}[\delta(\theta+1) + \delta(\theta-1)]$. Hence $\Psi(f) = \cos 2\pi f$.

To complete (4.43), we take the expectation of $E\{V_a(f)\}$ from (4.38) to get

$$|E\{V_a(f)\}|^2 = \left|\sum_{n=0}^{N-1} X(f,\ n)\Psi\left(\frac{1-\bar{a}(n)}{2} f\triangle\right)\right|^2 \tag{4.44}$$

The analysis for $E\{|V_{ab}(f)|^2\}$ proceeds similarly. Taking the expectation of the magnitude squared value of $V_{ab}$ in (4.41), we have

$$\begin{aligned} E\{|V_{ab}(f)|^2\} &= E\left\{\left|\sum_{n=0}^{N-1} X(f,\ n)\left[e^{-j2\pi f\left(\frac{1-\bar{a}(n)}{2}\right)\triangle\theta_n^a} - e^{-j2\pi fT/3} e^{-j2\pi f\left(\frac{1-\bar{a}(n)}{2}\right)\triangle\theta_n^b}\right]\right|^2\right\} \\ &= 2E\{|V_a(f)|^2\} - 2\ \mathrm{Re}\left[e^{j2\pi fT/3} E\left\{\sum_{n=0}^{N-1}\sum_{k=0}^{N-1} X(f,\ n)X^*(f,\ k)\right.\right. \\ &\qquad \left.\left. \cdot e^{-j2\pi f\left(\frac{1-\bar{a}(n)}{2}\triangle\theta_n^a - \frac{1-\bar{a}(k)}{2}\theta_k^b\right)}\right\}\right] \end{aligned} \tag{4.45}$$

where we have used $|a+b|^2 = |a|^2 + |b|^2 + 2\cdot\mathrm{Re}(ab^*)$.

The second expectation, inside square brackets in (4.45), would be identical to $|E\{V_a(f)\}|^2$ except for terms for which $k = n - N/3$. Making that correction gives

$$\begin{aligned} E\{|V_{ab}(f)|^2\} &= 2E\{|V_a(f)|^2\} - 2\ \mathrm{Re}\ \left\{e^{j2\pi fT/3}[|E\{V_a(f)\}|^2\right. \\ &\quad - \sum_{n=0}^{N-1} X(f,\ n)X^*(f,\ k)\Psi\left(\frac{1-\bar{a}(n)}{2} f\triangle\right)\Psi^*\left(\frac{1-\bar{a}(k)}{2} f\triangle\right) \\ &\quad \left. + \sum_{n=0}^{N-1} X(f,\ n)X^*(f,\ k)\Psi\left(\frac{\bar{a}(n-N/3)-\bar{a}(n)}{2} f\triangle\right)\right]\Big\}, \end{aligned} \tag{4.46}$$

where $k = n - N/3$.

Similarly, evaluating the first expectation in (4.45),

$$E\{|V_a(f)|^2\} = |E\{V_a(f)\}|^2 - \sum_{n=0}^{N-1} |X(f,\ n)|^2\Psi^2\left(\frac{1-\bar{a}(n)}{2} f\triangle\right)$$

$$+\sum_{n=0}^{N-1}|X(f,\ n)|^2, \tag{4.47}$$

where

$$|E\{V_a(f)\}|^2=\left|\sum_{n=0}^{N-1}X(f,\ n)\Psi\left(\frac{1-\bar{a}(n)}{2}f\triangle\right)\right|^2 \tag{4.48}$$

Here we note that if $p(\theta)$ is even, $\Psi(f)$ is real. Inserting $E\{|V_a(f)|^2\}$ in (4.47) and $|E\{V_a(f)\}|^2$ in (4.48) into (4.46) and assuming $p(\theta)$ even gives

$$\begin{aligned}
E\{|V_{ab}(f)|^2\} &= 2\left[|E\{V_a(f)\}|^2+\sum_{n=0}^{N-1}|X(f,\ n)|^2\left(1-\Psi^2\left(\frac{1-\bar{a}(n)}{2}f\triangle\right)\right)\right]\\
&\quad -2\cos(2\pi fT/3)|E\{V_a(f)\}|^2\\
&\quad +2\sum_{n=0}^{N-1}|X(f,\ n)|\ |V_a(f,\ n-N/3)|\left(\Psi\left(\frac{\bar{a}(n-N/3)-\bar{a}(n)}{2}f\triangle\right)\right.\\
&\quad \left.-\Psi\left(\frac{1-\bar{a}(n)}{2}f\triangle\right)\Psi\left(\frac{1-\bar{a}(n-N/3)}{2}f\triangle\right)\right).\\
&= 2|E\{V_a(f)\}|^2(1-\cos(2\pi fT/3))\\
&\quad +2\sum_{n=0}^{N-1}|X(f,\ n)|^2\left(1-\Psi^2\left(\frac{1-\bar{a}(n)}{2}f\triangle\right)\right)\\
&\quad +2\sum_{n=0}^{N-1}|X(f,\ n)|\ |V_a(f,\ n-N/3)|\\
&\quad \cdot\left[\Psi\left(\frac{\bar{a}(n-N/3)-\bar{a}(n)}{2}f\triangle\right)\right.\\
&\quad \left.-\Psi\left(\frac{1-\bar{a}(n)}{2}f\triangle\right)\Psi\left(\frac{1-\bar{a}(n-N/3)}{2}f\triangle\right)\right]
\end{aligned} \tag{4.49}$$

For the continuous line-to-line spectrum we combine (4.43) and (4.49):

$$\begin{aligned}
S_{c\ell\ell} &= \frac{1}{T}[E\{|V_{ab}|^2\}-|E\{V_{ab}\}|^2]\\
&= \frac{2}{T}\sum_{n=0}^{N-1}\frac{\sin^2(\pi f\bar{a}(n)\triangle)}{(\pi f)^2}\left(1-\Psi^2\left(\frac{1-\bar{a}(n)}{2}f\triangle\right)\right)\\
&\quad +\frac{2}{T}\sum_{n=0}^{N-1}\frac{\sin(\pi f\bar{a}(n)\triangle)\sin(\pi f\bar{a}(n-N/3)\triangle)}{(\pi f)^2}\\
&\quad \cdot\left[\Psi\left(\frac{\bar{a}(n-N/3)-\bar{a}(n)}{2}f\triangle\right)\right.
\end{aligned}$$

$$-\Psi\left(\frac{1-\bar{a}(n)}{2}f\triangle\right)\Psi\left(\frac{1-\bar{a}(n-N/3)}{2}f\triangle\right)\Big] \tag{4.50}$$

The discrete spectrum is defined as

$$S_{d\ell\ell}(f)=\frac{1}{T^2}\sum_{n=-\infty}^{\infty}|E\{V_{ab}(f)\}|^2\delta\left(f-\frac{n}{T}\right), \tag{4.51}$$

so the $k$th harmonic, using (4.43) and (4.48), has power

$$P_{\ell\ell}(k)=\frac{4}{(\pi k)^2}(1-\cos(2\pi k/3))\cdot\left|\sum_{n=0}^{N-1}\sin(\pi k\bar{a}(n)/N)e^{-j2\pi\frac{nk}{N}}\Psi\left(\frac{1-\bar{a}(n)}{2}\ \frac{k}{N}\right)\right|^2. \tag{4.52}$$

### 4.4.2 Line-to-Neutral Harmonic Power Spectra

The line-to-neutral voltages are of the form

$$v_{an}(t)=\frac{1}{3}[2v_a(t,\ \bar{a}(n),\ \theta^a)-v_b(t,\ \bar{a}(n),\ \theta^a)-v_c(t,\ \bar{a}(n),\ \theta^a)] \tag{4.53}$$

where $v_a(t,\ \bar{a}(n),\ \theta^a)$ and $v_b(t,\ \bar{a}(n),\ \theta^b)$ are as in (4.34) and (4.35) and

$$v_c(t)=v_c(t,\ \bar{a}(n),\ \theta^c)=v_a(t,\ \bar{a}(n-2N/3),\ \theta^a)=v_a(t-T/3,\ \bar{a}(k),\ \theta^c) \tag{4.54}$$

where $k=n-2N/3$.

Here $\theta^c_k=\theta^a_{k+2N/3}$, and because $\theta^a_{k+2N/3}$ is independent of $\theta^a_n$ unless $k=n-2N/3$.

The Fourier transform of $v_c(t)$ is

$$V_c(f)=\sum_{n=0}^{N-1}X(f,\ n)e^{-j4\pi fT/3}e^{-j2\pi f(\frac{1-\bar{a}(n)}{2})\triangle\theta^b_n} \tag{4.55}$$

Taking Fourier transform on (4.53) and using (4.38), (4.40), and (4.55), we get

$$\begin{aligned}3V_{an}(f) &= 2V_a(f)-V_b(f)-V_c(f)\\ &= 2\sum_{n=0}^{N-1}X(f,\ n)e^{-j2\pi f(\frac{1-\bar{a}(n)}{2})\triangle\theta^a_n}\end{aligned}$$

$$-e^{-j2\pi fT/3}\sum_{n=0}^{N-1}X(f,\ n)e^{-j2\pi f(\frac{1-\bar{a}(n)}{2})\triangle\theta_n^b}$$
$$-e^{-j4\pi fT/3}\sum_{n=0}^{N-1}X(f,\ n)e^{-j2\pi f(\frac{1-\bar{a}(n)}{2})\triangle\theta_n^c} \qquad (4.56)$$

Therefore, the expectation over the $3N$ variables in $\theta^a$, $\theta^b$ and $\theta^c$ gives for the Fourier transform of $v_{an}(t)$:

$$\begin{aligned} 3E\{V_{an}(f)\} &= \left(2-e^{-j2\pi fT/3}-e^{-j4\pi fT/3}\right) \\ &\quad \cdot\sum_{n=0}^{N-1}X(f,\ n)\Psi\left(f\frac{1-\bar{a}(n)}{2}\triangle\right) \qquad (4.57) \\ &= (2-e^{-j2\pi fT/3}-e^{-j4\pi fT/3})E\{V_a(f)\} \qquad (4.58) \end{aligned}$$

Taking the magnitude square on both sides of (4.58) we have

$$|E\{V_{an}(f)\}|^2=\frac{1}{9}(6-2\cos 2\pi fT/3-4\cos(4\pi fT/3))\cdot|E\{V_a(f)\}|^2, \qquad (4.59)$$

whereas before (4.44)

$$|E\{V_a(f)\}|^2=\left|\sum_{n=0}^{N-1}\frac{\sin\pi f\bar{a}(n)\triangle}{\pi f}e^{-j2\pi fn\triangle}\ \Psi\left(\frac{1-\bar{a}(n)}{2}f\triangle\right)\right|^2.$$

The discrete spectrum is defined as

$$S_{d\ell n}(f)=\frac{1}{T^2}\sum_{n=-\infty}^{\infty}|E\{V_{an}(f)\}|^2\delta\left(f-\frac{n}{T}\right), \qquad (4.60)$$

Assuming $p(\theta)$ an even function, the above three expressions give for the line-to-neutral discrete spectrum, $k$th harmonic power,

$$\begin{aligned} P_{k\ell n} &= \frac{4}{9(\pi k)^2}[3-\cos(2\pi k/3)-2\cos(4\pi k/3)] \\ &\quad \cdot\left|\sum_{n=0}^{N-1}\sin(\pi k\bar{a}(n)/N)e^{-j2\pi nk/N}\Psi\left(\frac{1-\bar{a}(n)}{2}\ \frac{k}{N}\right)\right|^2 \qquad (4.61) \end{aligned}$$

For the continuous spectrum we evaluate $E\{|V_{an}(f)|^2\}$ using (4.56) and get

$$\begin{aligned} 9E\{|V_{an}(f)|^2\} &= E\{|2V_a(f) - V_b(f) - V_c(f)|^2\} \\ &= 4E\{|V_a(f)|^2\} + E\{|V_b(f)|^2\} + E\{|V_c(f)|^2\} \\ &\quad -4 \text{ Re } \{V_a(f,\ \bar{a}(n),\ \theta^a)V_b^*(f,\ \bar{a}(n),\ \theta^b)\} \\ &\quad -4 \text{ Re } \{V_a(f,\ \bar{a}(n),\ \theta^a)V_c^*(f,\ \bar{a}(n),\ \theta^c)\} \\ &\quad +2 \text{ Re } \{V_b(f,\ \bar{a}(n),\ \theta^b)V_c^*(f,\ \bar{a}(n),\ \theta^c)\}, \end{aligned} \tag{4.62}$$

wherein we have used $|a-b-c|^2 = |a|^2+|b|^2+|c|^2-2\cdot\text{Re}(ab^*)-2\cdot\text{Re}(ac^*)+2\cdot\text{Re}(bc^*)$

Substituting expressions for $V_a(f)$, $V_b(f)$, and $V_c(f)$ into (4.62) we get

$$\begin{aligned} 9E\{|V_{an}(f)|^2\} &= 6E\{|V_a(f)|^2\} \\ &\quad -4 \text{ Re } \Big\{e^{j2\pi fT/3} \cdot [\ |E\{V_a(f)\Big\}|^2 \\ &\quad + \sum_{n=0}^{N-1} X(f,\ n)X^*(f,\ n-N/3)\Psi\left(\frac{\bar{a}(n-N/3)-\bar{a}(n)}{2}f\triangle\right) \\ &\quad - \sum_{n=0}^{N-1} X(f,\ n)X^*(f,\ n-N/3)\Psi\left(\frac{1-\bar{a}(n)}{2}f\triangle\right) \\ &\quad \cdot\Psi^*\left(\frac{1-\bar{a}(n-N/3)}{2}f\triangle\right)\Big]\Big\} \\ &\quad -4 \text{ Re } \Big\{e^{j4\pi fT/3} \cdot [\ |E\{V_a(f)\Big\}|^2 \\ &\quad + \sum_{n=0}^{N-1} X(f,\ n)X^*(f,\ n-2N/3)\Psi\left(\frac{\bar{a}(n-2N/3)-\bar{a}(n)}{2}f\triangle\right) \\ &\quad - \sum_{n=0}^{N-1} X(f,\ n)X^*(f,\ n-N/3)\Psi\left(\frac{1-\bar{a}(n)}{2}f\triangle\right) \\ &\quad \cdot\Psi^*\left(\frac{1-\bar{a}(n-2N/3)}{2}f\triangle\right)\Big]\Big\} \\ &\quad +2 \text{ Re } \Big\{e^{j2\pi fT/3} \cdot [\ |E\{V_a(f)\Big\}|^2 \\ &\quad + \sum_{n=0}^{N-1} X(f,\ n-N/3)X^*(f,\ n-2N/3) \\ &\quad \cdot\Psi\left(\frac{\bar{a}(n-2N/3)-\bar{a}(n-N/3)}{2}f\triangle\right) \end{aligned}$$

$$-\sum_{n=0}^{N-1} X(f,\ n)X^*(f,\ n-N/3)\Psi\left(\frac{1-\bar{a}(n-N/3)}{2}f\triangle\right)$$
$$\cdot\Psi^*\left(\frac{1-\bar{a}(n-2N/3)}{2}f\triangle\right)\Bigg]\Bigg\} \quad (4.63)$$

Assuming even $p(\theta)$, the continuous power spectrum is found by taking the indicated expectations over the $3N$ joint variables in $\theta^a$, $\theta^b$, and $\theta^c$; combining (4.59) and (4.63) gives

$$\begin{aligned}
S_{c\ell n} &= \frac{1}{T}[E\{|V_{an}|^2\} - |E\{V_{an}\}|^2] \\
&= \frac{1}{9T(\pi f)^2}\sum_{n=0}^{N-1}\Bigg[6\sin^2(\pi f\bar{a}(n)\triangle)\left(1-\Psi^2\left(\frac{1-\bar{a}(n)}{2}f\triangle\right)\right) \\
&\quad -4\sin(\pi f\bar{a}(n)\triangle)\sin(\pi f\bar{a}(n-N/3)\triangle) \\
&\quad \cdot\left(\Psi\left(\frac{\bar{a}(n-N/3)-\bar{a}(n)}{2}f\triangle\right)-\Psi\left(\frac{1-\bar{a}(n)}{2}f\triangle\right)\Psi\left(\frac{1-\bar{a}(n-N/3)}{2}f\triangle\right)\right) \\
&\quad -4\sin(\pi f\bar{a}(n)\triangle)\sin(\pi f\bar{a}(n-2N/3)\triangle) \\
&\quad \cdot\left(\Psi\left(\frac{\bar{a}(n-2N/3)-\bar{a}(n)}{2}f\triangle\right)-\Psi\left(\frac{1-\bar{a}(n)}{2}f\triangle\right)\Psi\left(\frac{1-\bar{a}(n-2N/3)}{2}f\triangle\right)\right) \\
&\quad +2\sin(\pi f\bar{a}(n-N/3)\triangle)\sin(\pi f\bar{a}(n-2N/3)\triangle) \\
&\quad \cdot\Bigg(\Psi\left(\frac{\bar{a}(n-2n/3)-\bar{a}(n-N/3)}{2}f\triangle\right) \\
&\quad -\Psi\left(\frac{1-\bar{a}(n-N/3)}{2}f\triangle\right)\Psi\left(\frac{1-\bar{a}(n-2N/3)}{2}f\triangle\right)\Bigg)\Bigg] \qquad (4.64)
\end{aligned}$$

wherein for $p(\theta)=\frac{1}{2}[\delta(\theta+1)+\delta(\theta-1)]$, $\Psi(f)=\cos 2\pi f$. For this $p(\theta)$, we have $\Psi(\alpha-\beta)-\Psi(\alpha)\Psi(\beta)=\sin(2\pi\alpha)\sin(2\pi\beta)$.

### 4.4.3 Verification of Spectral Formulas

An experimental system with a power MOSFET-based inverter has been built and investigated by S. Legowski[1] to verify the spectral formulas derived in the previous sections. An excellent agreement between the theoretical and the experimental results has been obtained as shown in the following examples.

Theoretical harmonic spectra of the output line-to-line voltage of the inverter at modulation index $m = 1$ and fundamental frequency $f_0 = 50$ Hz, along with the actual microprocessor controlled inverter output, are shown in figures 4.9 through 4.12. The following equations (symmetrical modulation) are used to compute the required duty ratio $a$, $b$, and $c$.

$$\bar{a}(n) = [1 + mF(\alpha_n)]/2$$

$$\bar{b}(n) = [1 + mF(\alpha_n - 120°)]/2$$

$$\bar{c}(n) = [1 + mF(\alpha_n - 240°)]/2$$

Two different modulation modes were used in the examples. They are the lead-lag (Bernoulli probability density) and the random location (uniform probability density) as defined in the previous section. The modulating functions used are the sinusoidal and trapezoidal functions. Figure 4.9, 4.10, and 4.11 show the line-to-line spectra using the trapezoidal modulation with the lead-lag mode randomization. The number of switching intervals was set at $N = 48$ (figure 4.9), $N = 120$ (figure 4.10) and $N = 480$ (figure 4.11). Trapezoidal modulation with uniform mode randomization ($N = 48$) is shown in figure 4.12.

Figure 4.13 shows the line-to-line discrete spectrum of the inverter using the

[1]Department of Electrical Engineering, University of Wyoming, USA

classical sinusoidal PWM (N=48). Notice that the spectrum contains a low-order harmonic close to the fundamental. In theory sinusoidal PWM should not generate any low-order harmonics. Due to the non-ideal nature of the switching device, it is possible to get low-order harmonic in the sinusoidal PWM inverter in practice.

To illustrate the effect of randomized modulation, the spectra for the sinusoidal modulation with lead-lag mode and uniform mode are shown in figure 4.14 and 4.15, respectively. The parameters used are the same as in the classical sinusoidal PWM. We can see that the harmonic power are reduced at the expense of introducing a continuous spectrum in the RPWM technique. In this case random modulation is not necessarily disadvantageous, since the spectrum can be significantly altered by a proper choice of modulation parameters or modulation statistics. Figures 4.9 to 4.11 illustrate that the central frequencies of the harmonic clusters can be controlled by adjusting the number of switching intervals. Figures 4.12 and 4.15 both show that the uniform mode spreads the continuous part of the spectra uniformly.

Figures 4.16 to 4.21 show the line-to-neutral spectra using the same set of parameters used in the previous examples on the line-to-line spectra (see figure 4.9 to 4.11). By comparing figure 4.9 to figure 4.16, or figure 4.10 to figure 4.17, or figure 4.11 to figure 4.18, we can see that the relation between the line-to-line and line-to-neutral voltage, i.e. $V_{ab} = \sqrt{3}V_{an}$, is verified.

The spectral formulas derived in this chapter are equations (4.50) and (4.52) for the discrete and continuous line-to-line spectra, respectively. Equations (4.61) and (4.64) are for the discrete and continuous line-to-neutral spectra. They have been implemented in the MATLAB software package contained in the Appendix (see m-file rpwm.m).

### 4.4.4 Optimal Solution Formulation

In this thesis, we have considered only two special forms of PDF to determine the pulse position in its switching interval. However we would like to show that the PDF can be generalized by having both the pulse position and the probability weight as random variables. The mathematical expression describing such a generalized PDF can be written as

$$p(\theta) = \sum_{i=1}^{I} p(\theta_i)\delta(\theta - \theta_i) \tag{4.65}$$

where $I$ is the number of PDF weights used, $p(\theta_i) \geq 0$ and $p(\theta_i)$ must be real and even. Further, $p(\theta_i)$ must satisfy the condition $\sum_{i=1}^{I} p(\theta_i) = 1$ in order to be a valid PDF. For instance, the Bernoulli randomization will give $p(\theta_i) = \frac{1}{2}$ and $\theta_i = -1, +1$ where $i = 1, 2$.

If we examine the line-to-line harmonic spectral formulas for both the continuous spectrum (4.50) and the discrete harmonic power spectrum (4.52), repeated below for convenience, we see that they are coupled by the term $\Psi(\cdot)$, where $\Psi(f) = \int_{-\infty}^{\infty} p(\theta)e^{-j2\pi f\theta}d\theta$ is the Fourier transform of the probability density function $p(\theta)$.

The continuous line-to-line spectrum is

$$\begin{aligned}
S_{c\ell\ell} &= \frac{1}{T}[E\{|V_{ab}|^2\} - |E\{V_{ab}\}|^2] \\
&= \frac{2}{T}\sum_{n=0}^{N-1} \frac{\sin^2(\pi f\bar{a}(n)\triangle)}{(\pi f)^2}\left(1 - \Psi^2\left(\frac{1-\bar{a}(n)}{2}f\triangle\right)\right) \\
&\quad + \frac{2}{T}\sum_{n=0}^{N-1} \frac{\sin(\pi f\bar{a}(n)\triangle)\sin(\pi f\bar{a}(n-N/3)\triangle)}{(\pi f)^2} \\
&\quad \cdot \left[\Psi\left(\frac{\bar{a}(n-N/3)-\bar{a}(n)}{2}f\triangle\right)\right. \\
&\quad \left. -\Psi\left(\frac{1-\bar{a}(n)}{2}f\triangle\right)\Psi\left(\frac{1-\bar{a}(n-N/3)}{2}f\triangle\right)\right]
\end{aligned} \tag{4.66}$$

The $k$th harmonic power spectrum is

$$P_{\ell\ell}(k) = \frac{4}{(\pi k)^2}(1-\cos(2\pi k/3)) \cdot \left| \sum_{n=0}^{N-1} \sin(\pi k \bar{a}(n)/N) e^{-j2\pi \frac{nk}{N}} \Psi\left(\frac{1-\bar{a}(n)}{2} \ \frac{k}{N}\right)\right|^2 . \tag{4.67}$$

There is no obvious solution for $p(\theta)$ such that the fundamental-to-harmonic power ratio is maximized. Finding $\Psi(\cdot)$ from the above formulas involves the use of constrained optimization theory. Our attempt to solve such a constrained optimization problem can be outlined as follows.

We want to find a function $\Psi_i(f) = p(\theta_i)e^{-j2\pi f\theta_i}$ in the frequency domain that minimizes the following cost function

$$\mathbf{J} = |\mathbf{S} - \mathbf{E}\mathbf{p}|^2 \tag{4.68}$$

where $\mathbf{S} = S(n,k) = \sum_{n=0}^{N-1} \sin(\pi k \bar{a}(n)/N) e^{-j2\pi \frac{nk}{N}}$ is the first term after the summation sign in the discrete formula. Using $\Psi_i(f) = p(\theta_i)e^{-j2\pi f\theta_i}$, the $\mathbf{E}$ and $\mathbf{p}$ terms are defined as follows.

For a single PDF term, we have

$$\Psi_i\left(\frac{1-\bar{a}(n)}{2} \ \frac{k}{N}\right) = p(\theta_i)e^{-j2\pi \frac{1-\bar{a}(n)}{2} \ \frac{k}{N}\theta_i} \tag{4.69}$$

Therefore the generalized PDF is

$$\Psi\left(\frac{1-\bar{a}(n)}{2} \ \frac{k}{N}\right) = \sum_{i=1}^{I} p(\theta_i)e^{-j\pi(1-\bar{a}(n)) \ \frac{k}{N}\theta_i} \tag{4.70}$$

We then let $\mathbf{E} = E_k(n,i) = e^{-j\pi(1-\bar{a}(n)) \ \frac{k}{N}\theta_i}$ and $\mathbf{p} = \sum_{i=1}^{I} p(\theta_i)$. As stated before the cost function is subject to satisfy the following constraints: $\sum_{i=1}^{I} p(\theta_i) = 1$, $p(\theta_i) \geq 0$ and real.

We can form an augmented cost functional by augmenting the cost function of the objective function $\mathbf{J}$ by the above constraints via Lagrange's multipliers $C_1$ and $\mathbf{C_2}$, where $C_1$ is a scalar used to satisfy the constraint $\sum_{i=1}^{I} p(\theta_i) = 1$ and $\mathbf{C_2}$ is a column vector for satisfying $p(\theta_i) \geq 0$. Both $C_1$ and $\mathbf{C_2}$ are constants to be determined.

Hence the objective function becomes

$$\mathbf{J} = |\mathbf{S} - \mathbf{E}\mathbf{p}|^2 - 2C_1\mathbf{1}^T\mathbf{p} - 2\mathbf{C_2}^T\mathbf{p} \tag{4.71}$$

where $\mathbf{1}^T$ is the transpose of a unity column vector of length I and the constant two is introduced for mathematical convenience.

### 4.4.5 Summary

The RPWM inverter output waveform is described in the form of a random pulse train. The pulse width is deterministic, and is described by the known modulating functions. Three modulating functions have been described. They are the sinusoidal, trapezoidal, and harmonic functions. It has been found that the trapezoidal modulating function results in the highest fundamental output current. The random pulse position modulation (RPPM) is described in terms of the random variable $\theta_n$. Two different types of position modulation modes were described. The lead-lag mode is described by means of a Bernoulli random variable, which gives only two pulse positions that can either be leading or trailing within each modulation interval. The randomized location is described in terms of a uniform probability density function.

The power spectral density of the random pulse train was given. The spectrum has a continuous part (power per Hz) and a discrete part with finite power (infinite

density) at harmonics of the fundamental $1/(N\triangle)$ Hz. The discrete components other than the fundamental represent wasted power. It is the main concern for the designer to reduce the unwanted discrete harmonic components at the PWM inverter output.

The derived formulas for a single switching variable were plotted for three different values of the switching interval. It has been confirmed that the higher number of switches within a modulation period, the lower the number of the low-order harmonics. The closed-form formulations for the line-to-line and line-to-neutral harmonic power spectra of the inverter have been derived. The formulas produce spectra which are in excellent agreement with the experimental results obtained for a typical trapezoidal modulation of the line-to-line output spectra.

Finally, the closed-form expressions for the power spectra of an RPPM inverter provide the key for optimization and design of the spectra so that without implementation and experimentation, the best compromise between the harmonic distortion and continuous noise of the output voltage is reached.

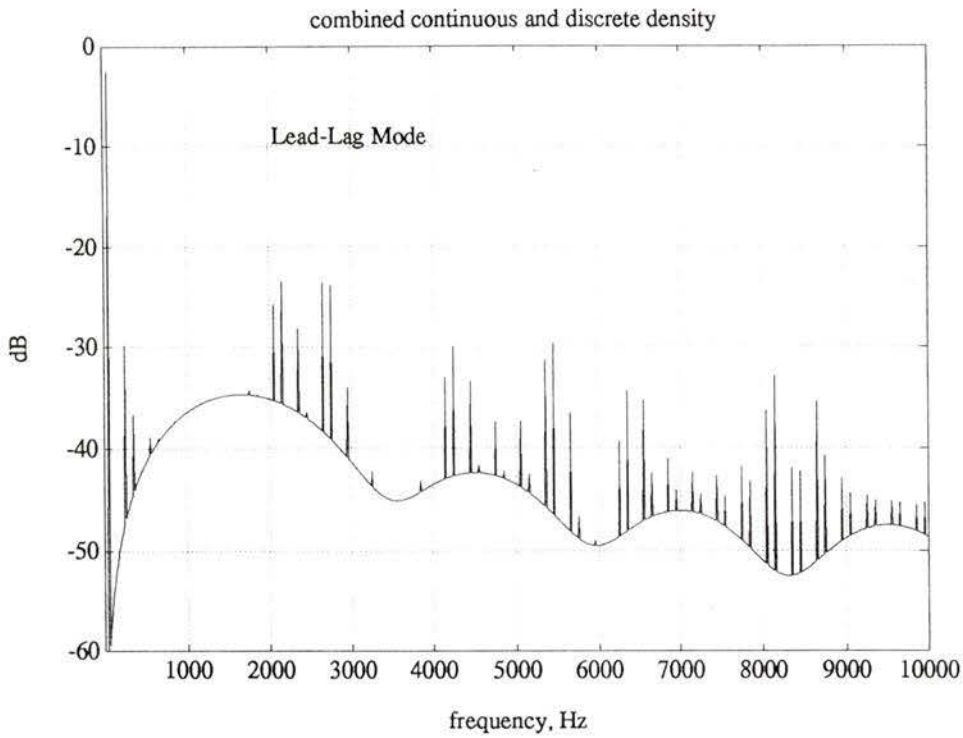


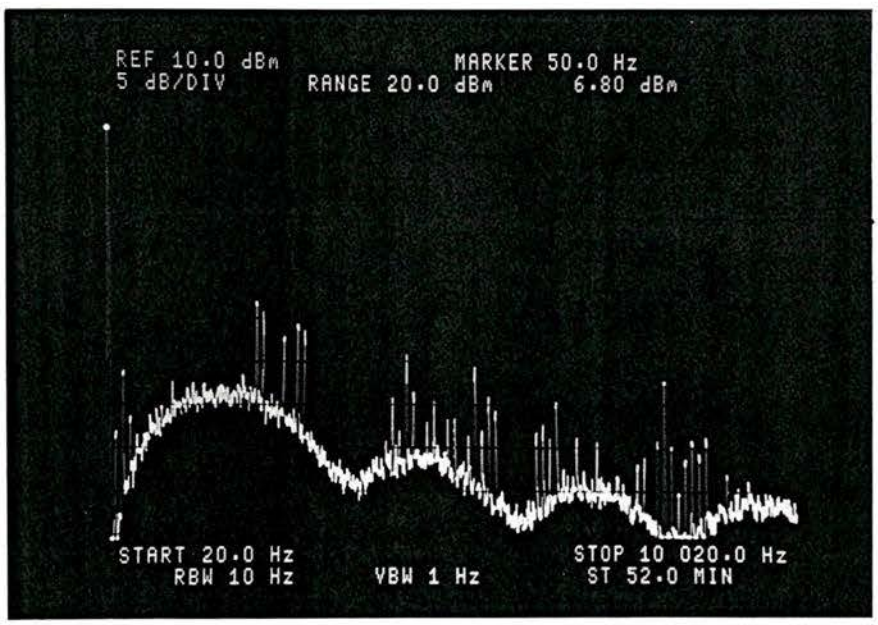


Figure 4.9: Trapezoidal Modulation (Lead-Lag Mode) N=48 m=1 fo=50Hz.

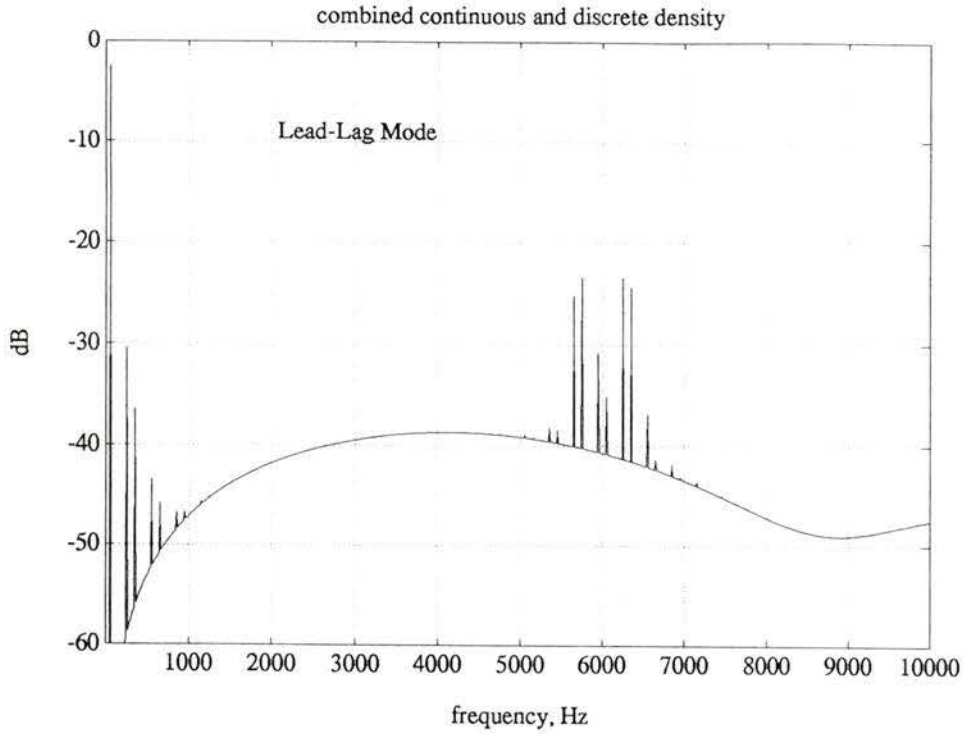


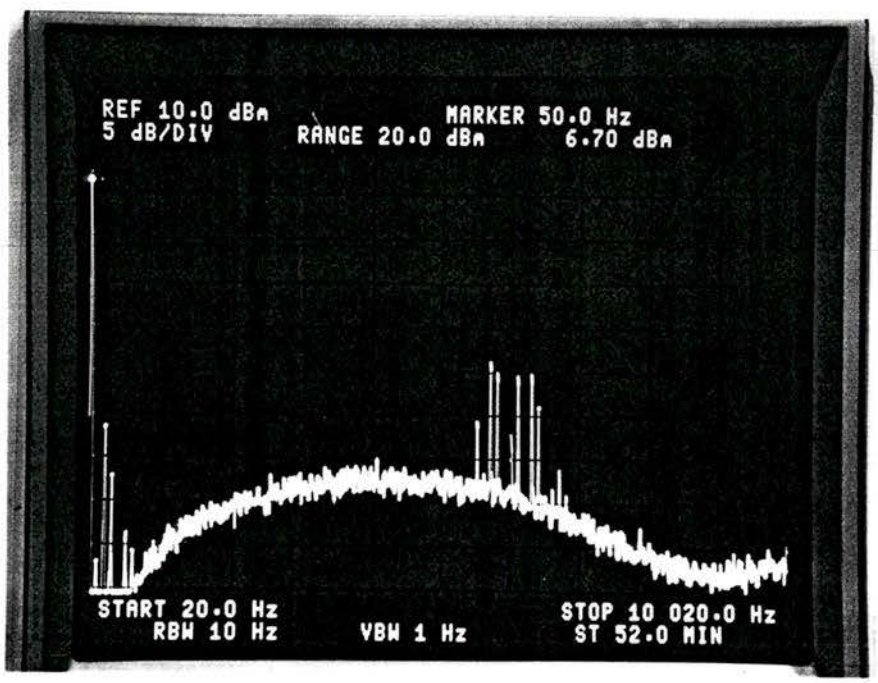


Figure 4.10: Trapezoidal Modulation (Lead-Lag Mode) N=120 m=1 fo=50Hz.

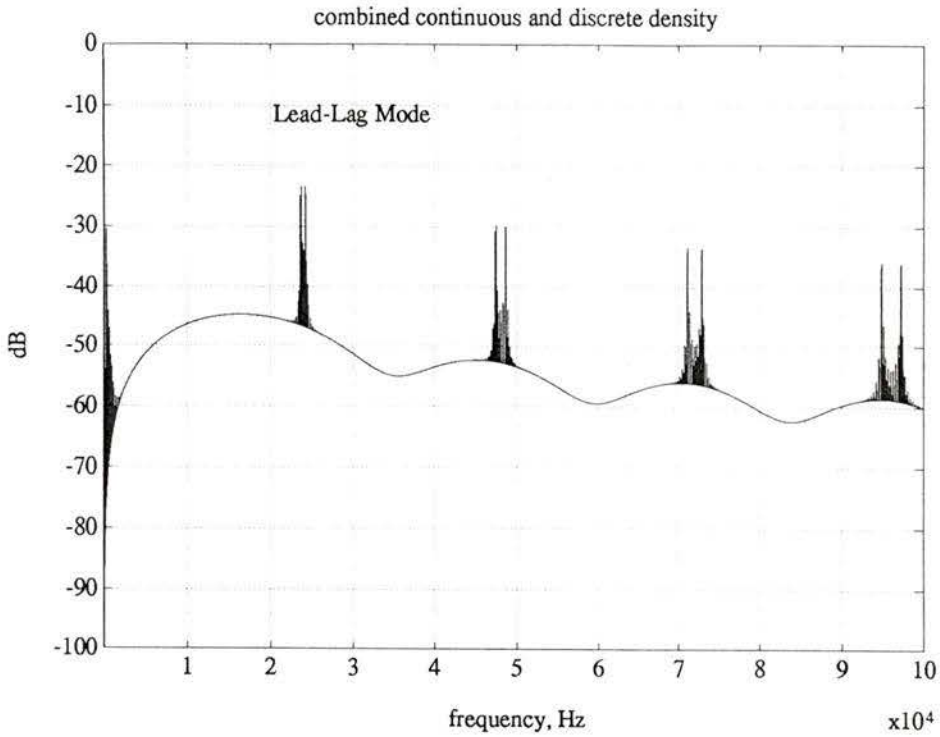


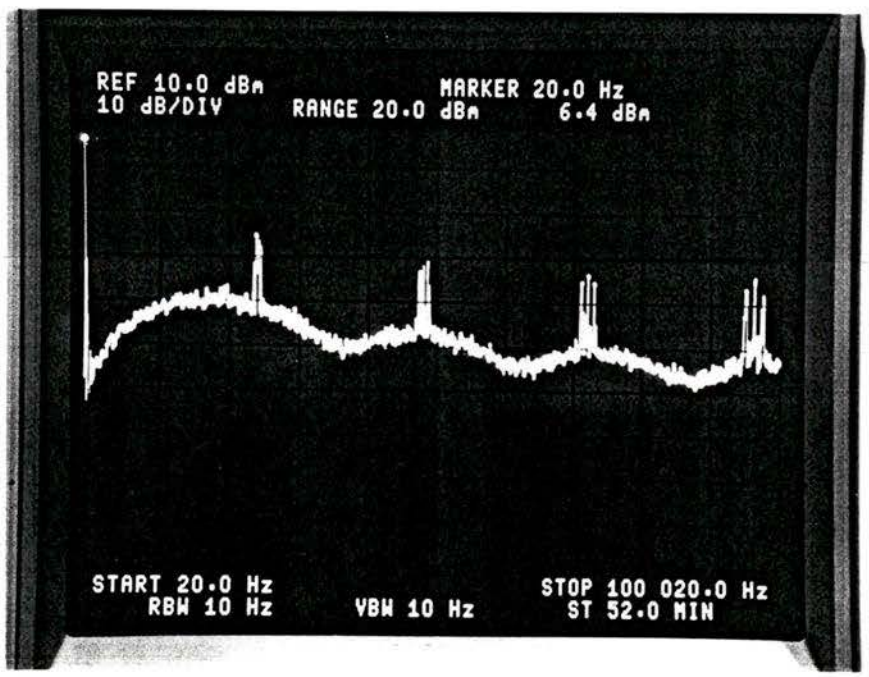


Figure 4.11: Trapezoidal Modulation (Lead-Lag Mode) N=480 m=1 fo=50Hz.

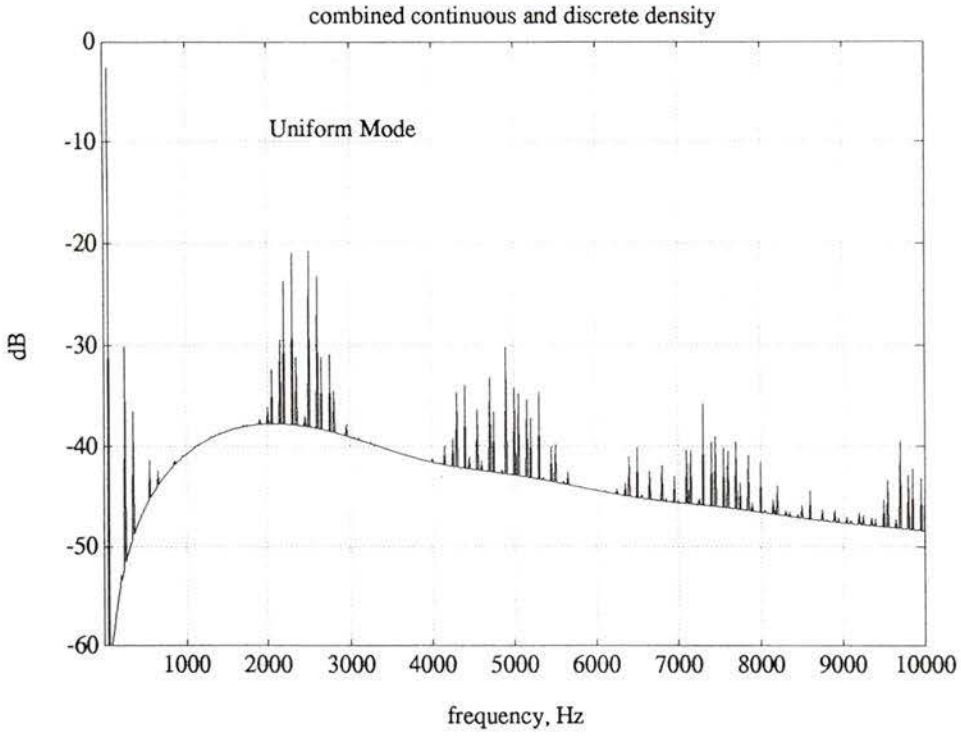


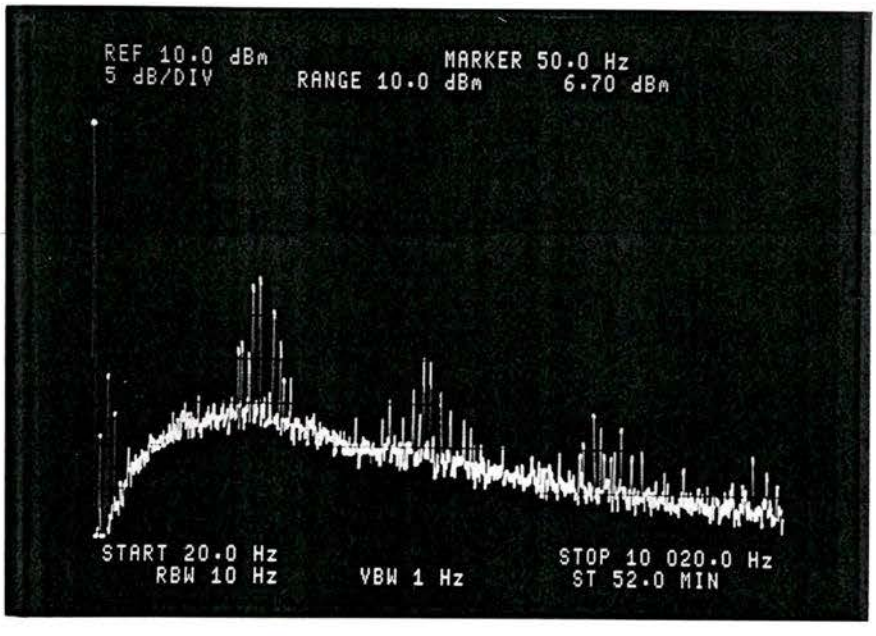


Figure 4.12: Trapezoidal Modulation (Random Location) N=48 m=1 fo=50Hz.

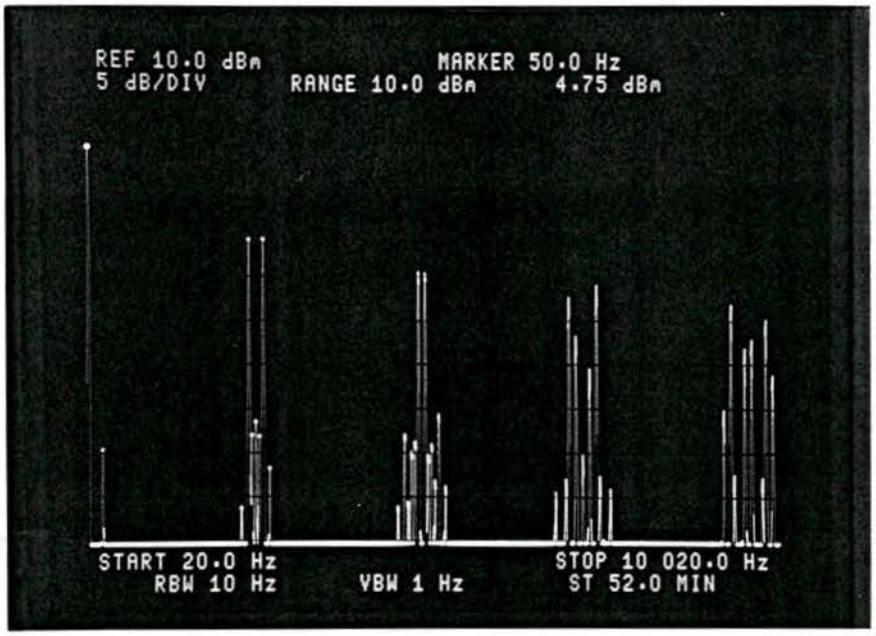


Figure 4.13: Classical Sinusoidal Modulation N=48 m=1 fo=50Hz.

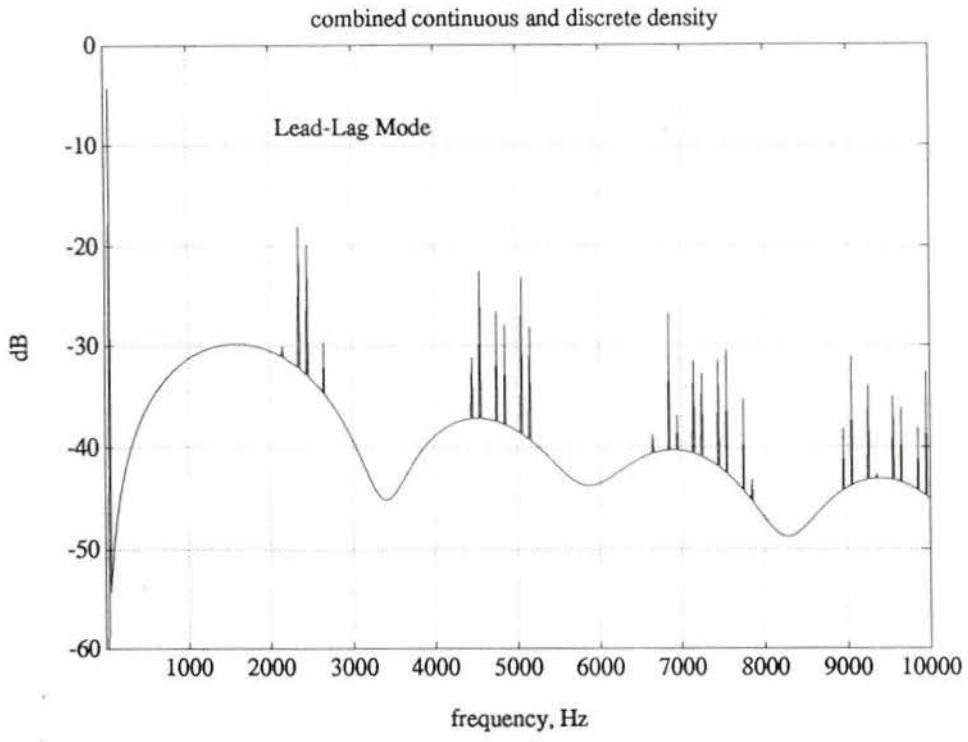


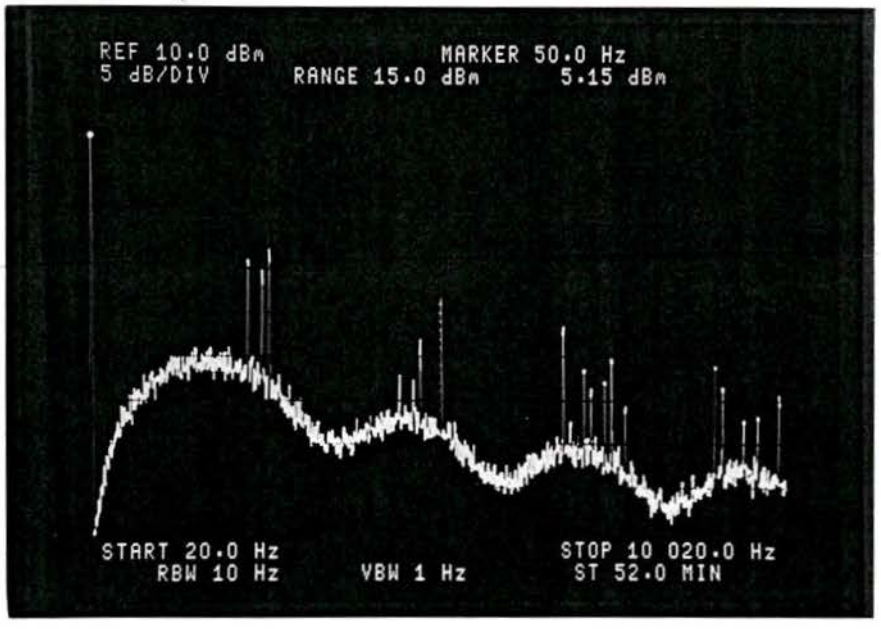


Figure 4.14: Sinusoidal Modulation (Lead-Lag Mode) N=48 m=1 fo=50Hz.

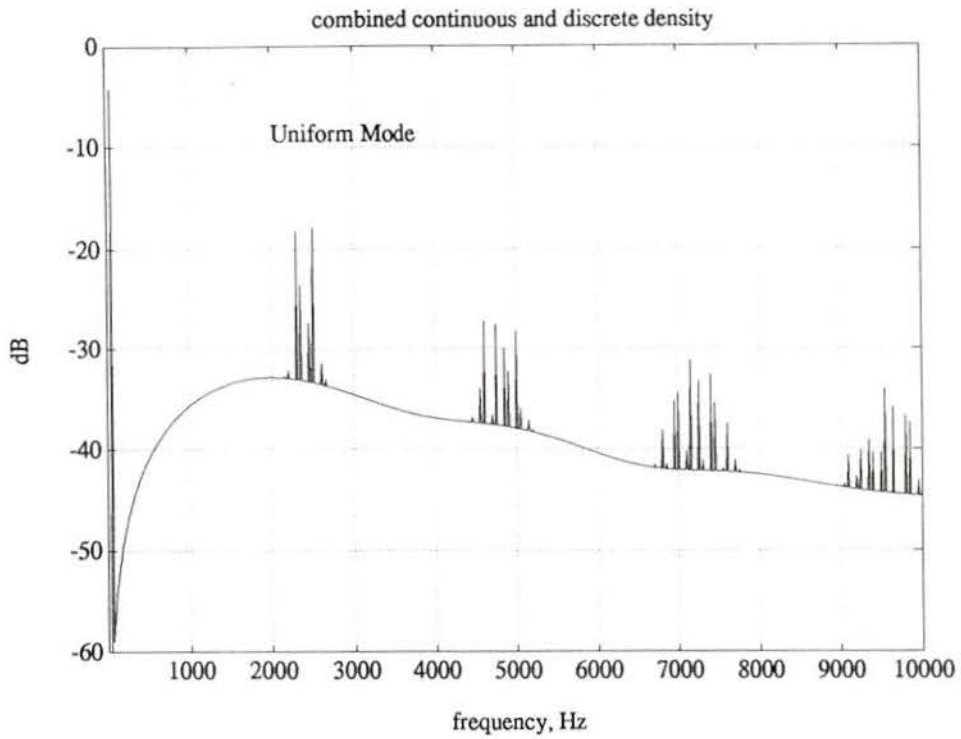


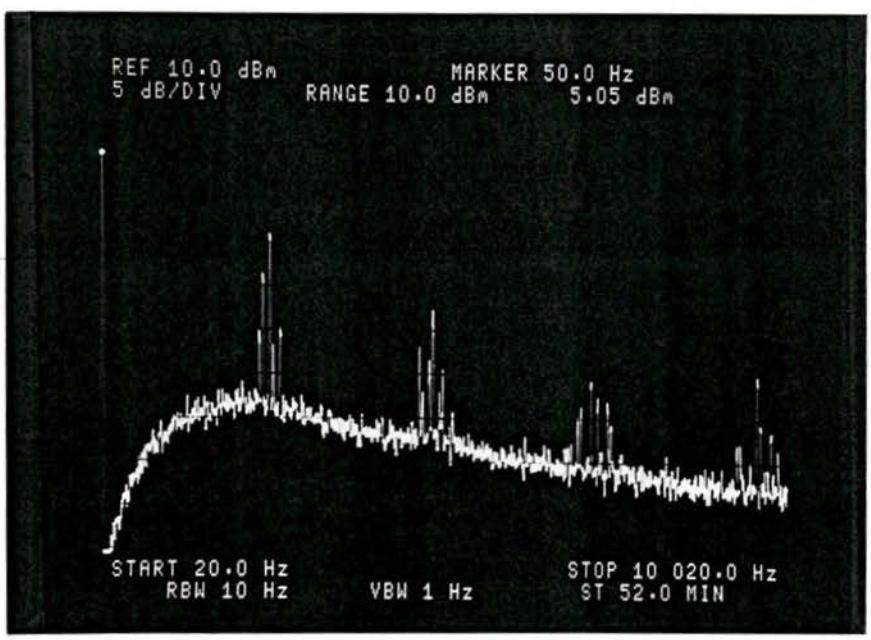


Figure 4.15: Sinusoidal Modulation (Random Location) N=48 m=1 fo=50Hz.

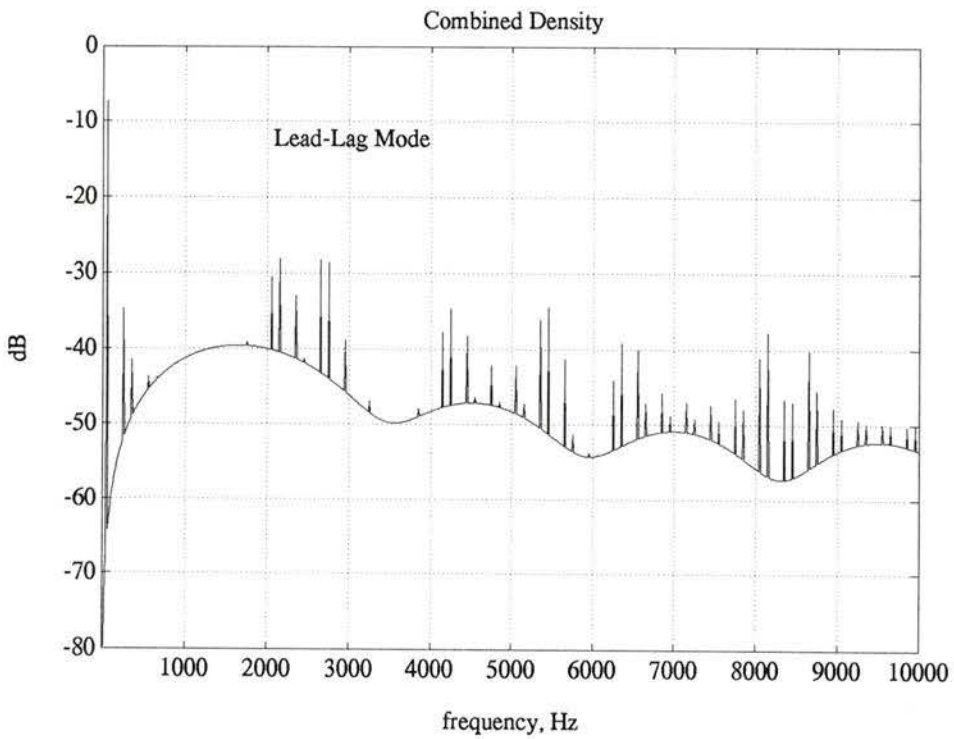


Figure 4.16: Trapezoidal Modulation, Line-to-Neutral (N=48).

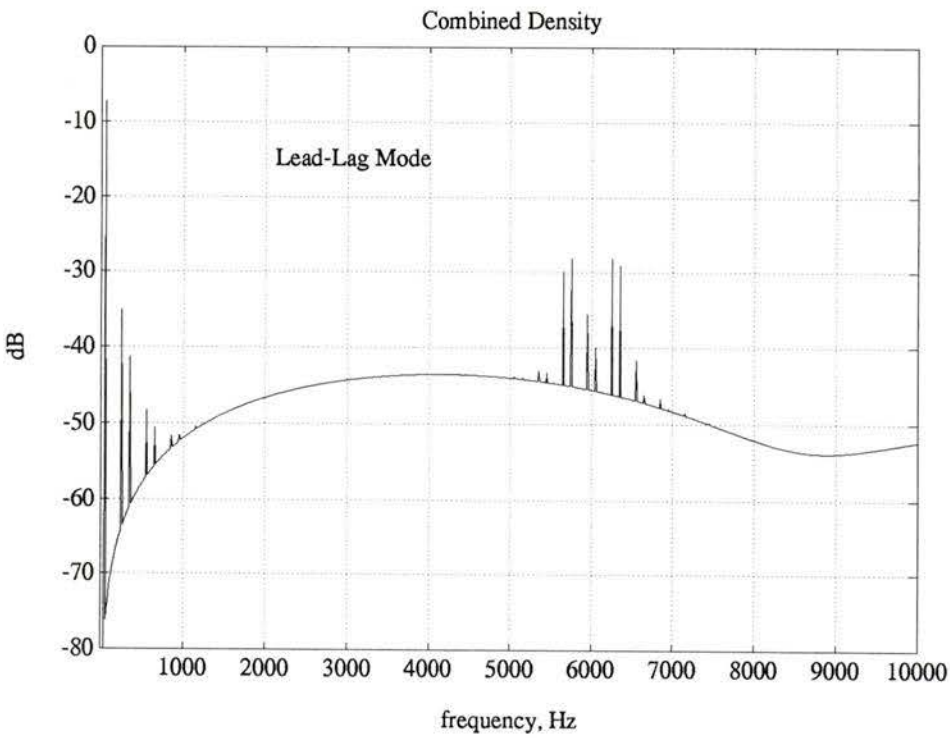


Figure 4.17: Trapezoidal Modulation, Line-to-Neutral (N=120).

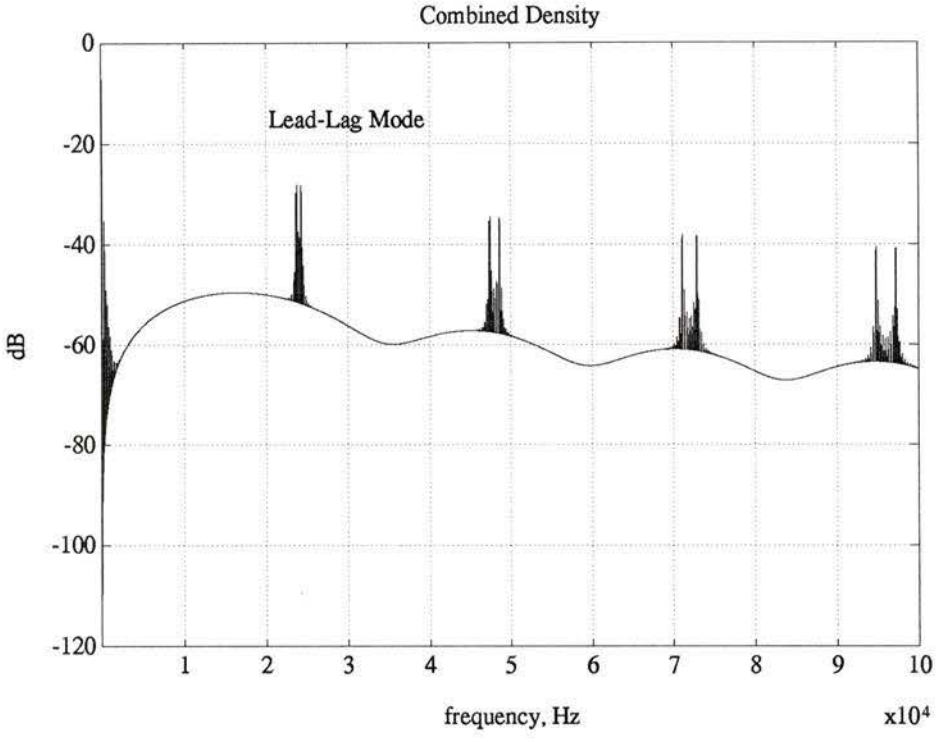


Figure 4.18: Trapezoidal Modulation, Line-to-Neutral (N=480).

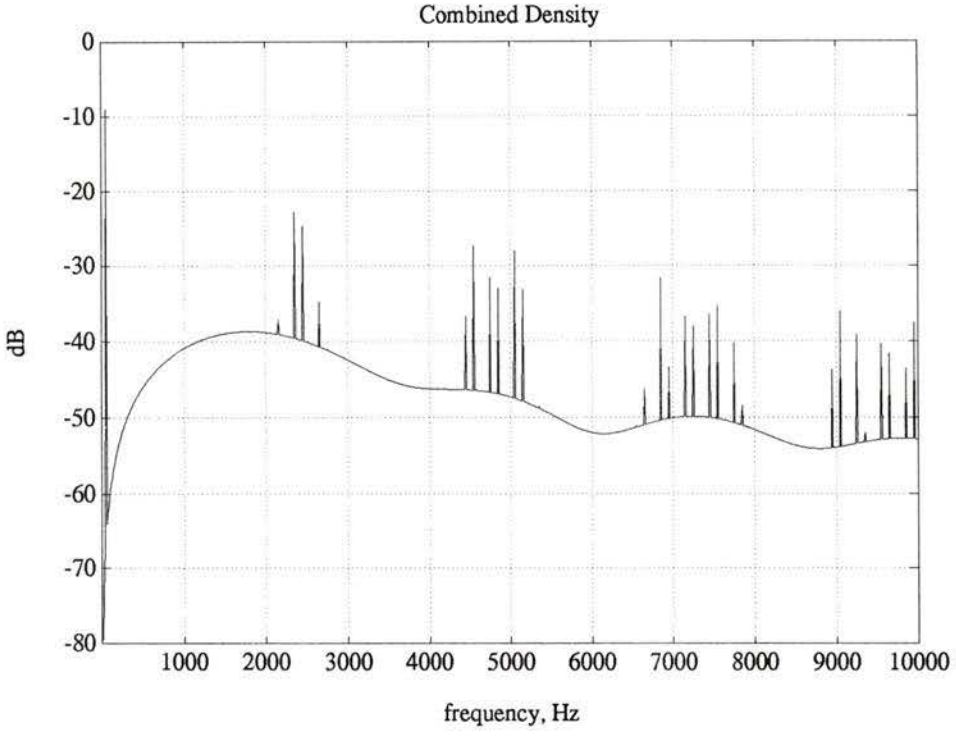


Figure 4.19: Sinusoidal Modulation (Lead-Lag Mode), Line-to-Neutral (N=48).

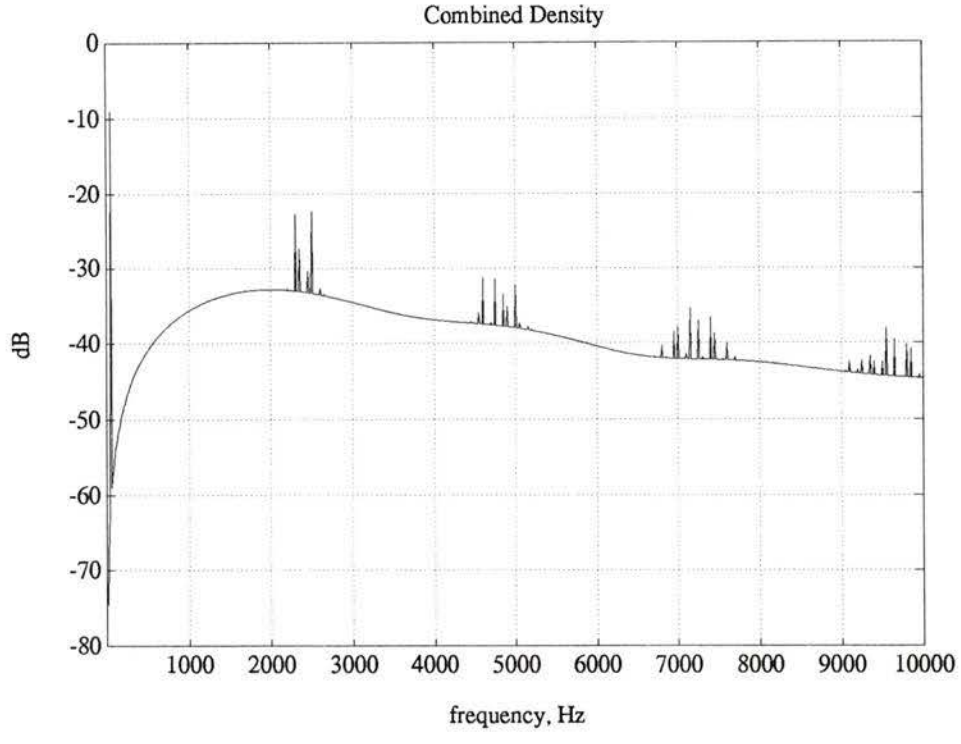


Figure 4.20: Sinusoidal Modulation (Random Location), Line-to-Neutral (N=48).

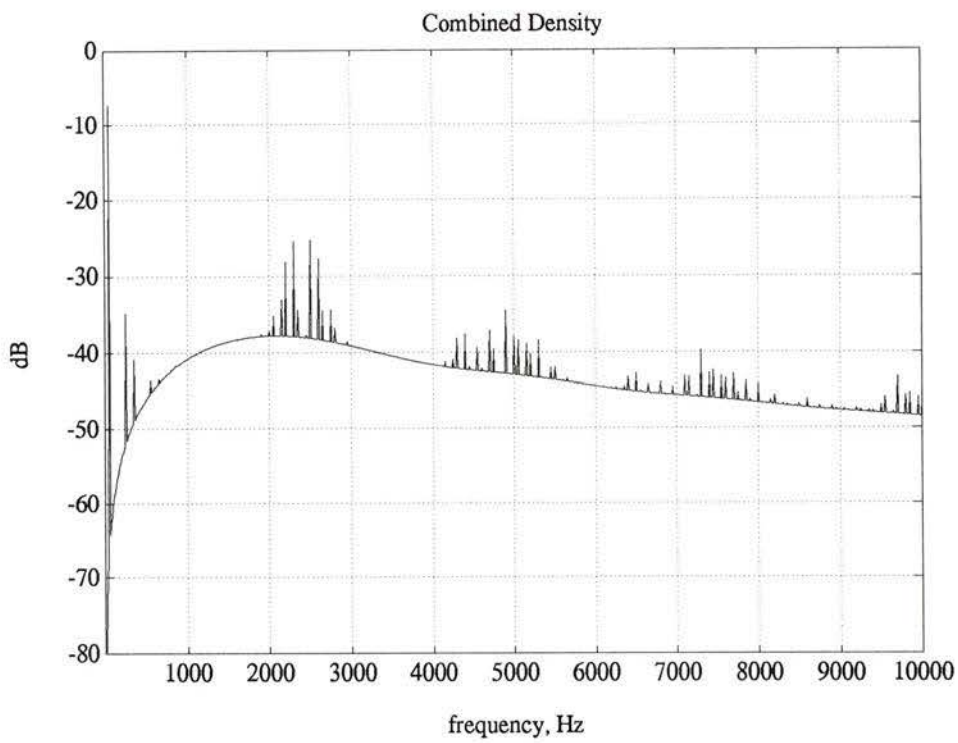


Figure 4.21: Trapezoidal Modulation (Random Location), Line-to-Neutral (N=48).

# Chapter 5

# Summary and Future Work

## 5.1 Summary

In this thesis we have studied and analyzed the effect of randomized switching strategies on the PWM d.c./a.c. inverter. We have first reviewed the deterministic PWM method in inverter control. We pointed out that the resulting PWM inverter output harmonic spectrum is characterized by distinct clusters of higher harmonic power. Most systems supplied from the inverter possess a frequency-dependent sensitivity to these harmonics. The typical adverse effects include an annoying tonal noise, resonant vibrations and electromagnetic interference (EMI).

Next, we have described an improved method called RPWM, which is based on randomized modulation. In particular, we have described two different schemes to randomly modulate the pulse position in its switching interval. They are called lead-lag and uniform randomization modes. The pulse widths are known *apriori* for both methods; they are a function of the desired a.c. waveform. In the lead-lag

mode the pulse can either occur at the beginning or at the end of the switching interval. In the uniform mode the pulse can be at any discrete location within the switching interval. These two randomization modes are described mathematically by the Bernoulli (lead-lag mode) and the uniform (uniform mode) probability density functions. The suppression of the low-order harmonics is due to the non-periodic nature of the switching pattern generated by RPWM. Different switching patterns generate different harmonic profiles. As a result, the harmonic power spectrum of the RPWM inverter tends to spread over a wider frequency range. This improves noise and vibration characteristics for a drive system supplied from an inverter.

We have also presented methods, based on the stochastic signal analysis and Fourier analysis techniques, for analyzing the RPWM schemes described in this thesis. The advantages of employing RPWM method for inverter control have been confirmed in practice by a number of researchers. Specifically the closed-form formulas presented in this thesis have theoretically confirmed the inverter harmonic power spectra obtained from the experimental results publised by A.M. Trzynadlowski and S. Legowski [2, 3, 6].

The closed-form expressions for the power spectra of a RPWM inverter are formulated in a way that is suitable for employing optimization techniques. The formulations provide the key for finding optimal design parameters, namely the probability density function and switching rate required to satisfy a given set of circuit operating constraints or spectral features. This can be accomplished without implementation and experimentation.

## 5.2 Suggestions for Future Work

The analysis and spectral formulas presented in this thesis provide the basis for further study in optimal design for randomized PWM control of power converters. Rather than using $ad - hoc$ design methods to minimize inverter harmonic power spectra, we can maximize the fundamental-to-harmonic power ratio by finding an optimal probability density function (PDF) in our analytical formulas. We suggest that the general analytical method presented in this thesis can also be applied to other PWM power converters (e.g. d.c. choppers) which employ similar randomization schemes.

It is worth mentioning that it is a difficult problem to determine the optimum PDF in the general case. The optimization formulation outlined in Chapter 4 (Section 4.4.4) remains a research problem.

Finally, it would be interesting to investigate the effect on the output power spectra of randomizing the width of the switching intervals $\triangle$t, and/or the number of switching intervals N over the switching period. Power spectral formulas can be derived using the analytical approach described in this thesis.

# Bibliography


[1] A.M. Trzynadlowski, S. Legowski, and R.L. Kirlin, "Random pulse width modulation technique for voltage-controlled power inverters," *International Journal of Electronics*, vol. 68, no. 6, 1990, pp.1027-1037.

[2] S. Legowski and A.M. Trzynadlowski, "Hypersonic MOSFET-based power inverter with random pulse width modulation," in *Conf. Rec. IEEE-IAS 1989 Ann. Mtg.*, pp.901-903.

[3] S. Legowski and A.M. Trzynadlowski, "Power-MOSFET, hypersonic inverter with high quality output current," in *Proc. APEC'90,* pp.3-7.

[4] A.M. Trzynadlowski, "Nonsinusoidal modulating functions for three-phase inverters," *IEEE Trans. on Power Electronics,* vol. 4, no. 3, 1989, pp. 331-338.

[5] S. Legowski and A.M. Trzynadlowski, "Advanced random pulse width modulation technique for voltage-controlled inverter drive system," in *Proc. APEC'91,* pp.100-106.

[6] S. Legowski and A.M. Trzynadlowski, "Analysis and implementation of a grey-noise PWM technique based on voltage space vectors," in *Proc. APEC'92,* pp.586-593.

[7] R.L. Kirlin, S. Kwok, S. Legowski and A.M. Trzynadlowski, "Power Spectra of a PWM Inverter with Randomized Pulse Position" in *Proc. PESC'93,* pp.1041-1047.

[8] T.G. Habetler and D.M. Divan, "Acoustic noise reduction in sinusoidal pwm drives using a randomly modulated carrier," IEEE Trans. on Power Electronics, vol.6, no.3, July 1991, pp. 356-363.

[9] T. Daly, "New technology makes power MOSFETs faster, more efficient," Powerconversion and Intelligent Motion, vol.14, no.1, 1988, pp.14-18.

[10] H.S. Patel and R.G. Hoft, "Generalized techniques of harmonic elimination and voltage control in thyristor inverters : Part I - harmonic elimination," *IEEE Trans. on Ind. Appl.,* IA-9(3):310-317, May 1973.

[11] H.S. Patel and R.G. Hoft, "Generalized techniques of harmonic elimination and voltage control in thyristor inverters : Part II - voltage control techniques," *IEEE Trans. on Ind. Appl.,* IA-10(5):666-673, Sept. 1974.

[12] K.A. Krishnamurthy, S.B. Mahajan, G.N. Revankar and G.K. Dubey, "Selective reduction of harmonics in inverters," *Int. Jour. of Electronics,* vol.46, 1979, pp.321-330.

[13] I. Takahashi and H. Machikawa, "A new control of PWM waveform for minimum loss operation of an induction motor drive," *IEEE Trans. on Ind. Appl.,* vol. IA-21, May-June 1985, pp.580-587.

[14] F.C. Zach and H. Ertl, "Efficiency optimal control for ac drives with PWM

inverters," *IEEE Trans. on Ind. Appl.,* vol. IA-21, July-Aug. 1985, pp.987-1000.

[15] F.C. Zach, R.Martinez, S. Keplinger, and A. Seiser, "Dynamically optimal switching patterns for PWM inverter drives (for minimization of the torque and speed ripples)," *IEEE Trans. on Ind. Appl.,* vol. IA-21, July-Aug. 1985, pp.975-986.

[16] B.K. Bose, "Adjustable speed ac drives - a technology status review," *Microcomputer Control of Power Electronics and Drives*, IEEE Press, 1987.

[17] S.R. Bowes, "New sinusoidal pulse width modulated inverter," *Proc. Inst. Elec. Eng.*, vol. 122, pp.1279-1285, Nov. 1975.

[18] S.R. Bowes, "Microprocessor control of PWM inverters," *IEE Proc.*, vol.128, Pt.B, no. 6, November 1981.

[19] A. Wang and S. Sanders, "Random and programmed pulse-width modulation techniques for DC-DC converters," in *Proc. IEEE 1990 Conf. on Systems Engineering*, pp.589-592.

[20] A.M. Stankovic and G.C. Verghese, "Randomized switching strategies in power converter control," Technical Report, MIT-LEES, 1992.

[21] Q. Jiang, D.G. Holmes, and D.B. Giesner, "A method for linearizing optimal PWM switching strategies to enable their computation on-line in real-time," in *Conf. Rec. IEEE-IAS Ann. Mtg.,* 1991, pp. 819-825.

[22] J.A. Houldsworth and D.A. Grant, "The use of harmonic distortion to increase the output voltage of a three-phase PWM inverter," *IEEE Trans. on Ind. Appl.,*

vol. IA-20, no. 5, 1984, pp.1224-1228.

[23] J. Holtz, P. Lammert, and W. Lotzkat, "High-speed drive system with ultrasonic MOSFET PWM inverter and single-chip microprocessor control," in *Conf. Rec. IEEE-IAS Ann. Mtg.,* 1986, pp. 12-17.

[24] J.M.D. Murphy and F.G. Turnbull. *Power Electronic Control of AC Motors,* Pergamon Press, 1988.

[25] B.K. Bose. *Power Electronics and AC Drives,* Prentice Hall, Englewood Cliffs, NJ, 1986.

[26] M.H. Rashid. *Power Electronic : Circuits, Devices, and Applications.,* Prentice Hall, Englewood Cliffs, NJ, 1988.

[27] G.K. Dubey. *Power Semiconductor Controlled Drives,* Prentice Hall, Englewood Cliffs, NJ, 1989.

[28] J.J. Stiffler. *Theory of Synchronous Communicaton,* Prentice Hall, Englewood Cliffs, 1971.

[29] A. Papoulis. *Probability, Random Variables and Stochastic Processes.* McGraw-Hill, second edition, 1984.

[30] A.V. Oppenheim and R.W. Schafer. *Digital Signal Processing,* Prentice Hall, 1975.

# Appendix

## MATLAB Source Code for Spectral Formulas

```
% ------------------------------------------------------------------
% This program calculates the continuous spectrum of a single phase
% output of a voltage controlled inverter.
% Trapzoidal modulating function is used.
% ------------------------------------------------------------------
% Call : continuous.m

clear, clc, clg
format long e;
N = input(' Modulation intervals (N= 48,120,480) = ');

% ------------------------------------------------------------------
% K is the number of samples in frequency domain.
% fd is the frequency interval.
% Delta is time interval between two pulses.
% N is number of intervals in a period.
% ------------------------------------------------------------------
delta=1/N;   T=N*delta;
fd=0.5;      K=1200;
m= zeros(1:N)';
% calculate the trapzoidal function
if N == 48,
    m(2:9) =  1/8*(1:8)';
    m(10:25) = ones(1:16)';
    m(26:33) = 1 -1/8*(1:8)';
    m(34:48) = zeros(1:15)';

elseif N == 120,
    m(2:21) =  1/20*(1:20)';
    m(22:61) = ones(1:40)';
    m(62:81) = 1 -1/20*(1:20)';
    m(82:120) = zeros(1:39)';

else
    m(2:81) =  1/80*(1:80)';
    m(82:241) = ones(1:160)';
    m(242:321) = 1 -1/80*(1:80)';
    m(322:480) = zeros(1:159)';
end, end, end,

s=zeros(1:K);
f=fd*(1:K)/T;
for k=1:K
 f1=0;
 fb=2*pi*delta*f(k)*(m-0.5);
```

```
 f1=0.5*cos(2*fb)'*ones(N,1)-2*(cos(pi*f(k)*delta).*cos(fb))'*ones(N,1);
s0=N*(cos(pi*f(k)*delta))^2+N/2;
 s(k)=(s0+f1)/(2*pi*f(k))^2;
end
plot(f,s);
title('The Continuous Power Spectrum')
xlabel('Frequency'), ylabel('Amplitude') pause;
plot(f,log(s));
title('The Continuous Power Spectrum - Log')
xlabel('Frequency'), ylabel('Amplitude')
```

```
% ------------------------------------------------------------------
% This program calculates the discrete spectrum of a single phase
% output of a voltage controlled inverter.
% ------------------------------------------------------------------
% Call : discrete.m

clear, clc, clg
format long e;
N = input(' Modulation intervals (N= 48,120,480) = ');
mod = input('Trapzodial(1), Sinusoidal(2), and Increased output(3) = ');

% ------------------------------------------------------------------
% K is the number of samples in frequency domain.
% fd is the frequency interval.
% Delta is time interval between two pulses.
% N is number of intervals in a period.
% ------------------------------------------------------------------

if mod == 1,        % trapzoidal modulation
   if N == 48,
      m(2:9) =  1/8*(1:8)';
      m(10:25) = ones(1:16)';
      m(26:33) = 1 -1/8*(1:8)';
      m(34:48) = zeros(1:15)';
   elseif N == 120,
      m(2:21) =  1/20*(1:20)';
      m(22:61) = ones(1:40)';
      m(62:81) = 1 -1/20*(1:20)';
      m(82:120) = zeros(1:39)';
   else
      m(2:81) =  1/80*(1:80)';
```

```
      m(82:241) = ones(1:160)';
      m(242:321) = 1 -1/80*(1:80)';
      m(322:480) = zeros(1:159)';
   end, end, end,
end,

if mod == 2,        % sinusoidal modulation
   F= zeros(1:N)';
   for n=1:N,
       F(n)=sin((n-1)*2*pi/N);
   end
   M=1;   m= M*(1+ F)/2;
end,

if mod == 3,        % increased output
   F= zeros(1:N)';
   for n=1:N,
       F(n)=2*(sin((n-1)*2*pi/N)+1/6*sin(3*((n-1)*2*pi/N)))/sqrt(3);
   end
   M=1;   m= M*(1+ F)/2;
end,

zo=exp(-j*2*pi/N);
alpha=2*pi*(m-0.5)/N;
f=(1:K)/T;
for k=1:K
  z=zo .^((0:(N-1))*k);
  alphab=sin(k*alpha);
  s(k)=(abs(z*alphab))^2/(2*(pi*k)^2);
end
axis([0 K 0 0.003]);   %
plot(f,s);
title('The Discrete Power Spectrum')
xlabel('Harmonic'), ylabel('Power'), pause;
plot(f,log(s));
title('The Discrete Power Spectrum - Log')
xlabel('Harmonic'), ylabel('Power')
```

```
% ------------------------------------------------------------------
% This program calculates both the "line-to-line" and "line-to-neutral
% discrete and continuous harmonic power spectra of a 3-phase voltage
% inverter modulated by RPWM technique.
% ------------------------------------------------------------------
% Call: rpwm.m
%
% Calls: trap.m - trapzoidal modulating function
% sine.m - sinusoidal modulating function
% increase.m - increase output modulating function
%
%
clear, clc, clg
format long e;

% ------------------------------------------------------------------
% 1.  Parameters input
% ------------------------------------------------------------------
ii = input(' Modulation index (0 < M < 1) = ');
freq= input(' Fundamental frequency in Hz = ');
flag =1;
while flag,
  N = input(' Modulation intervals (N= 48,120,480) = ');
  if (N==48) | (N==120) | (N==480),
     flag =0;
  else
     disp('  '); disp(' Error input, Please try again');
  end,
end,

% ------------------------------------------------------------------
% K is the number of samples in the frequency domain
% Delta is time interval between two pulses
% N is number of intervals in a period
% ------------------------------------------------------------------
if N == 480, K= 2000;
else  K= 200;  end

T= 1/freq;   delta= T/N;

notok = 1;
while notok,
  mt= input('"0" for trapezoidal,"1" for sinusoidal and "2" for Increased output=
  if mt == 0,
```

```
    abar=trap(ii,N); notok=0;
    axis([0 N 0 1.5]); plot(abar); title('Trapezoidal Modulation');
  elseif mt ==1,
    abar=sine(ii,N);  notok=0;
    axis([0 N 0 1.5]); plot(abar); title('Sinusoidal Modulation');
  elseif mt ==2,
    abar=increase(ii,N);  notok=0;
    axis([0 N 0 1.5]); plot(abar); title('Increased Output Modulation');
  else
    disp('  '); disp(' Error input, Please try again');
  end,
  xlabel('n'); ylabel('a'); axis;
  disp(' Hit return to continue'); pause;
end,

pdf= input('"0" for lead-lag, "1" for uniform = ');

% ------------------------------------------------------------------
% 2.  Calculation of the Harmonic Power Spectrum
% ------------------------------------------------------------------
disp('   '); disp(' Calculating the spectrum');

zo= exp(-j*2*pi/N);
alpha= pi*abar/N;
beta= pi*(1-abar)/N;       % A=1/2, T=2  (lower power on the harmonics)
%beta= pi*(1-abar)/(2*N);  % A=1, T=1  (this beta is for uniform only,
                           % otherwise same)
f=(1:K)/T;
for k=1:K,
 z= zo.^((1:N)*k);
 alphab= sin(k*alpha);

 if pdf==0,  % Bernoulli pdf
  % alphac= cos(k*beta);       % Fourier Transform of PDF
    alphac=  0.5*exp(j*k*beta) + 0.5*exp(-j*k*beta);
 end

 if pdf==1,  % Uniform pdf
    for i=1:N,          % alphac= sin(k*beta)./(k*beta);
        if beta(i)==0, alphac(i,:)=1;
        else  alphac(i,:)=sin(k*beta(i))/(k*beta(i));
        end
    end
 end
% Not implemented in Hardware
```

```
 if pdf==2,  % Triangular pdf
    for i=1:N,
        if beta(i)==0, alphac(i,:)=1;
        else  alphac(i,:)= ( sin(k*beta(i)/2) / (k*beta(i)/2) )^2;
        end
    end
 end

% Line-to-Line discrete
% ---------------------
 s(k)= (abs( sum(alphab.*z'.*alphac) ))^2 * 4/(pi*k)^2 *(1-cos(2*pi*k/3));

% Line-to-Neutral discrete
% ------------------------
% l2n= 4/(3*pi*k)^2 * (3-cos(2*pi*k/3) - 2*cos(4*pi*k/3));
% s(k)= (abs( sum(alphab.*z'.*alphac) ))^2 * l2n;

% Classical PWM
% -------------
% s(k)= (abs( sum(alphab.*z') ))^2 * 4/(pi*k)^2 *(1-cos(2*pi*k/3));

end

if N==480,
   ds2=zeros(1:10000); ds2(5:5:10000)=s;
else,
   ds2=zeros(1:1000); ds2(5:5:1000)=s;
end

axis; %
axis; %
plot(f,10*log10(max(s,1.16E-5))); grid;
title('Harmonic Power Spectrum (line-to-line)')
xlabel('Harmonic Number')
ylabel('dB')

%clear K f s k
disp(' Hit Return to see the continuous spectrum ');
pause;
l_or_n= input('"0" for line-to-line and "1" for line-to-neutral = ');
line_to_line = 0; line_to_neutral = 0;

if l_or_n == 0,
   line_to_line = 1;
else
```

```
   line_to_neutral = 1;
end,
% phase B is 120 degree phase shift with respect to phase A
% phase C is 240 degree phase shift with respect to phase A
bbar= [abar(N*2/3:N); abar(1:N*2/3-1)];
cbar= [abar(N/3:N); abar(1:N/3-1)];

if N == 480, K= 10000;
else  K= 1000;  end
fd= 10/freq;
% ---------------------------------------------------------------
% 3.  Calculation of the Continuous Noise Spectral Density
% ---------------------------------------------------------------
disp('   '); disp(' Calculating the spectrum');

s=zeros(1:K);   % express in terms of delta
f=fd*(1:K)/T;
t1=0; t2=0; t3=0;

if line_to_line == 1,
  if pdf==0, % Lead-Lag pdf
     for k=1:K,
         c1= pi*delta*f(k)*abar;
         c2= pi*delta*f(k)*(1-abar);
         c3= pi*delta*f(k)*bbar;
         c4= pi*delta*f(k)*(1-bbar);
         t1= sum( sin(c1).^2 - (sin(c1).*cos(c2)).^2 );
         t2= cos(c3-c1) - cos(c2).*cos(c4);
         t3= sum( sin(c1).*sin(c3).*t2 ); % need a cos term
         s(k)= 20*(t1+t3)/(pi*f(k))^2*(2/T);
     end
  end

  if pdf==1,      % Uniform pdf
     for k=1:K,
         c1= pi*delta*f(k)*abar;
         c2= pi*delta*f(k)*(1-abar);
         c3= pi*delta*f(k)*bbar;
         c4= pi*delta*f(k)*(1-bbar);
         c5= c3-c1;
         for i=1:N,
             if c2(i)==0, ut1(i,:)=1;
             else  ut1(i,:)=sin(c2(i))/c2(i); end
             if c5(i)==0, ut2(i,:)=1;
             else  ut2(i,:)=sin(c5(i))/c5(i); end
```

```
            if c4(i)==0, ut3(i,:)=1;
            else  ut3(i,:)=sin(c4(i))/c4(i); end
        end  % for i=1:N
        t1= sum( sin(c1).^2 - (sin(c1).*ut1).^2 );
        t2= ut2 - ut1.*ut3;
        t3= sum( sin(c1).*sin(c3).*t2 );
        s(k)= 20*(t1+t3)/(pi*f(k))^2*(2/T);
    end  % for k=1:K
  end  % if
end    % line_to_line == 1


if line_to_neutral == 1,
  if pdf==0,  % Lead-Lag pdf
    for k=1:K,
        c1= pi*delta*f(k)*abar;
        c2= pi*delta*f(k)*(1-abar);
        c3= pi*delta*f(k)*bbar;
        c4= pi*delta*f(k)*(1-bbar);
        c5= pi*delta*f(k)*cbar;
        c6= pi*delta*f(k)*(1-cbar);

        t1= sum( (6*sin(c1).^2).* (1-cos(c2).^2) );
        t2= sum( (4*sin(c1).*sin(c3)).* (cos(c3-c1) -cos(c2).*cos(c4)) );
        t3= sum( (4*sin(c1).*sin(c5)).* (cos(c5-c1) -cos(c2).*cos(c6)) );
        t4= sum( (2*sin(c3).*sin(c5)).* (cos(c5-c3) -cos(c4).*cos(c6)) );
        s(k) = 20*(t1 - t2 -t3 + t4)/ (9*T*(pi*f(k))^2);
    end  % for k=1:K
  end     % if

  if pdf==1,      % Uniform pdf
    for k=1:K,
        c1= pi*delta*f(k)*abar;
        c2= pi*delta*f(k)*(1-abar);
        c3= pi*delta*f(k)*bbar;
        c4= pi*delta*f(k)*(1-bbar);
        c5= c3-c1;
        for i=1:N,
            if c2(i)==0, ut1(i,:)=1;
            else  ut1(i,:)=sin(c2(i))/c2(i); end
            if c5(i)==0, ut2(i,:)=1;
            else  ut2(i,:)=sin(c5(i))/c5(i); end
            if c4(i)==0, ut3(i,:)=1;
            else  ut3(i,:)=sin(c4(i))/c4(i); end
        end  % for i=1:N
```

```
        t1= sum( sin(c1).^2 - (sin(c1).*ut1).^2 );
        t2= ut2 - ut1.*ut3;
        t3= sum( sin(c1).*sin(c3).*t2 );
        s(k)= 20*(t1+t3)/(pi*f(k))^2*(2/T);
    end  % for k=1:K
  end  % if
end  % line_to_neutral == 1


if N==480, cs = s(1:10000);
else  cs = s(1:1000);  end,
%save cs.mat cs f

clg
plot(50*f,10*log10(s));
title('Continuous Noise Spectral Density')
xlabel('Normalized Frequency')
ylabel('Power/Hz')
disp('  '); disp('Hit Return to see the combined spectra')
pause

% ----------------------------------------------------------------
% 4.  Plot of the Combined Spectrum
% ----------------------------------------------------------------
sum=cs+ds2;
if N== 480,
   axis([1 100000 -120 0]);
   plot(f,10*log10(sum))
   title('Combined Density')
   xlabel('frequency, Hz')
   ylabel('dB')
   grid
else,
   axis([1 10000 -80 0]);
   plot(f,10*log10(sum))
   title('Combined Density')
   xlabel('frequency, Hz')
   ylabel('dB')
   grid
end
```

```
% ------------------------------------------------------------
% m-file for calculating trapzodial modulating function
% ------------------------------------------------------------
function m=trap(M,N);

F= zeros(1:N)';
ver=1;
if ver==0,
  F(1) = 0;
  if N == 48,
    F(2:9) =  2/8*(1:8)'-1;
    F(10:25) = 2*ones(1:16)'-1;
    F(26:33) = 2 -2/8*(1:8)' -1;
    F(34:48) = zeros(1:15)'-1;
  elseif N == 120,
    F(2:21) =  2/20*(1:20)' -1;
    F(22:61) = 2*ones(1:40)' -1;
    F(62:81) = 2 -2/20*(1:20)'-1;
    F(82:120) = zeros(1:39)'-1;
  else
    F(2:81) =  2/80*(1:80)'-1;
    F(82:241) = 2*ones(1:160)'-1;
    F(242:321) = 2 -2/80*(1:80)'-1;
    F(322:480) = zeros(1:159)'-1;
  end, end, end,

elseif ver==1,
  F(1)=-1;
  if N == 48,
    F(2:9) =  1/4*(1:8)'-1;
    F(10:25) = ones(1:16)';
    F(26:33) = 1 -1/4*(1:8)';
    F(34:48) = -1*ones(1:15)';

  elseif N == 120,
    F(2:21) =  2/20*(1:20)' -1;
    F(22:61) = ones(1:40)';
    F(62:81) = 1 -2/20*(1:20)';
    F(82:120) = -1*ones(1:39)';

  else
    F(2:81) =  1/40*(1:80)'-1;
    F(82:241) = ones(1:160)';
    F(242:321) = 1 -1/40*(1:80)';
    F(322:480) = -1*ones(1:159)';
```

```
  end, end, end,
end

clg;
axis([0 N -1.5 1.5]);
plot(F);
title('Trapezodial Modulation')
xlabel('n'), ylabel('F'), keyboard

m= (1+M*F)/2;  %symmetrical
%m=  M*(1+F)/2;



% ------------------------------------------------------------------
% m-file for calculating the sinusoidal modulating function
% ------------------------------------------------------------------
function m=sine(M,N);

F= zeros(1:N)';
for n=1:N,
   F(n)=sin((n-1)*2*pi/N);
end

clg;  axis([0 N -1 1]);  plot(F);
title('Sinusoidal Modulation')
xlabel('n')
ylabel('F')
keyboard

m = (1 + M*F)/2;    % version (1) symmetrical modulation
%m= M*(1+ F)/2;     % asymmetrical


% ------------------------------------------------------------------
% m-file for calculating the increased output modulating function
% ------------------------------------------------------------------
function m=increase(M,N);

F= zeros(1:N)';
for n=1:N,
   F(n)=2*(sin((n-1)*2*pi/N)+1/6*sin(3*((n-1)*2*pi/N)))/sqrt(3);
end

clg;  axis([0 N -1 1]);  plot(F);
```

```
title('Increased-output Modulation')
xlabel('n')
ylabel('F')
keyboard

m = (1 + M*F)/2;    % symmetrical modulation
%m= M*(1+ F)/2;     % asymmetrical modulation
```

# VITA

Surname: Kwok | Given Names: Samuel (Tin-Chu)

Place of Birth: Hong Kong | Date of Birth: November, 1967

Educational Institutions Attended:

| | |
|---|---|
| University of Victoria, Canada | 1987 to 1991 |
| University of Victoria, Canada | 1991 to 1993 |

Degrees Awarded:

B.Eng.(Co-op), University of Victoria, Canada, May 1991

Publications:

1) R.L. Kirlin, S. Legowski, A.M. Trzynadlowski, Y. Cui, and S. Kwok, "Power Spectra of a three-phase inverter with random pulse width modulation modes," presented at 3rd IEEE workshop on computers in power electronics, UC Berkeley, August 1992.

2) R. Lynn Kirlin, Sam Kwok, Stanislaw Legowski, and Andrzej M. Trzynadlowski, "Power Spectra of a PWM Inverter with Randomized Pulse Position," In PESC Proceedings, pages 1041-1047. IEEE, 1993 (also submitted for publication to *IEEE Transaction on Power Electronics*).

# PARTIAL COPYRIGHT LICENSE



Title of Thesis :

**Power Spectra of a Three-Phase Inverter with Random Pulse-Width Modulation Modes**

Author: [redacted]

Samuel Kwok

August 12, 1993